b138 484 95

U.O.V.S. BIBLIOTEEK

University Free State
34300000407696
Universiteit Vrystaat

HIERDIE EKSEMPLAAR MAG ONDER GEEN OMSTANDIGHEDE UIT DIE BIBLIOTEEK VERWYDER WORD NIE

Using Monte Carlo Techniques to Evaluate the Dose Distributions from A Radiotherapy Treatment Planning System

BY

KAVUMA AWUSI

Dissertation submitted in partial fulfillment of the requirements for the M.Med.Sc degree in the Faculty of Health Sciences, Medical Physics Department, at the University of the Orange Free State.

JUNE 2000

Supervisor: Prof. M.G.Lotter

Co-supervisor: Dr.C.A. Willemse

Universiteit van die
Oranje-Vrystaat
BLOEMFONTEIN
- 2 MAY 2001
UOVS SASOL BIBLIOTEEK

Acknowledgements

I would like to thank the following people:

My supervisor Prof. M.G.Lotter for his devotion, the numerous contributions of advice and other essential guidance which made this work reach this its conclusion.

My co-supervisor Dr.C.A Willemse for his dedication to this work, all the discussions and suggestions which made the realization of this project possible.

All other staff, Medical Physics Department, University of the Orange Free State, who made a significant contribution and gave encouragement for making this work possible.

My sponsors, the International Atomic Energy Agency which granted a fellowship for facilitating my travel, leave and fees that has enabled me to study this course.

My employers, Mulago Hospital / Radiotherapy Department, who allowed me to go for further studies.

My family, for their support and bearing with me while I was away during this course.

Kavuma Awusi

Table Of Contents

List of Abbreviations used

CT	Computer Tomography
TPS	Treatment Planning System
MC	Monte Carlo
SSD	Source to Surface Distance
PDD	Percentage Depth Dose
TAR	Tissue Air Ratio
MU	Monitor Units
CM	Component Module
PSF	Phase Space File
ECUT	Electrons Cutoff Energy Value
PCUT	Photons Cutoff Energy Value
3D	Three Dimensional

ABSTRACT

In this study we used Monte Carlo techniques to simulate the SL25 linear accelerator treatment head using the BEAM Code. The main purpose of study was to evaluate the dose distributions obtained by the CADPLAN treatment planning system (TPS) for 8 MV photon beams of a SL25 linear accelerator in realistic patient models. Simulation of the treatment head involves modeling of the main components of the treatment head that have influence on the absorption and scattering of radiation. Simulation of the accelerator was done in two parts to minimize the simulation time.

Analysis of the data generated by the BEAM code was carried out using BEAMDP, another subsidiary of the BEAM code. We calculated the beam characteristics which are difficult to measure experimentally, such as angular distributions, spectral distributions, planar fluence and planar energy fluence at a plane located just above the jaws of the treatment head.

The phase space files at the isocenter were used as source input for DOSXYZ, a MC code to calculate 3D dose distributions in water or CT based phantoms. The DOSXYZ code was used to calculate depth dose and cross plane profiles in a water phantom. The data obtained with Monte Carlo methods were compared with that obtained by ionization chamber measurements. Depth dose and cross plane profiles obtained by Monte Carlo methods and ionization chamber measurements generally agreed within 2%.

We created patient models from CT data of real patients using the CTCREATE option of the DOSXYZ program. Dose distributions for a number of field sizes and different anatomical sites were calculated with the DOSXYZ code and compared with corresponding dose distributions calculated by the TPS. The modified BATHO and ETAR inhomogeneity correction methods used in the TPS were evaluated.

Results show that Monte Carlo methods can accurately reproduce ion chamber measurements in a water phantom. Monte Carlo techniques are very useful for evaluating

the accuracy of dose distributions generated by treatment planning systems in patient based models where measurements are impossible. The BATHO and ETAR methods showed comparable results to the Monte Carlo results. This could be due to the inefficiency of the method (visualization of the dose distributions) that we used for the comparison of the results. A more quantitative method like the use of the dose difference volume histogram could give a more comprehensive evaluation.

Key words: Monte Carlo, BEAM code, DOSXYZ code, Accelerator simulation, Photon beam and Dose distributions.

CHAPTER ONE

1.0 Introduction

1.1 Radiotherapy

Radiation therapy is the treatment of a defined volume of tissue in a patient by exposure to ionizing radiation in such a way that a desired biological or clinical effect is obtained as a result of the energy absorbed. Radiation use for the treatment of malignancies was born in 1896, the year following the discovery of X-rays. It remained ineffective, basically because of the side effects that were high at that time until the 1930's when more research on its application has been done. The progress of radiotherapy was due to (Tubiana et al, 1990) the developments in radiation dosimetry, better radiation beam collimation and more penetrating X-rays. During the past century, radiotherapy has tremendously changed and at present there is a wide range of radiation sources. Sources of radiation used in radiotherapy may be classified into natural and artificial sources. Natural sources are radioactive materials which spontaneously decay by emitting radiation e.g. cobalt-60, caesium-137, iridium–192, radium-226 and many others. Artificial radiation sources on the other hand appeared as the result of the development of high energy devices and initially included the cyclotron, betatron, microtron, kilovoltage units and later the linear accelerator. The increased availability of linear accelerators having with multi-energy photons and electron beams, with
high dose rate outputs and large field capabilities has given linear accelerators considerable edge in popularity over all other treatment modalities.

Radiotherapy may be classified according to whether the source of radiation is external or internal to the patient's body. In external radiotherapy the sources are situated at a distance from the surface of the body, a method of treatment called teletherapy. Teletherapy units include the linear accelerator, cobalt-60 units. kilovoltage units,

betatrons etc. On the other hand, for internal radiotherapy the sources are in contact with the patient and are mainly small sealed sources of radioactive nuclides such as Ra-226, Cs-137, Ir-192 etc. There are also unsealed radionuclides used for radiotherapy eg 1-131. This method of treatment is called brachytherapy. Brachytherapy is subdivided into two main categories: intracavitary, where radioactive sources are inserted into body cavities and interstitial, where radioactive needles are inserted into the patient's tissue.

This particular work is limited only to teletherapy units and more specifically to linear accelerators.

The main objective of radiotherapy is to deliver a high dose to a target volume (tumor) and spare as much as possible the normal surrounding tissue. In general radiotherapy is a compromise between tumor control and causing complication to the patient. Studies have shown that the dose-response curve is quite steep (Kutcher, 1992). There is evidence that a 7 to 10 % variation in the dose to the target volume may result in a significant change in both the tumor control and normal tissue complication probabilities (Brahme, 1984). A generally accepted criterion developed on the basis of clinical and dosimetric experience (Laughlin et.al, 1977 and Dahlin et.al, 1983) is that the administered tumor dose should be within ± 5% of that specified by the oncologist. This limit minimizes the chances of recurrence due to under dosage or causing complications due to doses exceeding normal tissue tolerance. Because of the above facts, ionizing radiation must be used wisely with full understanding of its injurious and therapeutic potentials. To achieve the above goals and objectives, it is essential that all aspects that maximize accuracy in dose delivery must be applied or adopted to obtain better therapeutic results in radiotherapy. The main concern in this project was to improve accuracy of dosimetry.

Radiotherapy demands more accurate dosimetry for good patients care. The demand has increased tremendously with the advent of computer technology like CT scanners, which allow detailed knowledge of the geometry and densities of the body to be irradiated. Taking into consideration the steepness of the dose response curve as mentioned above, methods that can be employed for the accurate determination of absorbed dose

distributions in the patient (section 1.4.3) have a big role to play. Such methods include the Monte Carlo simulation of radiation transport, that has been widely accepted (Ma et al, 1999) as one of the most accurate methods for predicting absorbed dose distributions in radiotherapy. In fact Monte Carlo simulation of radiotherapy treatment units is believed to be the next generation dose calculation engine (Mohan, 1997 and Ma et al, 1999) for radiation treatment planning systems in routine clinical practice.

1.2 Photon and electron beams in radiotherapy

1.2.1 Photon beams

Photons are interchangeably referred to as γ-rays or X-rays. γ-radiation is mainly a result of the decay of radioactive sources. X-radiation is mainly produced when fast moving electrons strike a high density target material and, depending on the energy of the incident electrons, either low or high (or a combination of both) energy X- rays may be produced. Strictly speaking, a photon is not a particle like an electron but a bunch of energy, though in many of its interactions it acts as a particle. Photons travel at the speed of light, which is 3×10^8 m/s. Photon beams with beam quality ranging between 4 to 20 MV have been commonly used in radiotherapy. Because photons have no charge, they are often referred to as indirectly ionizing radiation and this physical property plays a fundamental role in the interaction mechanism of the photons. When photons interact with matter, ionization is produced as a secondary effect, and this reaches a peak value at a certain depth from the surface, resulting in relatively less dose to the surface. This phenomenon leads to the skin sparing effect observed when patients are irradiated. An important consideration in the use of mega voltage photon beams (Petti et al, 1983) for the treatment of cancer is the amount of surface dose delivered to the patient. One of the main characteristics of a high-energy photon beam is its ability to penetrate deep into tissue while depositing energy in the form of radiation dose. Because of there capability to penetrate deeper in tissue, the principal application of photons is in the treatment of deep-seated tumors e.g cancer of cervix, esophagus, prostate, etc.

1.2.2 Electron beams

A number of different types of particles e.g. electrons, neutrons, protons, π-mesons and heavy ions are in use in radiotherapy and of these only electrons have gained wide spread use. The most clinically useful energy range for electrons is 4 – 22 MeV (Khan, 1994) and at these energies the electron beam can be used for the treatment of superficial tumors less than 5 cm deep. Because electrons are charged, they rapidly ionize the matter through which they are passing and therefore they are referred to as directly ionizing radiation. In the process they lose energy and their degree of ionization falls off rapidly with depth in matter, hence their inability to deliver high dosages to deeper tissues. Although there are many similarities between the behavior of electrons beams and that of photon beams, there are also many differences and chief among the differences are: (ICRU report 42)

(i) The steep fall-off of the depth-dose curve beyond the dose maximum; one of the main features of the electron beam that makes it attractive for radiotherapy.

(ii) The broadening of the dose distribution with depth resulting in a bulged shape in the penumbra region.

(iii) The complex behavior of electrons in and around tissue inhomogeneities due to multiple scattering.

(iv) The shape of the dose distribution particularly at depths greater than the electron beam range which may be due to the bremsstrahlung produced mainly in the radiation head of the accelerator and also in the patient.

The principal applications of electrons are in

(i) The treatment of skin cancers

(ii) Chest wall irradiation for breast cancers and boosting dose to nodes

(iii) The treatment of head and neck cancers

Although many of these sites can be treated with superficial X-rays or tangential photon beams, the electron beam irradiation offers distinct advantage in terms of dose uniformity in the target volume and in minimizing dose to deeper tissues.

1.3 Radiotherapy treatment planning

The process of radiation therapy is complex (Van Dyk et al, 1993) and involves a series of procedure steps beginning with patient diagnosis, disease staging and lastly the treatment of a specified target volume with predetermined radiation energies and beam parameters. Radiotherapy treatment planning is a process whereby sources of ionizing radiation are suitably arranged and combined to give a required distribution of absorbed dose in a particular region of the body. In summary, the goal of treatment planning is to produce a high and uniformly distributed dose throughout the target volume while keeping the dose to the surrounding normal tissue / organs at risk as low as reasonably achievable. The procedures of radiotherapy treatment planning (Williams et al, 1993) are:

(i) Acquisition of patient anatomical information

(ii) Definition of target volume and prescription of target absorbed dose

(iii) Selection of beam and field arrangements

(iv) Computation of dose distribution

(v) Simulation of each of the selected components of the plan on the patient by use of an X ray simulator

(vi) Set-up of patient on the therapy unit for treatment

In teletherapy it is usually necessary to combine a number of external beams of radiation entering the body from different directions in order to obtain the desired distribution of absorbed dose in the target volume and to minimize unwanted exposures else where. The combination of beams necessitates two important parameters in treatment planning and these are beam weighting and dose normalization. Two sets of data are needed for the initialization and accomplishment of treatment planning (ICRU report 42) and these are

(i) Beam data: This characterizes the radiation and implies measurement at the therapy machine. The number and type of measurements depend on the model

used for beam representation and the algorithm used to combine this information with the patient data.

(ii) Patient data: This describes the patient's anatomy (geometry) in a form that can be combined with the beam data. This data include information on the external surface of the patient, the target volume, organ at risk and relevant tissue inhomogeneities.

There has been an increase in the development of high-energy photon and electron sources of varying degree of complexity and capabilities, all of which permit a high degree of concentration of radiation. This necessitated the development of treatment planning as well, to make best use of these modalities. This has resulted in the increased use of computers in radiotherapy to handle the large amount of data involved, that is, beam/dosimetric related and patient data. The former refers to the use of computers for treatment dose calculation while the latter means the use of computers (CT) for more accurate localization of the tumor and other anatomical regions relevant to treatment planning.

CT images help to represent the patient in terms of physical parameters for use in dose calculations. The anatomical structures of the patient are assigned different bulk densities and the most commonly used physical parameters used in dose calculation are the electron density relative to that of water. Furthermore in computed tomography, CT numbers representing properties of volume elements of the body can be obtained. These CT numbers can be directly transformed into relative electron densities (Huizeng et al, 1985 and ICRU report 42, 1987) to be fed to a treatment planning system. In summary, the main applications of CT in radiotherapy are:

(i) diagnosis of diseases in patients

(ii) the acquisition of patient and tumor contours

(iii) obtaining density information concerning the patient in order to improve the dose calculations for therapy

(iv) the evaluation of the results of the radiation therapy.

1.4 Methods of obtaining dose distributions due to a radiation beam

Apart from direct measurement of radiation fields by ionization chamber, film dosimetry, calorimetry, chemical dosimetry and thermoluminescence dosimetry, there are several other possible methods, that can be used to predict the dose distribution due to an incident radiation beam (Metcalfe et al, 1997 and ICRU report 42, 1987). Some of these are:

1.4.1 Boltzman integral – differential equation

Solving the Boltzman integral –differential equation is an analytical method that allows the possibility of calculating the dose distribution from first principles using the laws governing the physics of photon and electron transport. Equations can be solved for specific beam and medium conditions e.g. energy, field size, etc. The limitation of the method is that there are so many variables affecting the resulting dose distribution that the equations are rendered almost impossible to solve. Therefore solutions can only be found after making many approximations both in formulating and solving the equations (Williamson, 1989). Thus the method can be employed only for simple interaction mechanisms. Furthermore since the technique solves the transport equation directly, it is not capable of answering questions about an individual particle's history (Rogers et.al, 1990) as Monte Carlo techniques can do (section 1.4.3).

1.4.2 Convolution Methods

This method is more realistic for generating a radiation beam dose distribution compared to the Boltzman integral–differential equation. The method uses a combination of both analytically calculated and Monte Carlo generated physical quantities to construct the dose distribution that is calculated directly from the known characteristics of the incident beam. Convolution algorithms have two essential components, one representing the

energy imparted to the medium by the interactions of the primary photons (Terma) and the other representing the energy deposited about a primary photon interaction site (Kernel). Similar to Monte Carlo (section 1.4.3), the convolution method does not rely on measured dose data (Metcalfe et al, 1997). The only major limitation of the method is that it does not consider individual particles but rather the macroscopic or statistically averaged effects of a large numbers of particles.

1.4.3 Monte Carlo Techniques

Of all the possible methods available at the moment for obtaining the dose distribution due to a radiation beam, the Monte Carlo (MC) method is one of the most powerful methods available (Ma et al, 1999 and Cunningham, 1982) for studying the complex behavior of the interaction of a broad beam of radiation with an absorbing medium. The MC method is a random sampling technique (statistical simulation method) (Bushberg et al, 1994). It consists of computer simulations that involve propagating a photon or electron beam through a computerized phantom and, photon by photon calculating the deposition of energy within the phantom by using the laws of probability and the known physical characteristics of scattering (attenuation coefficients, scattering angles, etc). The transport of an incident particle, and of the particles that it subsequently sets in motion, is referred to as a particle history and in MC each history is uniquely followed by random selection from the probability distribution that control each possible interaction. The procedure describes the distribution by tracing the histories of a very large number of individual photons or electrons as they interact, scatter and eventually disappear. At each interaction, the laws of radiation physics are used to predict the outcome. A dose distribution can be built by summing the energy deposition in each particle history. Because the MC method requires modeling a stochastic set of events, the computer essentially rolls the dice to calculate whether the radiation particle was absorbed, scattered or passed through the phantom unattenuated. In a computer, rolling the dice is performed by using a code that generates a pseudo random number. To employ MC methods practically in radiotherapy the simulation of the relevant components of the

radiation treatment head is required. The user has to describe the geometry and materials of the relevant components where interaction might take place and by so doing it provides the practical means for obtaining energy spectra and angular distributions (Mohan, 1988).

The MC simulation of photon beams is much simpler and faster compared to electron beams (Nahum, 1988). Photons on average undergo a moderate number of interactions and also the cross-section data needed for most applications are known to a high degree of accuracy, mainly using the Klein-Nishina cross-section. On the other hand, simulation of electron transport is time consuming, (Rogers et al, 1990) because an electron undergoes a large number of elastic scattering collisions during its history and also in the course of slowing down a large number of low energy electrons are set in motion. Even in photon simulations, it is the electron transport that consumes most of the computing time for high energies where the electron range is large. This is because there are usually many short electron transport steps corresponding to each photon step. Berger et al, 1988, estimated that an electron makes $\approx 10^4$ elastic collisions in the course of slowing down from 1 MeV to 1 keV. Therefore the simulation of electrons require a different approach from that of photons, involving a combination of multiple scattering and stopping power theories. In the simulation the condensed-history technique is used (Rogers et al, 1990) in which the electron path is broken into a series of steps for which the effects of the large number of individual interactions occurring during the step are grouped together.

1.4.3.1 Advantages of Monte Carlo methods

MC methods have several advantages over all other existing methods for predicting the dose distributions in a patient (Rogers, 1991; Ma et al 1999; Andreo, 1991; Metcalfe et al, 1997). Some of the advantages are:

(i) The method can precisely model the physical processes involved in radiation therapy and can be applied to any absorbing medium of any geometry and any radiation beam.

(ii) Secondary particles (electrons and positrons) produced in case of photon interactions can also be followed.

(iii) The method does not require measurements

(iv) Information about macroscopic quantities such as energy deposition can be obtained.

(v) The MC method has an upper hand in handling geometrically complex inhomogeneities whose densities deviate significantly from unity, in which case the available inhomogeneity correction methods fail to predict dose distributions properly compared to that of water. Regions of low or high densities, where electronic dis-equilibrium is present, have posed problems for correction methods (Metcalfe et al, 1997).

(vi) Monte Carlo simulation methods can handle backscatter from high-density materials such as bone and scatter perturbations by air cavities more accurately than any other existing dose calculation model (Rogers and Bielajew 1990).

(vii) The method can be used to answer questions that cannot be addressed by experimental investigation, such as what fraction of the electrons were generated in the collimator versus the filter, or how often have certain photons undergone Compton scattering.

(viii) The method can be used to obtain angular distributions, quantities that cannot be measured experimentally.

(ix) The method allows the generation of the energy spectrum, not only in the central part of the beam, but also in regions away from it.

(x) Last but not least, is the possible saving in manpower at the expense of computer time.

Monte Carlo simulation is therefore the method of choice for solving complicated transport problems (Williamson, 1989)

1.4.3.2 Limitations of Monte Carlo

(i) An extremely large number of histories are required before the statistical uncertainty in the distribution is small enough for it to be used in a treatment planning system (TPS). The lower the uncertainty the smoother the depth dose or cross beam profiles obtained from the distributions.

(ii) Because a large number of histories are simulated in the method, a large amount of computer memory long computing times are required.

Because of the limitations mentioned above, at present MC methods can only be used as a bench mark to compare other simpler and faster calculation methods. However the above computational shortcomings are becoming less severe due to the rapid increase in computer speed and memory as well as the decrease in the cost of computers. Currently, efforts are under way to develop MC based three dimensional (3D) treatment planning systems (TPSs) e.g. the OMEGA project (Rogers et al, 1995) and the Peregrine project (http://www-phys.llnl.gov/peregrine) Hopefully with these new developments the dose to be delivered to a patient will be calculated in few minutes.

1.5 Review of previous work done on Monte Carlo simulation of photon beams

For the past two decades, many investigations have been carried out on the MC simulations of radiation beams from radiotherapy treatment units (mainly linear accelerators and Co-60 units). MC simulation of photon beams has been studied extensively compared to electron beams due to the fact that the dose calculation for the latter requires more detailed beam phase space information on the patient surface than the former (Mackie, 1990). Also, electrons undergo thousands of interactions in the process of slowing down such that computing problems hindered investigators. Currently much work is being done in this area as there has been a tremendous improvement in computer technology. In the early years, due to the low speed of computers and the relatively simple MC codes that where available, a full simulation of the accelerator geometry was

an extremely difficult task (Ma et al 1999). Simulations were usually carried out for treatment heads with great simplification and only taking into account few components of dosimetric importance. A large amount of physical data e.g. dimensions and materials need to be obtained with high precision to carry out a full MC simulation of any therapy unit. The task of simulating the full accelerator head was first tacked by Udale (1988, 1990, 1992), who did many studies mainly on electron simulations using the EGS4 code system. Udale's work changed the MC simulation of accelerators in that simulation were no longer restricted to cylindrical symmetry as before, but any geometry could be simulated. However Udale's code could only be applied to other types of accelerators after a large effort, involving extensive modification of the program.

Monte Carlo simulations of photon beams have been carried out by quite a number of investigators. Patau et al (1978) simulated the generation of photons in a tungsten-copper target, the transport of photons through a flattening filter and collimators, and the attenuation of photons in slabs of various materials. McCall et al (1978) investigated the effects of various targets and flattening filters on the mean energy of photon beams using the EGS3 code. Mohan et al (1985) simulated an accelerator head using the EGS3 code system to calculate the photon spectra and fluence distributions from several accelerators. Han et al (1987) used the EGS3 code to simulate a Co-60 unit treatment head, where they approximated the geometry of the Theratron-780 unit as a source capsule, the source housing and the collimators. Similar studies were done by Nelson et al (1985) and Rogers et al (1988) using the EGS4 code system, whereby Rogers and his group investigated the source of electron contamination in a Co-60 beam. Lovelock et al (1994) developed McRad, an EGS4 user code that was a generic MC model of a photon linear accelerator. Lee (1997) simulated the 6 MV photon beam from a Varian Clinac 2100C accelerator using the EGS4 code system to study the differential beam hardening effect of the flattening filter.

The Rogers et al (1995) EGS4/BEAM code has been extensively used to simulate photon beams from various types of accelerators by different investigators. Some of these are:

- Liu et al (1997) simulated the photon beams from a Clinac 2100C accelerator and by analyzing the simulation results developed an extra-focal source model for the dose calculation using a convolution/superposition method.
- Jiang and Ayyangar (1998) simulated a Varian Clinac 1800 accelerator and studied the perturbation effect of compensators on photon beam characteristics.
- Balog et al (1999) did studies on multileaf collimator transmission by simulating a GE Orion 4 MV linear accelerator using the BEAM code and as the result of their study they redesigned the collimator for that unit.
- Faddegon et al (1999), after simulating the treatment head for the Siemens MXE accelerator with the BEAM code, re-designed a new flattening filter for the 6 MV photon beam for this machine.
-
- Verhaegen et al (1999) used the BEAM code to simulate a radiotherapy kV x-ray unit.
- Du Plessis (1999) used the BEAM code to simulate the 8 MV photons from a Philips SL14 linear accelerator in his study in which he used MC methods for the evaluation of a radiotherapy treatment planning system. He used the DOSXYZ code to calculate the beam data, that is, percentage depth dose and cross plane profiles in a 3D water phantom. The generic accelerator beam data, generated by the BEAM/ DOSXYZ codes were supplied to the treatment planning system. At the end of his study, he was able to compare the MC calculated absorbed dose distributions in CT based patient models with that calculated by the treatment planning system.

1.6 Monte Carlo simulations of linear accelerator heads

A number of MC codes are available which can be used to simulate therapy units. Examples are:

1) The ETRAN (Electron Transport) code system
2) The ITS (Integrated Tiger Series) code system
3) The EGS (Electron Gamma Shower) code system

Of these, the EGS code, and more specifically the fourth version EGS4, is the most widely used MC code in medical radiation physics today. The EGS4 code is written in MORTRAN language, that is based on FORTRAN, but has extensions to make it more flexible and easier to use (Metcalfe et al, 1997).

Monte Carlo simulations of radiation output of, radiation treatment machine heads provide practical means for obtaining energy spectra and angular distributions of photons and electrons emerging from such a machine, which are important in radiation dosimetry. The main task of the user is to set up the geometry for the problem This include arrangement and describing of the various relevant components of the head, in a manner that can be understood by the computer program. More discussion in sections 3.2 and 3.3.) There have been several applications developed using the EGS4 code, for example the McRad – Monte carlo Radiation Dosimetry (Lovelock et al, 1995) and BEAM (Rogers et al, 1995) which have successively been used in the simulation of radiotherapy units. One particular advantage of the BEAM code is the way it was designed and simplified in such a way that it can be accurately used to simulate treatment heads by other individuals with minimum efforts. The other advantage of the BEAM code is that the generated phase space files can be re-used by the BEAM its self, allowing the user to simulate a treatment head output in separate steps to reduce CPU time. A more detailed description of the BEAM code can be found in section 2.10.

In this study the BEAM code together with its subsidiary code, DOSXYZ were used to simulate the 8 MV photon beam from a Philips SL25 accelerator and to calculate the dose distribution in the phantom respectively. The BEAMDP was used for the analysis of the phase space files while CTCREATE program was used in simulation of CT based models.

1.7 The problem

The overall uncertainty in the delivered dose to a point in a patient is a combination of three distinct uncertainties (Van Dyk et al, 1993 and ICRU report 42, 1987) and these are

(i) Uncertainties in the determination of the absorbed dose at the reference point for the reference situation.

(ii) Uncertainties in the calculation of the dose by the computer at points in a patient relative to the dose at the reference point.

(iii) Uncertainties in the set up and treatment of the patient.

This study is mainly addressed to the first two of the above mentioned and there are several factors which may contribute to these uncertainties.

(i) For the first case, a number of factors may influence accurate dose determination which may include chamber accuracy and precision, errors in positioning of chamber in water phantom, electrometer sensitivity and variations in the atmospheric conditions e.g. temperature and pressure during the course of measurement.

(ii) In addition to the first two cases mentioned above, there is another factor of information transfer from the measuring conditions to the treatment planning computers.

(iii) Measurements are usually done with a perpendicular incident beam in a water phantom which is homogeneous, flat surface and unity density, yet the patient is heterogeneous in nature and with an irregular surface.

(iv) The computer algorithms used in the computation of dose distributions have posed great problems mainly when it comes to inhomogeneity correction effects. Different TPS employ different algorithms in the calculations, and some are more superior to others in their capabilities in handling inhomogeneity problems.

There is no overall solution to the above problems. However, since MC simulation methods do not require measurements, they can be used to accurately predict the dose in the two stages mentioned above. A MC treatment planning system needs detailed information about the beams incident on the patient and also to initiate the transport of particles in patient CT model, accurate phase space information about particles on the patient surface is required. A direct measurement of this information for a clinical beam is difficult or impossible. Calculation of beam phase space parameters using analytical

methods is not flexible and usually employs approximations (section 1.4.1). Currently the most practical way to obtain detailed information about the incident radiation beam is the MC simulation of the radiotherapy treatment head (Udale–Smith, 1992 and Rogers et al, 1988). With the BEAM Monte Carlo code it is possible to get beam data from a radiotherapy unit and use it as input beam data for a TPS. The output from the BEAM program can be used as input to the DOSXYZ code program to calculate dose distributions in a water phantom and this eliminates uncertainties in the measurements. By so doing MC simulations allows inter-comparison against which TPS calculations can be compared.

1.8 Aims of the study

The main aims of the study are

1) (a) Set up simulation of the 8 MV photons from a Philips SL25 linear accelerator with the BEAM program.
   (b) Generate phase space files, analyze the energy spectrum and angular distributions.
   (c) Use the phase space files to calculate depth dose and cross section profiles in a water phantom using the DOSXYZ program.
   (d) To compare the MC calculated dose profiles with dose profiles measured with an Ionization Chamber.
2) (a) Set up patient simulation using CT data and DOSXYZ program
   (b) Read CT data using CTCREATE program
   (c) Enter beams from phase space file to the created CT phantom and use DOSXYZ MC code to calculate the dose distributions.
   (d) Analyze dose distributions
   (e) Evaluate a CADPLAN treatment planning system by comparing its dose distributions to the MC calculated dose distributions.

CHAPTER TWO

2.0 THEORY

2.1 Production of photon and electron beams in a linear accelerator

A linear accelerator is a device that uses high frequency electromagnetic waves to accelerate charged particles such as electrons to high energies through a linear tube. Accelerators used in radiotherapy accelerate electrons either by travelling or stationary electro-magnetic waves at frequencies in the microwave region (≈ 3000 MHz), giving a wavelength = 10 cm in a vacuum. Figure 2.1 is a schematic block diagram showing the major components of a medical linear accelerator (Khan, 1994).

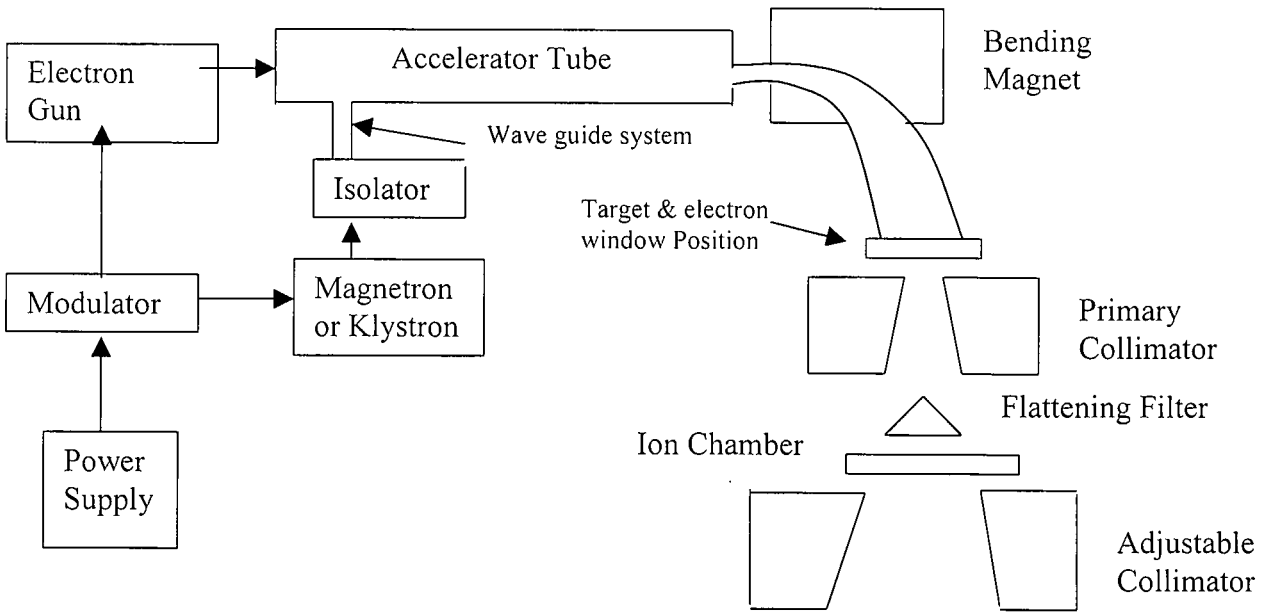

Fig 2.1 : A schematic block diagram of a medical Linear Accelerator

The power supply provides DC power to the modulator that includes the pulse- forming network. High voltage pulses from the modulator section are flat-topped DC pulses of a few μs in duration. These pulses are simultaneously delivered to the magnetron or klystron (both are devices for producing microwaves) and to the electron gun. Pulsed micro waves produced in the magnetron or klystron are injected into the accelerator tube or structure via a wave guide system and at the same instant electrons produced from the electron gun are also pulse injected into the accelerator structure. The accelerator structure consists of an evacuated copper tube with its interior divided by copper discs of varying aperture and spacing. As the electrons are injected into the accelerator structure with an initial energy of ≈ 50 KeV, the electrons interact with the electromagnetic field of the microwaves and hence electrons gain energy from the sinusoidal electric field. After the electron has been accelerated the full length of the wave guide, the electron energy will mainly depend on (Johns et al,1983):

1) the wave guide design
2) power applied to it
3) the current in the wave guide (the larger the current the lower the energy)

The high-energy electrons emerge from the exit window of the accelerator structure in a form of a pencil beam ≈ 3 mm in diameter. Low energy linear accelerators (4 to 6 MeV) have relatively short accelerator tubes, the electrons are allowed to proceed straight on to strike a target for X-ray production. In higher-energy linear accelerators the accelerator structure is too long, the electrons are bent through an angle (90° or 270°) between the accelerator structure and the target using bending magnets, focusing coils and other components such that the beam emerges facing down wards.

To make use of and control the produced radiation, all accelerators are designed with a treatment head, which provides sufficient shielding against leakage radiation. The treatment head consists of a thick shell of high-density shielding material such as lead or tungsten. It contains an X-ray target, primary fixed collimator, scattering foils, flattening filter, ion chamber, wedge, light localizing system and secondary adjustable collimator or jaws (Khan, 1994, Metcalfe et al, 1997 and Johns et al, 1983).

As mentioned above, the electron beam as it exits the window of the accelerator tube is a narrow pencil like beam ≈ 3 mm in diameter. In the photon mode, after electrons have been accelerated to relativistic velocities within the linear accelerator wave guide they strike a target and photons with a broad forward peaked energy spectrum are emitted due to bremsstrahlung production. X-rays are produced when high energy electrons are incident on a target of a high Z material such as tungsten. The target is thick enough to absorb most of the incident electrons and as a result the electron energy is converted into a spectrum of X-ray energies. In the electron mode of an accelerator, this beam, instead of striking the target, is made to strike an electron scattering foil (usually of lead) in order to spread the beam as well as get a uniform electron fluence across the treatment field (Khan, 1994)

The treatment beam is first collimated by a fixed primary collimator located immediately below the X-ray target. In case of X-rays the collimated beam then passes through the flattening filter whose main function is to modify the forward peaked X-ray beam to a uniform beam and to filter the low energy X-ray spectrum. In the electron mode the flattening filter is moved away and replaced by a scattering foil whose main function is to spread the electron beam. The flattened X-ray beam or the electron beam is incident on the dose monitoring chambers, whose main functions are to monitor dose rate, integrated dose and field symmetry. After passing through the ion chamber, the X-ray beam is further collimated by a continuously movable collimator consisting of two pairs of lead or tungsten block jaws that provide a rectangular opening. For electron beams an applicator of appropriate size is used. The field size localizer is provided by a light source system in the treatment head (located between the ion chamber and the jaws) which is a combination of a mirror and a light source (Johns et al, 1983).

2.2 Photon Interaction processes

The most important phenomena during interactions of radiotherapy photon beams are

1) attenuation of photons by scattering and absorption

2) energy transfer to charged particles, mainly electrons and positrons

3) transport of charged particles

4) deposition of energy.

The three most important photon interaction types relevant at energies used in radiotherapy (Metcalfe et al, 1997) are photoelectric, compton and pair production processes. The fourth interaction process is the coherent (classical or rayleigh) scattering, although its cross section is small at radiotherapy energies.

2.2.1 Photoelectric absorption

This type of interaction is more probable to occur at low photon energies and interaction occurs with inner shell electrons e.g. the K or L shells.

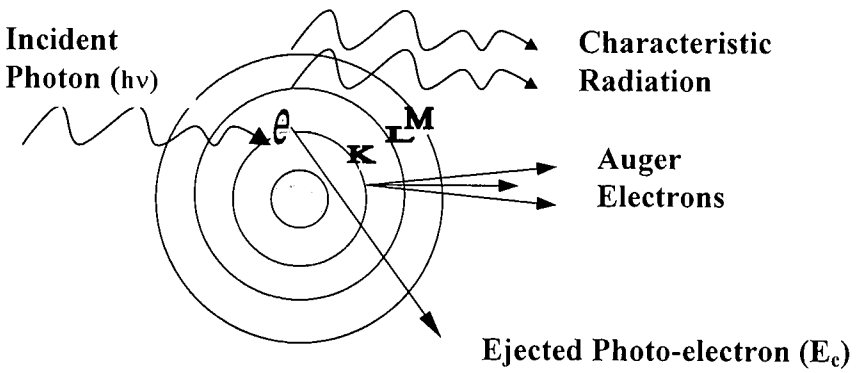

Fig 2.2: Diagram illustrating the Photoelectric effect.

All the energy hν of the incident photon is transferred to a bound electron which is ejected from the atom with kinetic energy $E_e = E_p - E_b$ where E_b is the binding energy of the electron and E_p is the incident photon energy (hν). After interaction the photon is totally absorbed. A vacancy left in the shell after the ejection of the photoelectron is filled by electrons from the outer orbits, and in the process characteristic X-rays are emitted. There is also a possibility of emission of Auger electrons, which are mono-energetic electrons produced by the absorption of characteristic X-rays internally by the atom. The

photoelectric component of the atomic cross section (σ_{pe}) is directly proportional to Z^3 and inversely proportional to E_p^3, where Z is the atomic number. Thus

$$\sigma_{pe} \propto Z^3 E_p^{-3} \qquad 2.1$$

The mass attenuation coefficient is given by the equation

$$\frac{\mu}{\rho} = \frac{N_A}{A}\sigma \qquad 2.2$$

Where A is the atomic mass, N_A is the Avogadro's number, μ is the attenuation coefficient and ρ is the density.

$$\left(\frac{\mu}{\rho}\right)_{pe} \propto \frac{N_A}{A} * Z^3 E_p^{-3} \propto \frac{Z^3}{AE_p^3} \qquad 2.3$$

Thus photoelectric effect is most probable to take place in high Z material and at low energies (< 200 keV).

2.2.2 Compton scattering (Incoherent)

The most important photon interaction process at beam energies used in radiotherapy is Compton scattering, replacing the photoelectric effect as the chief means of removing photons from the initial beam. It is the only predominant interaction in soft tissue at energies 200 keV to 2 MeV. In these energy ranges the energy of the incident photon is much greater than the binding energy of the atomic electrons. The interaction occurs with the outermost (valence) shell electrons that have negligible binding energy.

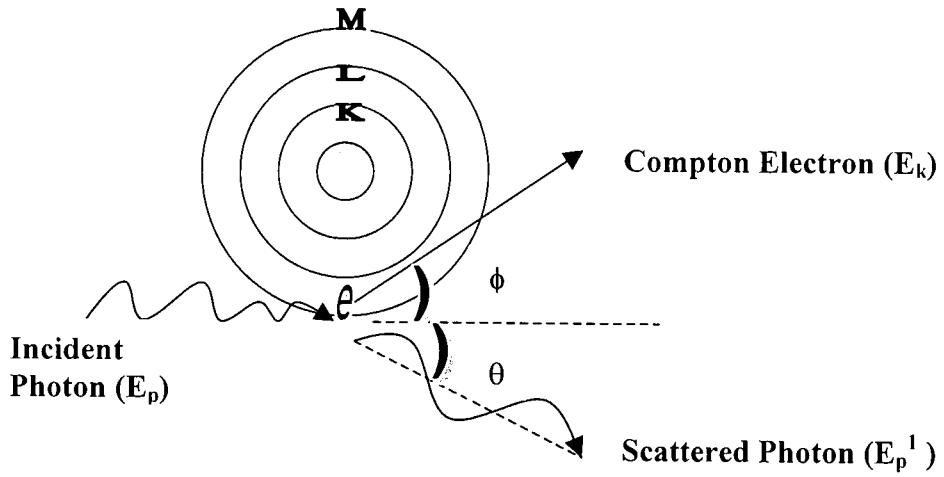

Fig 2.3: Diagram illustrating the Compton process.

The electron and scattered photons are ejected from the atom. By energy conservation, the energy of the incident photon E_p is equal to the sum of the energy of the scattered photon E_p' and kinetic energy E_k of the ejected electron. That is $E_p = E_p' + E_k$. Compton scattering results in the ionization of the atom and division of the incident photon energy between the scattered photon and the ejected electron. It can be shown that

$$E_p' = \frac{E_p}{1+\alpha(1-\cos\theta)} \qquad 2.4$$

Where $\alpha = E_p/ m_o c^2$ and $m_o = 0.511$ MeV is the electron rest mass.

Also it can be shown that the total energy E is given by the equation

$$E = E_p \frac{\alpha(1-\cos\theta)}{1+\alpha(1-\cos\theta)} \qquad 2.5$$

The Compton mass attenuation coefficient is proportional to the number of electrons per unit mass (Z/A) and inversely proportional to the square root of the energy, and given by

$$\left(\frac{\mu}{\rho}\right)_{comp} \propto \frac{Z}{A} E_p^{-1/2} \propto \frac{Z}{AE_p^{1/2}} \qquad 2.6$$

2.2.3 Pair production

This type of interaction is more predominant at high energies and has a threshold photon energy greater than of $2m_oc^2$ or 1.022 MeV. This energy is needed to supply the rest energy of the two particles.

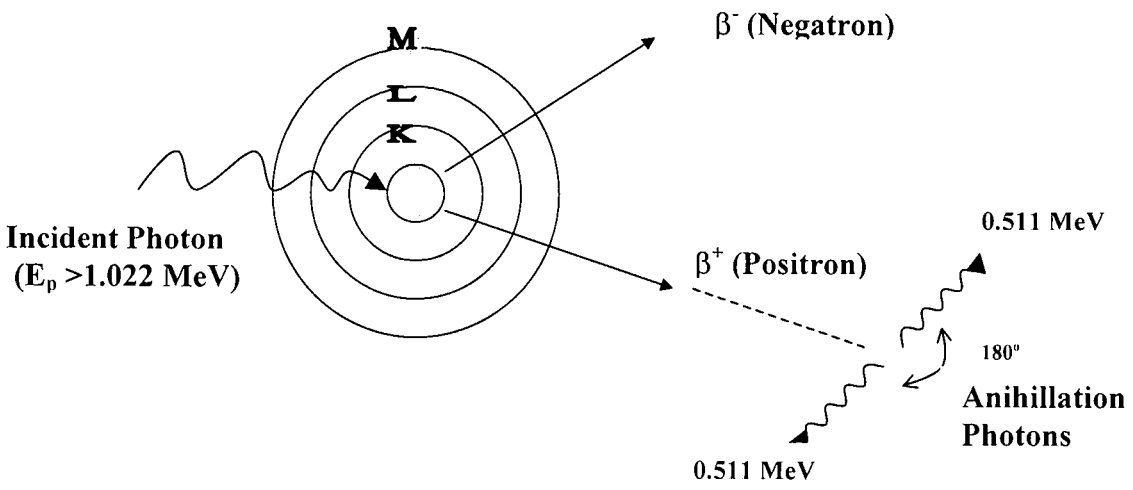

Fig 2.4: Diagram illustrating the Pair Production process.

Pair production can occur upon the interaction of a high energy photon near the nucleus of an atom. The photon disappears totally resulting in the formation of two oppositely charged ion particles, a positron and a negatron. The photon's energy in excess of the threshold is imparted to the ion pairs as kinetic energy. That is, the total kinetic energy shared by the ion pairs K.E = $E_p - 2m_oc^2$. Annihilation radiation occurs from the conversion of the rest mass of the positron. The pair production cross section is proportional to Z^2 and to the log of the energy. Thus

$$\sigma_{pair} \propto Z^2 \log E_p \Rightarrow \left(\frac{\mu}{\rho}\right)_{pair} \propto \frac{Z^2}{A} \log E_p \qquad 2.7$$

2.2.4 Coherent scattering

In this process the interaction cross section is small at radiotherapy energies. Coherent scattering is only important in the deflection of low energy photons and it does not contribute to energy deposition by ionization or excitation.

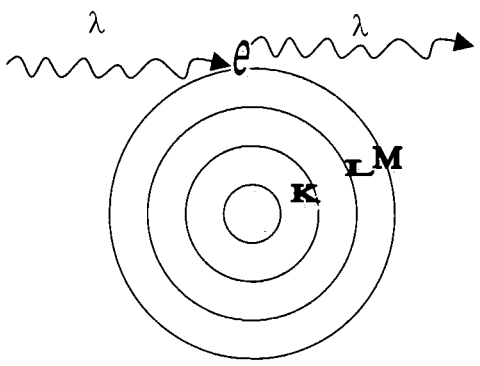

Fig 2.5: Diagram illustrating the Coherent scattering process

The interaction consists of an incident photon passing near the electron and setting it into oscillation. The oscillating electron radiates at the same frequency as the incident electromagnetic wave. These scattered X-rays have the same wavelength (λ) as the incident photon. Thus no energy is transferred and no energy is absorbed in the medium. Coherent scattering is probable in high atomic number materials and with photons of low energy.

$$\left(\frac{\mu}{\rho}\right)_{coh} \propto \frac{Z^{2.5}}{AE^{2}} \qquad 2.8$$

2.2.5 Total mass attenuation coefficient

The total mass attenuation coefficient is the sum of the attenuation coefficients due to photoelectric, compton, pair production and coherent processes.

That is

$$\left(\frac{\mu}{\rho}\right)_{\text{total}} = \left(\frac{\mu}{\rho}\right)_{\text{pe}} + \left(\frac{\mu}{\rho}\right)_{\text{comp}} + \left(\frac{\mu}{\rho}\right)_{\text{pair}} + \left(\frac{\mu}{\rho}\right)_{coh} \qquad 2.9$$

2.3 Attenuation of photons

Figure 2.6 shows an experimental arrangement for the measurement of photons attenuated through an absorbing material. A well-collimated monoenergetic photon beam is incident on an absorber of thickness Δx. A device that can record the number of photons that pass through it (detector) is placed in the beam direction at a distance. Only the primary or transmitted (radiation that pass through the absorber with out interaction) photons are detected. The scattered radiation with a narrow beam geometry will be limited to a small fraction of the primary photons.

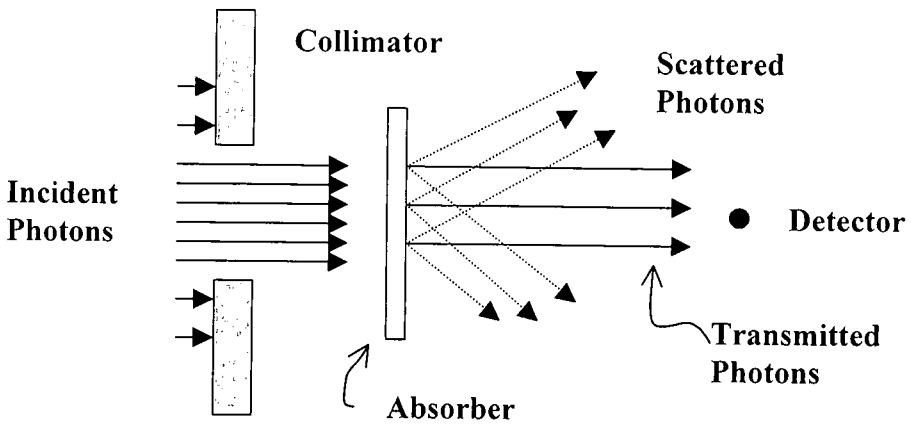

Fig 2.6: Experimental arrangement for attenuation of the photon beam through an absorber.

With such an arrangement, it is assumed that if a photon interacts with an atom, it is either absorbed or scattered away from the absorber according to the photoelectric, compton and pair production processes. The intensity of an X ray beam is reduced as a layer of an absorbing material of thickness Δx is placed in a beam .The reduction in intensity of photons (ΔI) is proportional to the intensity of incident photons (I) and to the thickness of the absorber. Mathematically,

$$dI \propto I.dx \Rightarrow dI = -\mu I\, dx \qquad 2.10$$

Where μ is a constant of proportionality called the linear attenuation coefficient and the minus sign indicates that the intensity of photons decrease as the absorber thickness increases. The solution of the equation is given by,

$$I(x) = I_0 e^{-\mu x} \qquad 2.11$$

where I(x) is the intensity transmitted by thickness x and I_0 is the incident. Equation 2.11 indicates that the attenuation of a monoenergetic beam follows an exponential law. Taking the natural logarithm on both sides of equation 2.11 , then

$$\ln I(x) = \ln I_0 - \mu x \qquad 2.12$$

A plot of ln I(x) versus x gives a straight line with a negative slope equal to μ.

2.4 Photon beam description

A photon beam emitted from a target consists of a large number of photons usually with a wide range of energies. A beam of photons can be described by a number of quantities, some of which are described below; Attix (1986), Khan (1994) and Johns et al, (1983)

2.4.1 Photon fluence

Photon fluence (Φ) is defined as the number of photons ΔN striking a finite sphere of cross-section area Δa, during the time interval extending from t_o to a later time t. That is

$$\Phi = \frac{\Delta N}{\Delta a} \qquad 2.13$$

The units of Φ are m^2 or cm^{-2}. It is also possible to describe the photon beam in terms of planar fluence, which is the number of particles crossing a fixed plane in either direction per unit area of the plane by analyzing the variation of fluence versus position in the X-direction, figure 2.7.

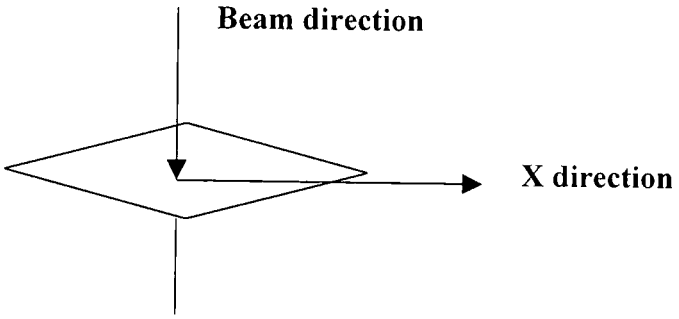

Figure 2.7: Show the X direction relative to the beam direction

2.4.2 Photon fluence rate (flux density)

At any time t within the interval t_o to t_{max}, the photon fluence rate or flux density (ϕ) is defined as the rate of change of fluence that is the number of photons crossing an area per unit time. Thus

$$\phi = \frac{\Delta N}{\Delta a . \Delta t} \qquad 2.14$$

Units of ϕ are $m^{-2}\ s^{-1}$ or $cm^{-2}\ s^{-1}$. From equations 2.13 and 2.14, the relation between fluence and flux density is given by

$$\Phi = \phi \,.\, \Delta t \qquad 2.15$$

2.4.3 Energy fluence

Energy fluence (Ψ) is the term used to describe the beam by taking into account the energies of the individual rays. If we let R be the expectation value of the total energy carried by ΔN rays striking a finite sphere during the time interval extending from t_o to a later time t. The energy fluence is the defined as the quotient of differential of R by Δa.

$$\Psi = \frac{dR}{da} \qquad 2.16.a$$

Units of Ψ is Jm^{-2}.

For a mono energetic beam $R = E*\Delta N$, the energy fluence is then given by

$$\Psi = \frac{\Delta N}{\Delta a} * E \qquad 2.16.b$$

From equations 2.13 and 2.16.b, the relationship between fluence and energy fluence is given by the equation

$$\Psi = \Phi * E \qquad 2.17$$

2.4.4 Energy fluence rate or energy flux density

Energy fluence rate or energy flux density (ψ) is the term used to describes the rate of energy flow for a beam. At any time t within the interval t_o to t_{max} , the energy flux density is the rate of change of the fluence rate. That is

$$\psi = \frac{d\Psi}{dt} = \frac{d}{dt}\left(\frac{dR}{da}\right) \qquad 2.18.a$$

where $d\Psi$ is the increment of energy fluence during the infinitesimal time interval dt at time t. Units of ψ is $Jm^{-2}s^{-1}$. For a mono energetic beam flux density may be given by

$$\psi = \frac{\Delta N}{\Delta a}.\frac{E}{\Delta t} \qquad 2.18.b$$

From equations 2.14 and 2.18.b, the relationship between flux density and energy flux density is given by the equation

$$\psi = \phi . E \qquad 2.19$$

2.4.5 Energy spectra:

The spectral distribution of a photon field is characterized by the distribution of energy fluence with respect to energy. Suppose $\Phi(E)$ denotes fluence Φ of photons with energy between 0 and E. The differential distribution (Φ_E) of the fluence with respect to energy is given by

$$\Phi_E = \frac{d\,\Phi(E)}{d\,E} \qquad 2.20$$

The product Φ_E dE is the fluence of photons with energies lying between E and E+dE. The total fluence Φ is given by

$$\Phi = \int_0^{Emax} \Phi_E \, dE \qquad 2.21(a)$$

and the mean energy is given by

$$\bar{E} = \frac{\int_0^{Emax} \Phi_E . E \, dE}{\int_0^{Emax} \Phi_E \, dE} \qquad 2.21(b)$$

2.4.6 Angular distribution

The direction of emission of X-rays from a target depend on the energy of the incident electrons. At electron energies 100 KeV, X-rays are emitted almost isotropically in all directions and as the kinetic energies of the electrons increase, the direction of X-ray emission becomes increasingly forward (Johns et al, 1983). At low energies the relative intensity is small in the forward direction and it is seen that maximum intensity occurs at angles around 50° with the direction of the electron beam. As the energies increase, the intensity at large angles drops and maximum intensity now shifts to small angles less than 5° and it is seen to be at 0° at high energies. This effect poses a difficulty in using the beam directly for radiotherapy treatment. However the difficulty is overcome by use of a flattening filter, which reduces the intensity along the axis of the beam and a relatively uniform beam is formed.

2.5 Factors affecting dose distribution in a patient

2.5.1 Variations in source to skin distance

The photon fluence emitted by a point source of radiation is inversely proportional to the square of the distance from the source. Linear accelerators and other external beam units have a finite source size. The source-surface distance is usually chosen to be large (80 – 100 cm) so that the source can be considered as a point source. Thus, assuming we are dealing with the primary source alone without scatter from the collimators and other scattering materials, then the exposure or dose rate in free space from such a source varies inversely as the square of the distance. Due to the inverse square law, a change in SSD (ICRU report 42, 1987) affects the depth-dose curve, the divergence of the beam, penumbra width and dose at the edge of the beam.

The dose rate at a point decreases with increase in distance from the source but the percentage depth dose (PDD), which is a relative dose with respect to a reference point, increases with SSD because of the effects of the inverse square law. SSD is a very important parameter in radiotherapy because of the PDD's dependence on SSD. Measured PDD values are required by treatment planning systems to calculate dose distributions at specific points in a patient.

2.5.2 External contour shape

Reference dosimetry data are normally obtained under standard conditions, which include a homogeneous unit density phantom, perpendicular beam incidence, and a flat surface. During treatment however, the beam may be incident at an oblique angle with respect to the surface and further more the surface may be curved and irregular in shape. In such circumstances the standard dose distributions can only be applied after making corrections for the shape of the patient or if boluses or compensators are used. There are several methods used by different treatment planning systems to take into account the

external body curvature and oblique incidence of the beam (Khan, 1997 and ICRU report 24, 1976). Some of these are: the isodose shift method, the effective SSD method and the tissue- air (or tissue maximum) ratio method.

2.5.3 Volume irradiated

Beam data is usually obtained in a reference condition involving a semi-infinite medium with a flat surface. However in practical situations, the irradiated volume has a complicated shape and differs a lot from that of the reference situation. Determination of the dose at a point such as P in figure 2.8 then requires correction methods which can take into account the actual shape of the scattering volume. Because of the finite shape of the patient, there is always a lack of scattering radiation near the edge and also at the exit surface. There are several methods (ICRU report 42, 1987) with varying accuracy that can be used to take into account the volume effects

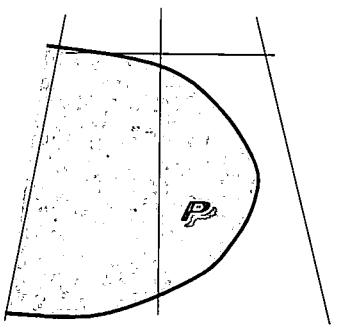

Fig 2.8: Diagram showing the radiation beam and typical scattering volume shape

In some cases the lack of lateral scatter can be accounted for by using boluses and compensators which are placed over the region where tissue is missing.

2.5.4 Composition and density (tissue inhomogeneities)

The human body is composed of different tissues of different composition and density. Inhomogeneities in the body are tissues and organs that differ from water by density or atomic composition or both. For example in a patient the beam of radiation may traverse layers of muscle, fat, bone, lung and air. Lung and air cavities differ from water only by density, whereas bone and to a lesser extent fat, differ from water in density and composition. When a radiation beam passes through a patient, it is absorbed and scattered depending mainly on the composition of the tissue in which the radiation is passing through, energy of the beam and geometry. Both the inhomogeneities within the body and the irregularities of the entrance surface have a considerable modifying effect on the beam distribution. The presence of inhomogeneities will produce changes in the dose distributions. The two main effects of tissue inhomogeneities (Klevenhagen, 1985 and Khan, 1997) are:

i) The different attenuation in the various tissues, which depends on the densities of the tissues involved (changes in the attenuation of the primary beam and the associated pattern of photons). These attenuation differences due to density may result in a shift of isodose in terms of depth.

ii) The alterations in the electron scattering pattern, which depend on the atomic number of the tissues in the electron beam path (changes in the secondary electron fluence). These scatter perturbations may affect the dose distributions in the neibourhood of the inhomogeneity.

Dose distributions are normally measured in a homogeneous medium and water that is assumed to be of unity density is most commonly used. These distributions have to be related to the human body that is heterogeneous in nature, in order to get a dose distribution in a patient for any particular beam energy and field size. Most treatment planning systems take into account the heterogeneity of tissue by calculating an inhomogeneity correction factor. There are several inhomogeneity correction algorithms (Cunningham, 1982) that have been employed by different TPSs and most of these have variable capabilities. Some of the algorithms that have been employed for tissue inhomogeneity corrections in photon beam treatment planning are:

1) Effective attenuation coefficient method
2) Ratio of tissue air ratio's method
3) Effective SSD method
4) Isodose shift method
5) Batho power law tissue air ratio method
6) Equivalent tissue air ratio method

All the methods above are applied if the dose is first calculated under the assumption that there is complete water equivalence and then a correction factor C is determined, where C is defined by

$$C = \frac{\text{dose at point P in a heterogeneous phantom}}{\text{dose at same point in a homogeneous water - like phantom}} \qquad 2.22$$

The first four methods involve the computation of an equivalent (radiological) path length d^l in water, given by

$$d^l = l_1\rho_1 + l_2\rho_2 + \ldots \qquad 2.23$$

where l_1, l_2,...are the thicknesses of the inhomogeneities along the ray passing through the point of interest and ρ_1, ρ_2,.. are the relative electronic densities. Figure 2.9 shows a point P at an actual depth d from the surface and three different tissue materials of densities ρ_1, ρ_2, ρ_3 and thicknesses l_1, l_2, l_3 respectively.

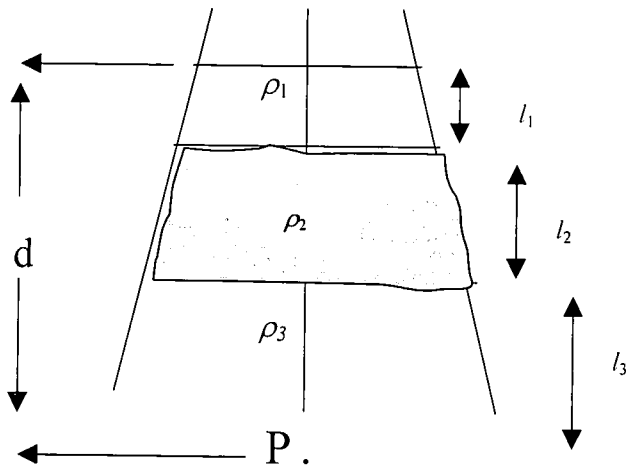

Fig 2.9: Show point P located below three layers of different densities and thickness.

The methods above are described in more details in the next subsections.

2.5.4.1 Effective attenuation coefficient method (EAC)

If we consider point P at an actual depth d (cm) in figure 2.9, the water equivalent depth d^1 is given by the equation

$$d^1 = \ell_1\rho_1 + \ell_2\rho_2 + \ell_3\rho_3 \qquad 2.24$$

If for example, the densities ρ_1 *and* ρ_3 are both equal *to* one (the density of water) and if density ρ_2 is less than one, then d^1 would be less than d. Because of the low density of the tissue, an equivalent of $d\text{-}d^1$ cm of water is missing and this would result in a higher dose at P because of the lower attenuation. If on the other hand ρ_2 is greater than one, then d^1 would be more than d because of the high density of tissue. The term $(d\text{-}d^1)$ will then be negative and a lower dose at P will result due to the higher attenuation. In this method, it is assumed that the dose at point P is increased by a certain fraction for each centimeter of water–equivalent material missing. This quantity plays the role of an attenuation coefficient for the radiation beam. In this method the correction factor for the dose at point P is given by the equation

$$C = e^{\mu(d-d^1)} \quad \Leftrightarrow \quad C \approx 1.0 + \mu(d - d^1) \qquad 2.25$$

where the attenuation coefficient, μ equals 0.05 cm^{-1} for Co-60, 0.04 cm^{-1} for 4 MV and 0.02 cm^{-1} for 25 MV. Frequently the calculations are carried out as a linear rather than exponential correction, that is, the first term of the expansion of the exponential. The method takes into account only the path-length of the radiation. The limitation of this method is that it does not consider the field size, position of structure, shape of the structure and electronic equilibrium.

2.5.4.2 Ratio of tissue air ratios method (RTAR)

This method uses a ratio of two tissue air ratios (TARs). In this method the correction factor for the dose at point P in Figure 2.9 is given by

$$C = \frac{T(d^1, W_d)}{T(d, W_d)} \qquad 2.26$$

where - d is the depth at point of interest P

- d^1 is the water-equivalent depth
- W_d is the field size of the beam at depth d

Compared to the EAC method, the RTAR method takes into account the field size in addition to the depth through the use of the TAR. The RTAR method does not take into account

i) The internal dimensions of the inhomogeneity,

ii) The position of the inhomogeneity with respect to the point of calculation P. In other words the correction factor will not change as long as d and d^1 remain constant.

iii) Electronic equilibrium.

2.5.4.3 Effective source to skin distance method (ESSD)

The ESSD method is entirely equivalent to the RTAR method but makes use of percentage depth doses (PDDs) rather than TARs. If a dose correction factor is to be calculated for a point P at depth d as in figure 2.9, an isodose chart is superimposed on the tissue lay out diagram. If we assume that all the tissue material present were homogeneous, then the PDD could be read off directly and can be represented symbolically as $P(d,W_o,F)$ where d is the depth of point P, W_o is the field size and F is the SSD. To take into account the inhomogeneity the isodose chart is adjusted either upwards or downwards by a distance $d-d^1$, so that the depth to point P is equal to the water-equivalent depth d^1. The new PDD for point P can be read off and can be represented symbolically as $P(d^1,W^1_o,F)$, but should be adjusted to take into account the new SSD (F^1 rather than F) and this necessitates the use of the inverse square corrections. From the definition of PDD (Khan, 1994),

$$P(d,W,F) \propto 100 . \left(\frac{F+d_m}{F+d}\right)^2 . e^{-\mu(d-d_m)K_s} \qquad 2.27$$

where d_m is the depth of maximum dose

μ is the attenuation coefficient for the primary beam and

K_s is a function that which accounts for the change in scattered dose.

If we ignore the change in the value of K_s from one SSD to another, we can rewrite $P(d,W_o,F)$ and $P(d^1,W^1_o,F)$ in a similar way, thus

$$P(d^1,W_o,F) \propto 100 . \left(\frac{F+d_m}{F+d^1}\right)^2 . e^{-\mu(d-d_m)K_s} \text{ and } P(d^1,W_o,F^1) \propto 100 . \left(\frac{F^1+d_m}{F^1+d^1}\right)^2 . e^{-\mu(d-d_m)K_s} \qquad 2.28$$

By combining the two functions in equation 2.28 above, then

$$P(d^1,W_o,F^1) = P(d^1,W_o,F) . \left(\frac{F+d^1}{F+d_m}\right)^2 . \left(\frac{F^1+d_m}{F^1+d^1}\right)^2 \qquad 2.29$$

The percentage depth dose is expressed as a percentage of dose at the reference point (at depth d_m) and this point has been moved from distance $F+d_m$ to F^1+d_m. Therefore the dose correction factor can be obtained as

$$C = \frac{P(d^1, W_o, F^1)}{P(d, W_o, F)} \cdot \left(\frac{F + d_m}{F^1 + d_m} \right)^2 \qquad 2.30$$

By substituting equation 2.29 into equation 2.30 then

$$C = \frac{P(d^1, W_o, F)}{P(d, W_o, F)} \cdot \left(\frac{F + d^1}{F + d_m} \right)^2 \cdot \left(\frac{F + d_m}{F^1 + d_m} \right)^2 \cdot \left(\frac{F^1 + d_m}{F^1 + d^1} \right)^2 \qquad 2.31$$

and equation 2.31 simplifies to

$$C = \frac{P(d^1, W_o, F)}{P(d, W_o, F)} \cdot \left(\frac{F + d^1}{F^1 + d^1} \right)^2 \Leftrightarrow C = \frac{P(d^1, W_o, F)}{P(d, W_o, F)} \cdot \left(\frac{F + d^1}{F + d} \right)^2 \qquad 2.32$$

where $F^1+d^1 = F+d$.

By using the relationship between TAR and PDD, that is

$$P(d, W_o, F) = 100 \cdot \frac{T(d, W_d)}{T(d_m, W_{dm})} \cdot \left(\frac{F + d_m}{F + d} \right)^2 \qquad 2.33$$

a similar expression can be obtained for $P(d^1, W_o, F)$, that is

$$P(d^1, W_o, F) = 100 \frac{T(d^1, W_d)}{T(d_m, W^1_{dm})} \left(\frac{F + d_m}{F + d^1} \right)^2 \qquad 2.34$$

and substitution of equations 2.33 and 2.34 in equation 2.32 ,then the correction factor C reduces to

$$C = \frac{T(d^1, W_d)}{T(d, W_d)}\left[\frac{T(d_m, W_{dm})}{T(d_m, W_{dm}^1)}\right] \qquad 2.35$$

Similar to RTAR method, the ESSD also takes into account only the path length of the radiation beam and field size.

2.5.4.4 The Isodose –shift method

Greene et al, 1965 proposed the isodose–shift method and it is essentially a simplification of the ESSD method. It was introduced largely for manual manipulation of isodose charts to account for the presence of inhomogeneities. . In its application the isodose lines are moved only a fraction n of the distance d-d^1 and the corrected dose values can be read off directly, eliminating the need for the inverse square term. The correction factor for the dose at point P in figure 2.9 using this method is given by the equation

$$C = \frac{P(d^{11}, W_o, F)}{P(d, W_o, F)} \qquad 2.36$$

$$\textit{where,}\quad d^{11} = d - n(d - d^1) \qquad 2.37$$

The value of n depends on the beam energy; n = 0.67 for Co-60, 0.65 for 4 MV and 0.5 for 25 MV.

2.5.4.5 Batho power law tissue- air ratio method (PTAR)

Batho, 1964 and Young et al, 1970 were the first to propose an inhomogeneity correction method involving the use TAR's raised to a power that depends on density for points lying below an inhomogeneity. The limitation of the method (Khan, 1994) was that the

correction factor depended on the location of the inhomogeneity relative to point P but not relative to the surface and the method was inapplicable for points inside an inhomogeneity.

A more generalized form of the power law was later suggested by Sontag and Cunningham (1977), that allows for correction of the dose to points with in an inhomogeneity as well as bellow it. The dose correction factor with this method is given by

$$C = \frac{T(d_1, W_d)^{\rho_1 - \rho_2}}{T(d_2, W_d)^{1-\rho_2}} \qquad 2.38$$

where ρ_1 is the density of the material in which the point of calculation lies and d_1 is the distance to the bottom surface of the overlying inhomogeneity, within this material. ρ_2 is the density of the next or overlying material and d_2 is the distance of P from its upper surface. Figures 2.10.a and 2.10.b show the two situations when point P is inside and outside of the inhomogeneity.

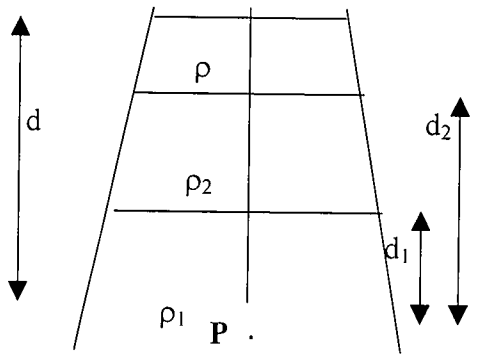

Fig 2.10.a: P outside of the inhomogeneity

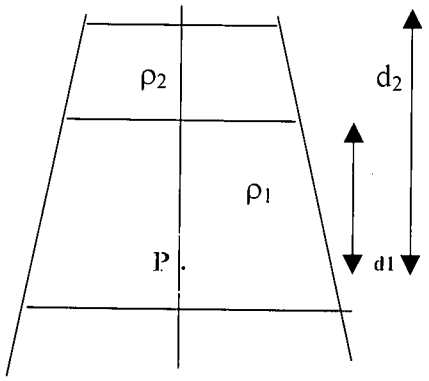

Fig 2.10.b: P inside of the inhomogeneity

The generalized PTAR method compared to the previous methods has an added advantage, in that it takes into account the position of the inhomogeneity with respect to the point of calculation.

2.5.4.6 The equivalent tissue–air ratio method (ETAR)

The ETAR method was first suggested by Sontag and Cunningham (1978), and it also uses a ratio of tissue-air ratios. The method is a variation of the simple ratio of tissue-air ratios, but also in its numerator not only the depth is altered to take into account the inhomogeneity but so is the field size. The alteration of the field size follows from the idea that a beam irradiating a homogeneous but non-water equivalent phantom, is equivalent to a beam irradiating a water phantom with all linear dimensions such as depth and field size scaled in proportion to the density (electronic density) of the non-water equivalent material. The ETAR method operates on the assumption that at any point in an inhomogeneous phantom, it is possible to find an equivalent homogeneous phantom with relative electron density $\tilde{\varepsilon}$ and that a correction factor can be obtained accordingly using an equivalent tissue-air ratio given by the expression

$$C = \frac{T(d^{1}, r^{1})}{T(d, r)} \qquad 2.39$$

where d is the depth of the point of calculation and r is the radius of an equivalent circular field as applied to the patient. d^{1} is the water equivalent depth, $r^{1} = r \,.\, \tilde{\varepsilon}$ is the scaled field size dimension and $\tilde{\varepsilon}$ is the weighted density of the irradiated volume. The problem in applying the method is that of choosing the proper scaling procedure for the two parameters. Depending on the implementation, the effective depth and radius may be used in a tissue-air ratio split into a zero-area tissue-air ratio and a scatter-air ratio to account for the perturbation in primary and scattered dose respectively as in the equation,

$$T(d^{1}, r^{1}) = T(d^{1}, 0) + S(d^{1}, r^{1}) \qquad 2.40$$

Cunningham suggested that the primary and scatter component be considered separately. Thus for the primary component the proper depth to use is the water-equivalent depth d^{1}.

CT input data may be employed in the mathematical manipulations of the scaling procedure. The scaled beam radius and the weighted density $\tilde{\varepsilon}$ can be determined by the averaging procedure, and given by the equation

$$r^{1} = r\bar{\varepsilon} \text{ where } \bar{\varepsilon} = \frac{\sum_{i}\sum_{j}\sum_{k} \varepsilon_{ijk} \cdot W_{ijk}}{\sum_{i}\sum_{j}\sum_{k} W_{ijk}} \qquad 2.41$$

where ε_{ijk} are the relative electron densities of pixels in a series of CT images of the irradiated volume. W_{ijk} form a set of weighting factors that expresses the relative importance of each of the ε_{ijk}. The advantage of the method compared to all the previous methods is that it takes into account the three dimensional shape of the structure.

None of the methods discussed above can claim an accuracy of less than ± 5% (Khan, 1994) for all irradiation conditions encountered in radiotherapy. The above goal can only be achieved by algorithms that take into account the three-dimensional shape of the irradiated volume and electron transport. However these methods are still under development and include: volume integration of differential scatter-air ratio method, convolution methods and Monte Carlo methods; Khan, (1994) and Rogers et al, (1991). These methods are much more effective in handling inhomogeneity corrections because in addition to all the factors taken into consideration by the methods discussed so far, they take into account the electronic equilibrium at the tissue interface. However they have not been used in TPSs because of the time required to calculate a dose distribution, which is long for daily routine purposes.

2.6 CT data in treatment planning systems

2.6.1 Use of CT data in treatment planning system

With the help of CT scans a detailed knowledge of the anatomical structures, cross-sectional information and accurate body outline can be obtained. Inhomogeneities pose a problem when calculating the dose distributions and thus it is necessary to know their shape, dimensions, exact position, atomic number and density. Composition and density data of body tissues is a prerequisite in dosimetry involving radiation interactions in humans (Woodard et al, 1986). Thus CT to significantly improves the accuracy of the calculated dose distributions in treatment planning. Computer tomograms obtained from x-ray transmission scannings are distributions of linear attenuation coefficients (Sontag et al, 1977) that depend on both the atomic number and the electron density of the tissue being imaged. For photon beams used in radiotherapy, compton scattering is the dominant interaction mechanism in soft tissue and consequently the dose delivered to such tissue is mainly dependent on the distribution of electrons density (e/cm^3) in the irradiated volume. Thus a relationship between these coefficients and electron densities is required for use in treatment planning. The reconstruction of the body image by CT is a mathematical process, and the reconstruction algorithm generates what is known as CT numbers. CT numbers are essentially attenuation coefficients for x-rays of diagnostic energies and thus they cannot be used directly for dose computation at mega voltage energies which requires knowledge of the electron density of the irradiated tissue relative to that of water (Satish et al, 1979).

2.6.2 CT numbers and attenuation coefficients

Before using CT data in treatment planning computers, the scan data should be calibrated in terms of relative electron density versus CT number (Metcalfe et al, 1997). CT numbers range from -1000 for air to +1000 for bone, with that of water set at 0. CT numbers normalized in this manner are called Hounsfield numbers (H) and the theoretical

relationship between CT number and linear attenuation coefficient is given by the equation

$$H = 1000\left(\frac{\mu_{tissue} - \mu_{water}}{\mu_{water}}\right) \qquad 2.6.a$$

where : μ_{tissue} is the linear attenuation coefficient for a tissue at a specific energy

μ_{water} is the linear attenuation coefficient of water at the same energy.

Because CT numbers bear a linear relationship with attenuation coefficient it is possible to infer electron densities. The product of electron density, ρ_e (electrons per cm^3) and total electron cross-section, σ_e (cm^2 per electron) is equal to μ (per cm) (Metcalf et al, 1997),

where $\sigma_e = \sigma_{pe} + \sigma_{comp} + \sigma_{pair} + \sigma_{coh}$ is the sum of component electron cross-sections due to photoelectric absorption (σ_{pe}), Compton scattering (σ_{comp}), pair production (σ_{pair}) and coherent scattering (σ_{coh}).

Although CT number can be correlated with electron density, the relationship is not linear in the entire range of tissue densities (Khan, 1994). The non-linearity is caused by the change in atomic number of tissues that affects the propagation of beam attenuation by Compton versus photoelectric interactions. Usually there is a linear relationship between lung and soft tissue but non-linear between soft tissue and bone, (section 3.8.2).

2.7 The CADPLAN treatment planning system

As was mentioned in section 1.7, one of the aims of this study is the evaluation of the accuracy of dose distribution obtained with CADPLAN treatment planning system. This section gives a brief review on CADPLAN modeling for external photon beams (CADPLAN user manual, 1999). Also the study will be limited to open fields only, therefore wedged fields and irregularly shaped fields will be omitted in the discussion. The models used in CADPLAN for inhomogeneity corrections and how the system handles skin obliquity corrections will be briefly discussed.

2.7.1 Models

For external photon beam modeling, beam reconstruction and patient models are required. The former is used to calculate dose distributions in a water-equivalent material using the regular beam model, while the latter applies the dose distribution in a water equivalent material to the patient anatomy taking into account inhomogeneities and skin external shape.

The dose at point P is given by the equation

$$\boldsymbol{DOSE(P)} = \mathrm{DD(d)}.\mathrm{OA(x,z,d)}.\mathrm{CO}.\mathrm{CF} \qquad 2.42$$

where DD(d) = depth dose value at depth d

OA(x,z,d) = off-axis factor at point (x,z) in a plane perpendicular to the beam central axis (taken to be parallel to the y-axis) at depth d.

CO = skin obliquity correction factor

CF = tissue inhomogeneity correction factor

The product DD(d).OA(x,z,d) gives the dose value in a water equivalent material for rectangular, symmetrical and asymmetrical fields. The regular beam model is used to calculate the dose value. This homogeneous dose distribution is then corrected for inhomogeneities and skin obliquity.

2.7.2 Beam Model

For open fields the CADPLAN regular photon beam model requires measured data for:

1) Depth dose curve for square field sizes that are measured along the field central axis.
2) Open field profiles on field lateral main axis which are measured at user-defined depths. Measurements are required for five standard depths which are 25 cm, 15 cm, 10 cm, 5 cm and at d_{max} (2 cm for 8MV).
3) Diagonal profiles for the largest possible open field.

For open fields, the CADPLAN photon beam model requires measured data for depth dose curves and open field profiles. The depth dose value at d for equivalent field size A at the central axis source skin distance (CSSD) is calculated according to the equation

$$DD(d) = DD_m(d, A).CF_{dd}(d).CF_{inv} \qquad 2.43$$

Where DD_m is the measured depth dose value for equivalent field size A

CF_{dd} is the modification of the depth dose curve due to changed SSD.

CF_{inv} is the inverse square law factor

The equivalent field size A is calculated by the equation

$$A = \left[\frac{2.W.H}{W+H}\right].\left[\frac{CSSD}{SAD}\right] \qquad 2.44$$

where, W is the field width, H is the field height and SAD is the source to axis distance.

Modification of depth-dose-value correction factor is calculated by the equation

$$CF_{dd} = \left[\frac{T(d, A_2)}{T(d, A_1)}\right].\left[\frac{CSSD + D_{max}}{CSSD + d}\right]^2.\left[\frac{SPD + d}{SPD + D_{max}}\right]^2 \qquad 2.45$$

where A_1 and A_2 are defined by

$$A_1 = \left[\frac{SPD + d}{SPD}\right].A \quad \text{and} \quad A_2 = \left[\frac{CSSD + d}{CSSD}\right].A \qquad 2.46$$

where SPD is the source to phantom distance

T(d,A) is the TAR/TPR value at depth d for field size A

D_{max} is the depth-of-dose maximum

The inverse square law correction factor is calculated by the equation

$$CF_{inv} = \left[\frac{SSD_S + D_{max}}{CSSD + D_{max}}\right]^2 \quad 2.47$$

where SSD_S is equal to the SPD for standard fixed SSD and isocentric fields.

The off-axis value in regular beam model for open fields at point (x,z) at depth d′ is calculated according to the equation

$$OA_o(x,z,d') = P_c(r,d').P_B(x,d',FS_x).P_B(z,d',FS_z) \quad 2.48$$

where

$r = \sqrt{x^2 + z^2}$

$P_c(r, d')$ is the envelope profile value at radial distance r at depth d^1

$P_B(x, d',FS)$ is the boundary profile value at distance x at depth d^1 for field size FS

2.7.3 Patient Model

The patient model determines how the patient outline and inhomogeneities are handled when applying the dose distribution of a beam to the patient anatomy.

2.7.3.1 Skin obliquity correction factor

Skin obliquity correction is performed using the TAR/TPR ratio and inverse square law. The skin obliquity factor (CO) is calculated according to the equation

$$CO = \left[\frac{CSSD + d_{bc}}{CSSD + d_{fe}}\right] \cdot \left[\frac{T(d_{bc} \cdot A_4}{T(d_{bc} \cdot A_3)}\right] \quad 2.49$$

where T(d,A) is the TAR/TPR value at d for field size A

d_{bc} is the distance between the grid point and the body contour along the fanline from the grid point to focus.

d_{fe} is the distance along the fanline between the grid point and the plane perpendicular to the field central axis, where the central axis intersects the body contour.

$$A_3 = \left[\frac{CSSD + d_{bc}}{CSSD}\right].A \quad \text{and} \quad A_4 = \left[\frac{FSSD + d_{bc}}{FSSD}\right].A \qquad 2.50$$

where FSSD is the focus source skin distance

2.7.3.2 Inhomogeneity correction factor

The inhomogeneity correction factors are calculated either by using the modified Batho power law or the equivalent tissue air ratio (ETAR) method as described previously in section 2.5.4. The dose value calculated in a water equivalent material is then multiplied with the inhomogeneity correction factor.

2.7.4 Calculation of treatment times

For accelerators, monitor units (MU), instead of treatment time is, is the appropriate quantity. Calculation of MU requires a prescribed dose in Gy and corresponding percentage isodose value. The calculation of MU needs a dose rate (output factor) table which is expressed as MU/Gy for accelerators (or MU/min for Co-60 units). The dose rate values are obtained for each square field from minimum to maximum possible field size. For the CADPLAN TPS, the dose rate DOSERATE(FS) in MU/Gy is given by the relation

$$DOSERATE(FS) = \frac{100.OUT\_FCT_{calib}}{OUT\_FCT_m(FS).D\_REF} \qquad 2.51$$

where,

- $OUT\_FCT_m(FS)$ is the measured output factor for selected field sizes FS and the values for other fields are linearly interpolated.

- OUT_FCT_{calib} is the measured output for calibration field
- D_REF is the calibrated dose rate (Gy/100 MU)

The MU setting is calculated according to the equation

$$MU = \text{DOSE\_NORM} \cdot \left[\frac{\text{DIST\_NORM}}{\text{DIST\_CALIB}}\right]^2 \cdot \left[\frac{\text{TAR\_CALIB}}{\text{TAR\_NORM}}\right] \cdot \text{DOSERATE} \qquad 2.52$$

where

DIST_NORM is the distance of the normalization point from the focus

DIST_CALIB is the distance of the calibration point from the focus

TAR_CALIB is the TAR/TPR value at the calibration point

TAR_NORM is the TAR/TPR value at the field normalization points

$\text{TAR\_CALIB} = T(d_{calib}, A_5)$

where d_{calib} = depth of calibration point and

$$A_5 = \left[\frac{\text{DIST\_CALIB}}{\text{SPD}}\right] \cdot A \qquad 2.53$$

For fixed SSD, the ratio TAR_CALIB to TAR_NORM equals 1.

DOSE_NORM is the field normalization dose corresponding to the dose in Gy at the depth dose maximum and is given by the equation

$$\textbf{\textit{DOSE\_NORM}} = \left[\frac{D_{pre}}{\%_{pre}}\right] \cdot CF_{iso} \cdot CF_{sum} \cdot \text{PLAN\_FCT(p)} \cdot 100 \qquad 2.54$$

where

D_{pre} is the prescribed dose at the plan reference point

$\%_{pre}$ is the reference point percentage

CF_{iso} is the correction factor for an isocentric field or 1.0 for fixed SSD fields

CF_{sum} is the field summation factor

PLAN_FCT(p) is the plan normalization factor for plan p.

2.8 Monte Carlo simulation of photon transport

In MC simulations (Metcalfe et al, 1997) the individual history of a photon is determined from :

a) Medium geometry and composition and this has to be defined by the user
b) Initial state of the photon such as incident position, angle and energy which are randomly determined.
c) Random selection from the set of probability distributions governing the possible interactions of the photons.

The probability that a photon will travel a particular path is determined by an appropriate expression involving a random number (Cunningham, 1982). The main steps taken into consideration during photon simulations are:

1) Distance to next interaction:

During photon simulation, the probability of selecting a particular distance is determined by the mean free path corresponding to the photon energy and medium in which the photon currently resides. At a given energy, the probability that a photon will go a distance x before interacting and then interacts between x and x + Δx is given by

$$p = \mu e^{-\mu x} \qquad 2.55$$

The cumulative probability density (CPD) is then

$$P = \int_0^x p\,dx = 1 - e^{-\mu x} \Rightarrow 1 - P = e^{-\mu x} \qquad 2.56$$

where P varies between 0 and 1. The path length x can be sampled by setting P equal to a random value, R, between 0 and 1 and solving x. Because, if P is random then 1-P will also be random, the same results can be obtained by setting $e^{-\mu x} = R$ and solving for x

$$x = -\frac{1}{\mu} \ln R \quad , \text{ where } \mu = \frac{1}{\lambda} \qquad 2.57$$

μ is the linear attenuation coefficient and λ is the mean free path.

2) The type of interaction, energy and angle:

The interaction type is randomly chosen from photoelectric, Compton and pair production depending on the photon energy, medium and using the relative value of the total cross-section for these interactions. At radiotherapy energy ranges the Compton interaction is the most probable event. If a Compton interaction is selected, the energy of the scattered photon is selected on a random basis and then its scattering angle θ is determined from the kinematic equations of the interaction. The azimuthal scattering angle ϕ is chosen randomly between 0 and 2π. The process is continued for further interactions until the photon is absorbed by a randomly chosen photoelectric effect or else exits from the phantom.

3) New particles :

As a result of some photon interactions, depending on the energy, new particles are created and / or set in motion. The position, direction and energy of these particles are also followed in a similar manner as described above. For example, if pair production had taken place, electrons and positrons are set in motion and in fact the absorbed dose connected with photon interaction is actually a result of electrons that are set in motion by the photon interaction. It is these electrons that consume most of the computing time during MC photon calculation as each electron suffers thousands of collisions (Nahum, 1988) in the process of slowing down.

2.9 Random number generators

The aim of any MC procedure is to draw independent random samples from some probability law via intermediate steps involving the use of independent random numbers (Raeside, 1976). A significant proportion of the computing time in a simulation is spent generating random numbers so it is important that the code used for generating these numbers is efficient (Metcalfe et al). For the EGS4 code, the random number generator

U.O.V.S. BIBLIOTEEK

1152 182 11

is of the multiplicative congruential type. The n^{th} random number is found recursively using the expression

$$X_n = (aX_{n-1}) \bmod 2^k \qquad 2.58$$

Where a is a constant multiplier and k is the integer word size of the computer. The first number in the sequence X_0 is called the seed and is usually specified by the user.

2.10 The BEAM code

2.10.1 General description of the code

BEAM is a MC code (Rogers et al, 1995) that was designed to simulate radiation beams from linear accelerators, Co-60 units and orthovoltage units. BEAM is based on the PRESTA extension of the EGS4 MC system for simulating radiation transport. The BEAM code runs under the UNIX operating system and is written in MORTRAN 3, a Fortran 77 pre-processor that is used for the EGS4 system. With the BEAM code it is possible to model almost all therapy sources with the Z-axis taken as the beam axis and in case of linear accelerators, the origin is usually taken to be the center of the beam as it exits from the accelerator vacuum window. For photon beams, the origin is at the target. Modeling a therapy unit using this code involves arranging a series of individual component modules (CMs) to describe the main components of the accelerator head relevant in radiation interaction e.g. the target, primary collimator, flattening filter, ionization chamber, wedges, mirror, jaws, etc. The code comprises of a number of CMs with each CM dealing with a specific class of geometric shapes, of which the user has to set the physical dimensions and materials during simulation. This feature makes the code capable of simulating a wide range of therapy units. The CMs used in the model are:

a) SLABS: models parallel slabs in the x-y plane.
b) CONS3R: models a stack of truncated cones including cylinders.
c) CONESTAK: models a series of stacked truncated cones (may be cylindrical).
d) FLATFILT: models flattening filters used in photon beams.

e) CHAMBER: models an ionization chamber and other structures with cylindrical symmetry and centered on the beam axis.
f) JAWS: models pairs of opposing flat surfaces perpendicular to the X or Y axes
g) MIRROR: models the mirror for the field localization
h) XTUBE: models an x-ray tube as the photon source.
i) APPSQ: models a series of square applicators or scrapers
j) PYRAMIDS: models a series of truncated pyramids.
k) APPLICAT: models the electron beam applicators.

2.10.2 Running the BEAM code

Running the BEAM code consist of three main steps (Rogers et al, 1996) and these are:

A) **Specifying an accelerator**: This is the fist step, and it involves defining or specifying the component modules in order as they are to be used in the simulation. A CM can be used more than once where necessary as long as the user uses different identifier names that the user can be able to remember. The user also specifies the accelerator model by giving it a name representing the machine they are modeling.

B) **Building an accelerator**: The accelerator after specification is then built. Building an accelerator consists of gathering all the source code, automatically editing it to avoid duplicate names. The user has to specify the modules to use.

C) **Compiling an accelerator**: After specifying and building of the accelerator, next is compiling the resulting Mortran and Fortran code. The user has to specify the name of the specification module they are running and once that is done the user is presented with a compilation menu with several options to select and modify before BEAM is compiled.

During simulation with the BEAM code, some of the main tasks of the user are:

- Interactively specify the geometry of the accelerator, that is the dimensions and materials of the treatment head.
- Which variance reduction techniques to use (section 2.11.2)
- What transport parameters to use, e.g. the PCUT and ECUT values.
- Specify the physical properties of each material to be used in the simulation. The cross-section data for BEAM is created by an EGS4 pre-processor called PEGS4 (Rogers, et al 1996). This program generates parameters such as scattering cross-sections, mean free paths and electron stopping powers for a user-defined energy range that may be 521 or 700 keV up to 55 MeV in both cases. These data are based on the density effect as specified by the ICRU report 37. The user has to specify the medium to be used which is given as either MEDIUM700ICRU or MEDIUM521ICRU depending on the user's selected cut-off energies to be used by the program during simulation.
- How to track a particle's history. The LATCH feature (optional) allows detailed information about each particle's history and information about dose scored from various accelerator components to be traced. This feature can be used for particle tracking and bits 1 to 23 can be optionally set by the user during input for the code to register a particle's interaction in any particular region.
- Define the location of the output planes (scoring planes) of interest to the user.

2.11 Efficiency and variance reduction

2.11.1 Efficiency of any Monte Carlo procedure

All MC calculations suffer computing time problems (Raeside, 1976 and Metcalfe et al, 1997) and thus it has been customary to assign an efficiency when comparing different MC procedures used to estimate the same quantity. The efficiency of a particular simulation is inversely proportional to the time taken for the simulation and also to the variance of the results (Metcalf et al, 1997), thus the efficiency should increase as the amount of computer time required to carry out the simulation decreases. The efficiency ε, of any MC procedure is given by the equation (Bielajew et al, 1987)

$$\varepsilon \propto \frac{1}{t.\sigma^2} \Rightarrow \varepsilon = \frac{K}{t.\sigma^2} \qquad 2.59$$

where

- t is a measure of computing time required to complete a MC simulation and depends on the computer being used.
- σ^2 is the sampling variance associated with estimating the quantity of interest.
- K is a proportionality constant.

Since t is directly proportional to N, the number of histories, and assuming ε to be a constant, then equation 2.59 can be rewritten as

$$\varepsilon = \frac{K}{N\sigma^2} \Rightarrow \sigma = \frac{\kappa}{\sqrt{N}} \qquad 2.60$$

Where $\kappa = K/\varepsilon$, is another constant.

From equation 2.59, the possible ways of increasing efficiency is by reducing either the time or the variance, however since time depends on the computer being used, it is not ideal to think of increasing efficiency by ways of reducing time. The most realistic way of increasing efficiency is by reducing sampling variance and hence the subject " variance reduction".

2.11.2 Variance reduction techniques

Variance reduction means reducing the time it takes to calculate a result with a given statistical uncertainty or variance. Variance reduction techniques render possibilities of increasing efficiency and by applying these techniques, the necessity of accumulating massive amounts of data to achieve a certain precision in the quantity being estimated is avoided. There are various techniques for variance reduction (Bielajew et al, 1988), but those employed by the BEAM code are:

i) **Range rejection**: This technique saves time by discarding or terminating all particle histories which can not reach some region of interest e.g. a scoring plane.

The terminated particles have low energies and therefore they are going to result in thousands of low energy electrons which will not be of any importance except increasing the computing time as the BEAM code keeps track of all these histories. BEAM can automatically compute the minimum energy needed by electrons as they leave each CM if they are to reach the scoring plane and this can be the energy used in the range rejection routines. In BEAM, it is recommended that the secondary particle creation threshold as well as the transport cut-off energies be set at ECUT = AE = 0.521 MeV for electrons and PCUT = AP =0.01 MeV for photons.

ii) **Bremsstrahlung splitting and russian roulette**: Bremsstrahlung splitting is a variance reduction feature mainly used in the simulation of photon beams and it is used to increase the number of bremsstrahlung photons created in the simulation geometry. Biasing of the results is avoided by adjusting the weights assigned to particles. During photon simulation most of the time is spent tracking the electron histories created after the interaction. BEAM can use Russian roulette on the electrons created in the multiplicity of photons. Russian roulette means the number of electrons followed is restricted to the same number as would occur if bremsstrahlung splitting were not used. A 10 – 20 bremsstrahlung split may increase the efficiency by a factor of 10 (Rogers et al, 1995).

iii) **Forcing Photon Interactions**: This variance reduction feature is mainly applied in studying electron contamination in accelerator beams since virtually no photons interact in air and yet that is the major source of electron contamination. In BEAM, photons can be forced to interact in any subset of a component module.

2.12 Phase space files

After running the BEAM code simulation, a phase space file (PSF) is created for each simulation. The PSF contains data about each individual particle crossing the scoring plane and this file can be output at any time. Also the PSF can be used as source file for other simulations or used as input file for the DOSXYZ program. Typical data found in a PSF include:

i) Particle position, direction and energy

ii) Particle charge e.g. positive charge for positrons, negative charge for electrons or zero charge for photons.

iii) Total number of particles in a file

iv) Total number of photons, electrons and positrons in a file

v) Maximum and minimum kinetic energy of the particles stored in a file

vi) Number of particles (histories) incident from the original source used to generate the PSF.

The PSFs created can be analyzed by another program BEAMDP.

2.13 BEAMDP program

BEAMDP or BEAM Data Processor is a subsidiary of the BEAM program used for analyzing PSFs (Ma et al, 1995) generated by the BEAM code. The program is capable of analyzing the PSF allowing the user to get information relating to a particular simulation. Some of the several options that can be analyzed are:

a) Derivation of planar fluence distributions from a phase space data file. The program gives the total number of particles scored in spatial bins of equal area. Usually a plot of fluence versus position in the X-direction is given.

b) Derivation of spectral distributions from a phase space data file. The program gives the total number of particles scored in each energy bin of user specified bin width within a specified spatial region. Usually a graph of planar fluence per incident particle versus energy (MeV) is plotted.

c) Derivation of the mean energy distributions from a phase space data file. The program gives the ratio of the total particle energy to the total number of particles scored in a spatial bin of equal area.

d) Derivation of angular distributions from a phase space data file. The program gives the total number of particles scored in an angular bin of user specified bin width within a specified spatial region. Usually a plot of particles per bin versus angle in degrees is given.

The user has to describe the input parameters for the program e.g.

- the file name of the PSF to be processed by BEAMDP
- field type e.g. square ring, annular bins or rectangular bins
- Particle type, that is photons, electrons, positrons or all particles
- Graph type, which might be normal or histogram
- Scoring regions for spectrum and angular distributions
- Energy ranges which should be between zero and maximum energy of the particles in the PSF.
- Range of angles for angular distributions.

BEAMDP analyzes the BEAM phase space data and generates energy distributions for particles inside and outside the treatment field.

The PSF can be used as source data file for DOSXYZ which is another subsidiary code of BEAM, capable of calculating the dose distribution in a homogeneous water phantom.

2.14 DOSXYZ

DOSXYZ is an EGS4 MC code which can use use PSF from BEAM as source input (Ma et al,1995). DOSXYZ is used to calculate the absorbed dose distribution in a rectilinear 3-dimensional volume when irradiated by a beam described by the phase space output from BEAM. The geometry is a rectilinear volume with the X and Y-axes as cross plane

and the Z-axis as the depth. Every volume element can have a different material of varying densities for use with CT data. The program can use different input source files that include phase space data generated by a BEAM simulation or using a model-based beam reconstruction produced by BEAMDP.

2.15 CTCREATE

CTCREATE is a CT phantom option of DOSXYZ that allows calculation of dose distributions in phantoms that are derived from CT data sets. It is possible to generate a CT phantom from CT data sets since all the required material and geometry information is contained in the data set. There are several input parameters that the user has to specify in order to use the CTCREATE program:

1) The CT data format, and at the moment only Pinnacle, CADPLAN and DICOM formats are handled by the program.
2) The user also has to create a file containing a list of files that make up the full CT image data set (the files must be in order of increasing Z).
3) The user has to define the lower and upper X, Y, Z boundaries to form six planes that describe a cube. The intersection of the original CT data with this cube then determines the CT phantom.
4) The user has to specify the X, Y and Z voxel dimensions to be used for DOSXYZ.
5) The user has to specify the number of materials and ramps (functions for converting each voxel's CT number to material and density). The default material values in the program are for Air, Lung, Tissue and Bone. However it is possible for the user, if not satisfied with the default material values, to sub-sample the CT data set to create their own CT ramp.
6) Transport parameters e.g. the ECUT and PCUT values.

After the successful data input of CTCREATE, the relevant CT phantom information is stored into "file.egs4phant", where "file" is the original CT data set name. This CT phantom file created can then be read in and used by the DOSXYZ program to calculate the dose distribution in each voxel of the phantom. The CT phantom option in DOSXYZ

is used by setting the number of materials (nmed) of the DOSXYZ input file to zero, which causes the program to execute differently than when nmed > 0. Instead of geometry, material and density data being input in the DOSXYZ input file, DOSXYZ reads data from a CT phantom file that has been created using CTCREATE.

CHAPTER THREE

METHODS

3.1 Introduction

In this study MC simulation for the linear accelerator head was done to obtain the beam data for the 8 MV x-ray photons. Phase space files were generated, and then analyzed to get the energy spectrum and angular distributions. The BEAM and the BEAMDP, MC codes (Rogers et al, 1995) were used for the simulation of the accelerator and analysis of the data files. The DOSXYZ and the CTCREATE MC codes were used for the calculation of the 3D dose distributions in the water phantom and CT based patient models. The beam data obtained by the DOSXYZ code in the water phantom was verified by comparing it with similar data obtained by ionization chamber measurements in a water phantom on the same accelerator. For the evaluation of the treatment planning system (TPS), the dose distributions obtained by the MC data were directly compared with those calculated by the TPS using the BATHO and ETAR inhomogeneity correction algorithms.

In this chapter, in section 3.2 the procedure of the construction of the Philips SL25 accelerator, in the 8 MV mode that was used for the simulations is described. Section 3.3 outlines the detailed modeling of the upper part of the accelerator from the target to the mirror to obtain a master phase space file (MPSF). The MPSF was then used in the simulation of the lower part of the accelerator to obtain phase space files (PSF's) for the different field sizes. Both source to surface distance technique (SSD = 100 cm) and isocentric technique (SAD = 100 cm) were used in the simulations. Section 3.4 gives a brief discussion on how the MPSF was analyzed. In section 3.5, the procedure for the calculation of the absorbed dose distributions in a water phantom from the generated PSF's with the DOSXYZ MC code is discussed. In section 3.6 the procedure followed in the measurement with ionization chamber on the SL25 accelerator to obtain beam profile

data (percentage depth dose and cross plane profiles) is discussed. In section 3.7 the method used for the comparison of the MC calculated data and the ionization chamber measured data is outlined. In section 3.8 a procedure followed in CT based MC simulation using the CTCREATE program is discussed. This data is then used directly for the preparation and running of the DOSXYZ MC code to calculate 3D dose distributions in patients with cancer of the maxillary sinus, esophagus, breast and cervix patient models. In Section 3.9 a procedure for the comparison of the dose distributions from the MC method and the TPS is presented.

3.2 Construction of the radiation head of a Philips SL25 accelerator

The Philips SL25 accelerator was used in this study. Figure 3.1 shows the main components of the SL25 in the low energy (8 MV) x-ray configuration mode. This study is only limited to open beam fields, thus although the wedge is included in the diagram it was not simulated. Also included as part of the accelerator is the air gap between the jaws and the isocenter, which is located 100 cm from the target.

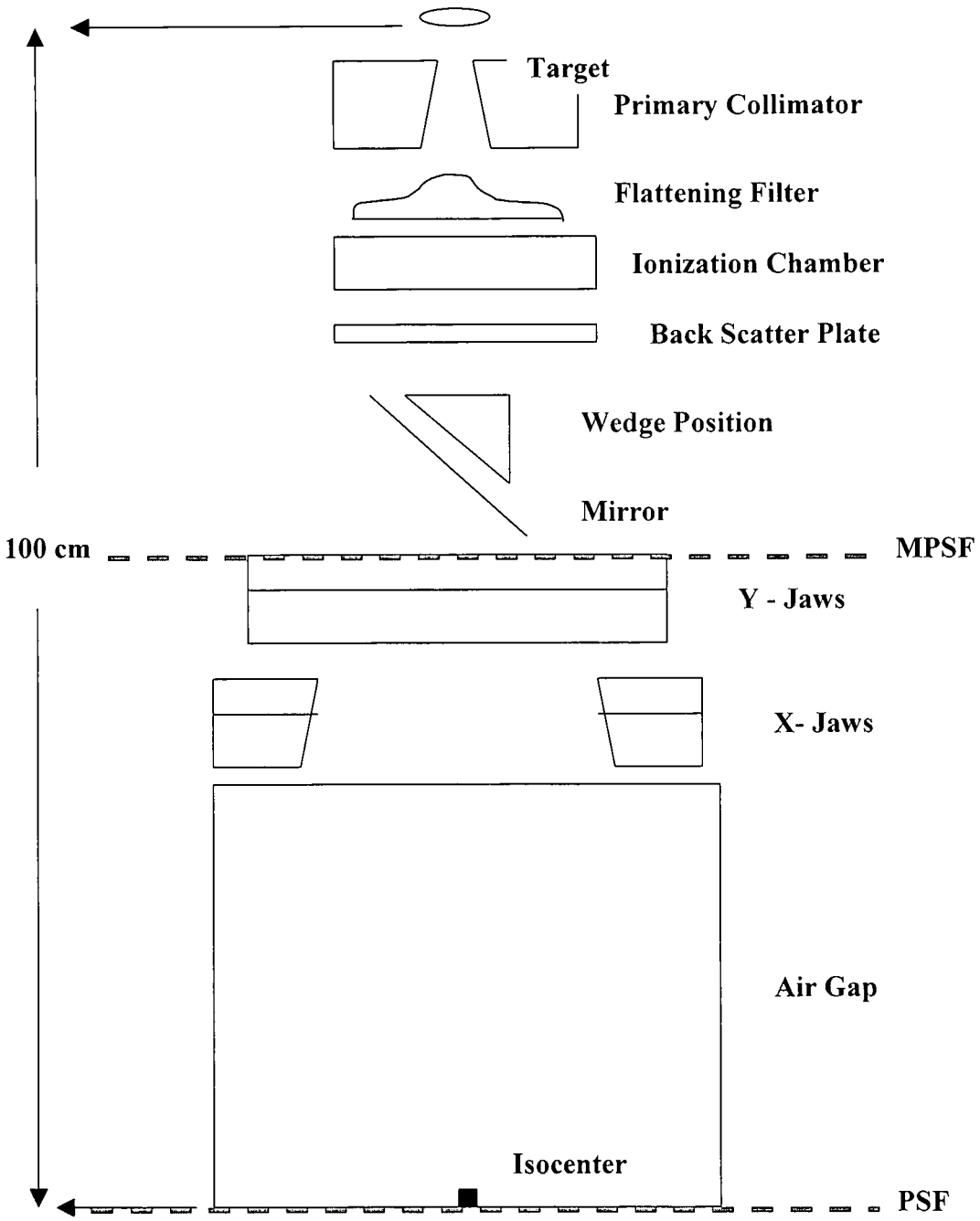

Fig 3.1: Main Components of the SL25 Radiation Head.

3.3 Monte Carlo simulation of the SL25 accelerator

The BEAM98 code was used to simulate output of the accelerator. The simulation was done on a Pentium II, 400 MHz processor with 8 Gbytes hard disk drive and 128 Mbytes of memory. The simulation of the accelerator was done in two stages. In the first stage, the upper part of the accelerator was simulated (from target to mirror). This was done only once. In the second stage radiation output of the lower part of the accelerator (from jaws to the isocenter) was simulated. Simulating the accelerator output as a whole would have resulted in long simulation times. Breaking the simulation into two stages saves time because only the jaws located in the lower part are to be varied to get the different field sizes and so there is no need of simulating the upper part of the accelerator every time the field size is changed. This reusability of the PSFs is one of the advantageous features of the BEAM code.

3.3.1 First stage of simulation

This stage involved modeling the top part of the accelerator, from the target all the way down to the lower end point of the mirror. Six component modules (CMs) were used for the modeling and these are:

1) CONESTAK used to model the x-ray target
2) CONS3R used to model the primary collimator
3) FLATFILT used to model the flattening filter
4) CONESTAK used to model the ionization chamber
5) CONESTAK used to model the back scatter plate
6) MIRROR used to model the mirror

The 700 ICRU cross section data for materials as stated in the Pegs4 data file wereused in the modeling. Mono energetic 8 MeV electrons were directed at the target to produce x-ray photons. 18 million histories were used to generate the photons. Bremsstruhlung splitting was set at 50 to increase the photon yield and Russian roulette was set on to reduce or decrease the computer processing unit (CPU) time. Photon forcing was not

used. The electron cut-off (ECUT) and photon cut-off (PCUT) values were set at 0.7 MeV and 0.01 MeV respectively in all six CMs. The next subsections give brief descriptions of the individual CMs modeled.

3.3.1.1 The target

The "CONESTAK" CM was used for modeling the target. The main function of the target is to generate x-rays when fast moving electrons strike on it. The CONESTAK CM was used because the target was modeled as a circular disk. It started at Z = 0 cm and this point also marked the origin of the coordinate system used in the modeling.

3.3.1.2 The primary collimator

The "CONS3R" CM was used for modeling the primary collimator. The main function of the primary collimator is to collimate the target produced photons. The CONS3R was used because the primary collimator is cone shaped, though the CONESTAK CM can also effectively be used to model the primary collimator (Du Plessis, 1999). The medium inside the cone is air such that photons can go through uninterrupted.

3.3.1.3 The flattening filter

The "FLATFILT" CM was used for modeling the flattening filter. The main function of the flattening filter in an accelerator is to modify the forward peaked x-ray beam to a beam with uniform intensity. The top is conical shaped with a wider flat shaped base as shown in figure 3.1.

3.3.1.4 The Ionization chamber

The "CONESTAK" CM was used to model the ionization chamber. Though the CHAMBER CM could be used, we found the former to be much easier to use than the latter in the modeling.

3.3.1.5 The back scatter plate

The "CONESTAK" CM was used to model the back scattering plate. The main function of this plate is to prevent photons back scattering from the wedge to reach the chamber.

3.3.1.6 The mirror

The "MIRROR" CM was used to model the mirror, whose main function is to reflect light from a light source for field localization during patient positioning.

The six CMs comprised the first simulation stage of the accelerator and at this plane, just below the mirror a master phase space file was scored. The PSF that was generated at this scoring plane had a particle yield of about 400% with respect to the number of primary histories, that is, about 73 million compared to 18 million particles that were incident on the target. The CPU time was about 42 hours giving a simulation rate of about 470000 histories per hour. The disk space occupied by this PSF was about 2.15 Gbytes.

3.3.2 Second Stage of Simulation

In this stage the lower part of the accelerator was modeled from the previous scoring plane which is located below the mirror, to the phantom surface at the isocenter which is at Z = 100 cm. Three CMs were used in this stage, and these are:

1) JAWS used to model the secondary adjustable jaws
2) CONESTAK used to model the accessory ring
3) CONESTAK used to model the air gap

The master PSF collected in the first stage was used as the source input for the second stage. Bremsstrahlung splitting, Russian roulette or photon forcing were not used. The values for the ECUT and PCUT as used in the first stage were maintained (0.7 MeV and 0.01 MeV respectively). The next subsections give a brief description of the CMs used.

3.3.2.1 The jaws

The "JAWS" CM was used for modeling the secondary adjustable jaws, whose main function is to collimate and define the field size at the isocenter. The accelerator jaws consists of upper (Y-direction) jaws and the lower (X-direction) jaws. The positive and negative lateral coordinates at the jaws positions were adjusted such that square field sizes of 2, 4, 6, 8 and 10 cm^2 (or any other rectangular fields field size e.g. 6x4, 10x6, e.t.c) at the isocenter could be obtained. Applying the range rejection technique to this CM by setting high ECUT and PCUT values (8 MeV) in the jaws, so as to only transport those particles that could clear the jaws aperture, decreases the simulation time by a large factor (Du Plessis, 1999). However, in this study the ECUT and PCUT for this CM were not changed, as we noticed a 7% reduction in the number of particles in the PSF by setting high ECUT and PCUT values (section 4.3).

3.3.2.2 The accessory Ring

The "CONESTAK" CM was used to model the accessory ring.

3.3.2.3 The Air Gap

The "CONESTAK" CM was used to model the air gap between the accessory ring to the isocenter plane with an outer radial boundary of 30 cm. For the SSD techniques the air gap extended from Z = 50.19 to Z = 100.0 cm, that is a thickness of 49.81 cm. For simulations using isocentric techniques, the air gap extended from Z = 50.19 to Z = 80.0 cm; that is a thickness of 29.81 cm. In otherwords PSFs were created at Z = 100 and Z = 80 cm for SSD and isocentric respectively.

The three CMs comprised the second simulation stage of the accelerator and at this plane PSFs were scored for each of the 2, 4, 6, 8 and 10-cm square fields or rectangular field sizes. The number of particles used in the simulation were the same for all the field sizes and was equal to the number obtained in the MPSF, that is ≈ 73 million histories. Each of the PSFs was used as source file for the DOSXYZ program to obtain the dose distribution in the phantom. Also the same PSFs were used as source beam data for the CT based models using the CTCREATE program.

3.4 BEAMDP - Analysis of the master phase space file

The MPSF created after the simulation of the upper part of the SL25 accelerator at a distance of 27.7 cm from the target was analyzed using the BEAMDP program. In this study the photon fluence variations with lateral position, energy fluence variations with lateral positions, spectral distributions and angular distributions were obtained. More detailed discussion of the results are presentedin chapter four, section 4.2.

3.5 DOSXYZ – Calculation of dose distribution in 3D phantoms

3.5.1 The Construction of the water Phantom

The DOSXYZ code was used for the calculation of the absorbed dose in a water phantom. This allowed calculation of percentage depth doses and cross beam profiles for different field sizes for comparison with ion chamber measurements. The PSFs generated by the BEAM program for the different field sizes were used as source input files for the DOSXYZ code. The scoring plane for the PSFs was at the surface of the phantom. ECUT and PCUT were set at 0.70 MeV and 0.01 MeV respectively. The PEGS4 data file was used for the supply of cross section data for water and air media. The PRESTA algorithm and the ISMOOTH option were set on during simulations. With the former the history simulation rate is increased (saves CPU time without loss of accuracy), while the latter allows the re-use of PSF particles if the number of histories required for the simulations is greater than the number of particles stored in the PSF (Ma et al, 1995).

The isocenter at Z = 100 cm for the accelerator was made to coincide with the isocenter for the DOSXYZ simulation at Z = 0cm on the surface of the water phantom. The water phantom was constructed in such a way that the **X** by **Y** by **Z** dimensions were 29.50 x 30 x 44.75 cm^3. The X direction consisted of one region with boundaries in cm of $-14.75 \leq X \leq +14.75$. There were 59 sub-regions of equal widths, each 0.5 cm. Setting the voxel dimension to 0.5 cm aimed at matching the TPS dose calculation grid. The Y-direction consisted of three regions with outer boundaries in cm of $-15.0 \leq Y \leq +15.0$. There was one sub region in each of the three regions and their widths were 14.50, 1.0 and 14.50 respectively. The Z-direction was made of three regions with boundary in cm $0 \leq Z \leq 44.75$. There are 1, 79, and 1 sub-regions in the first, second and third regions respectively. Their corresponding widths were 0.25, 0.5, and 5.0 cm respectively. The first voxel dimension in the Z-direction was set at 0.25 cm to allow calculation of the surface doses.

3.5.2 Number of histories for DOSXYZ and the uncertainty of dose calculation

From equation 2.59, the uncertainty in any Monte Carlo process is inversely proportional to the square root of the number of histories used (Bielajew et al, 1988). Mathematically

$$\sigma = \frac{\kappa}{\sqrt{N}} \qquad 3.1$$

where N is the number of histories and σ is the uncertainty.

If we let the uncertainties σ_1 and σ_2 correspond to the number of histories N_1 and N_2 respectively, then equation 3.1 can be rewritten as

$$\sigma_1 = \frac{\kappa}{\sqrt{N_1}} \text{ and } \sigma_2 = \frac{\kappa}{\sqrt{N_2}} \qquad 3.2$$

Equation 3.2 can be simplified to

$$\frac{\sigma_1}{\sigma_2} = \sqrt{\frac{N_2}{N_1}} \qquad 3.3$$

From equation 3.3, two observations can be made:

1) To find the number of histories that are needed to reduce the uncertainty by half, we let σ_2 be equal to $\sigma_1 / 2$, and substituting in equation 3.3:

$$\frac{\sigma_1}{\sigma_1/2} = \sqrt{\frac{N_2}{N_1}} \Leftrightarrow 2 = \sqrt{\frac{N_2}{N_1}} \Leftrightarrow N_2 = 4 N_1 \qquad 3.4$$

Thus four times more histories are required to reduce the uncertainty by half.

2) To find the number of histories that are needed to reduce the uncertainty to within 1%, we let σ_2 be equal to 1% and substitute in the equation 3.3:

$$\frac{\sigma_1}{1} = \sqrt{\frac{N_2}{N_1}} \Leftrightarrow N_2 = N_1 . \sigma_1^2 \qquad 3.5$$

Thus the number of histories required to reduce the uncertainty to within 1% is equal to the initial number of histories multiplied by the square of the uncertainty (expressed as a percentage).

The above equations were utilized in trying to establish the appropriate number of histories to be used for each field size for the DOSXYZ program that will give an uncertainty which is within 1%. Trial simulation tests were made for a 2x2 cm^2 field size, the number of histories being set at 2.5, 10, and 40 millions (as implied by equation 3.4). Several parameters were analyzed after simulation e.g. the uncertainty in the depth dose curve, CPU time, and computer memory space for each number of histories. The results are shown in section 4.4 and the depth dose graph comparing the number of histories also shown. In conclusion of this trial test, 10 million histories were found adequate for a 2x2-cm^2 field size giving an uncertainty which was within 1%. This implied a photon density of 2.5 million per square centimeter. This photon density was maintained for all other field sizes. Table 3.1 shows a summary of the number of histories used for the simulations of different field sizes with the DOSXYZ program in the water phantom.

Table 3.1: Number of histories used for different field sizes

Field Size (cm^2)	Area (cm^2)	Number of Histories (Millions)
2 x 2	4	10
4 x 4	16	40
6 x 6	36	90
8 x 8	64	160
10 x 10	100	250

The output file generated by DOSXYZ consists of a 3D dose array. The file is a ASCII file that can be read and displayed after writing suitable computer programs. After running the DOSXYZ program, graphs of depth dose and cross beam profiles for each

field size were ploted using a plot program (xvgr). The obtained profile data was compared with similar data obtained by measurements with an ionization chamber and the results are shown in Section 4.4.

3.6 Ionization Chamber Measurements

3.6.1 Set-up of water phantom

The procedure started with the leveling of the accelerator gantry such that the central axis was vertical. The water tank (phantom) was then filled with water and adjusted until it was well leveled and in the center of the beam axis, using metallic bobs and the collimator cross wires. The limits of movement of the detector in the tank were set in the X, Y, and Z directions before scanning began.

The depth dose and cross plane profiles were measured by an ionization chamber in a 3D water phantom system. A computer driven system consisting of two chambers, one acting as a probe (field detector) and the other acting as the monitor (reference) were used. The chamber size was small (0.1 cm^3), so that measurement could be made in regions of:

- high dose such as at the central axis
- high dose gradients such as near the edges of the beam
- steep gradient such as in the build-up region

The probe was arranged such that it could move in the tank of water to sample the dose rate at various points whereas the reference chamber was fixed at some point in the field to monitor the beam intensity with time. The probe is made waterproof by a thin plastic sleeve that covers the chamber as well as the portion of the cable immersed in water and its movement within the water tank was controlled by the computer program. The ratio of the probe to the reference chamber response is recorded as the probe is moved within the water phantom and thus the final response is independent of fluctuations in the accelerator output.

3.6.2 Measurement of accelerator beam data

Measurements were done on the SL25 accelerator for 8 MV photons at 100 cm SSD and for 2, 4, 6, 8 and 10 cm square field sizes. The percentage depth dose profiles were measured on the central axis of the beam. The probe to reference ratio was sampled as the probe moved from the surface down the phantom to a depth of 40 cm at increments of 0.25 cm and the data was stored by the computer program in a table matrix form of dose versus depth. For the cross plane profiles, the probe to monitor ratio was sampled as the probe moved across the field also at 0.25 cm increments. The cross plane profiles were measured at preset depths of 2, 5, 10, 15 and 25 cm, and the data was stored by the computer program as a table matrix of dose versus position for each depth in the water phantom.

3.7 Comparison of Monte Carlo and ion chamber profile data

The beam data calculated by the DOSXYZ MC method and that obtained by the ionization chamber measurements were compared to each other. The beam data included percentage depth dose curves and cross beam dose profiles for field sizes ranging from 2 to 10 cm square field sizes. During simulations, we limited ourselves to smaller field sizes because large field sizes require a large number of histories to reduce the uncertainty to be within 1%, and thus very long simulation times.

The PDD was measured on the central axis for all the field sizes by both methods. The data was sampled in increments of 0.5 cm for MC and 0.25 cm for the ion chamber to a depth of 40 cm in both cases. The data was then normalized to 100% in both MC and ion chamber and the corresponding data in terms of field sizes were plotted on the same graph for comparison; section (4.4.2).

The data for cross plane profiles were also sampled across the central axis of all the field sizes, in increments of 0.5 cm for MC and 0.25 cm for the chamber. In both cases the data were obtained at preset depths of 2, 5, 10, 15, and 25 cm. All data were normalized to 100% relative to the peak dose (at 2cm depth), for both the MC method and chamber measurements. Corresponding data in terms of field sizes were then plotted on the same graph for comparison (section 4.4.6).

3.8 Monte Carlo simulations in selected realistic cases

3.8.1 CT based simulations

In order to compare the treatment planning system with the MC dose distributions, CT scans on a Rando phantom and on real cancer patients were made on a Siemens Somatom HiQ-S CT scanner. The slice thicknesses were 1 cm and slices were 1 cm apart at regions of interest. The scans were transferred via a computer network to the TPS. Using the SL25 unit on the TPS with data obtained by measurement with an ion chamber, treatment plans were calculated for:

1) Rando Phantom:

(i) Anterior maxillary sinus plans using the SSD technique for four different field sizes.

(ii) Typical esophagus plan in the thorax region was made with three isocentric fields, one anterior and two posterior obliques.

2) Real Patients:

(i) Breast plan with two tangential fields using the SSD technique.

(ii) Cancer of the cervix plan with a three-field and four-field isocentric technique.

These plans together with all the CT slices making up the different regions of interest were sent via the network to two (400 MHz and 333 MHz) Pentium II PCs on which the simulations were carried out.

3.8.2 CTCREATE program

3.8.2.1 Data input

As discussed in section 2.14, the CTCREATE program is a DOSXYZ option that allows calculation of dose distributions in CT data sets. CTCREATE can be used to convert CT data from the CADPLAN format, where each CT slice is stored as a separate file. For each particular plan, all the slices were listed in one file (in order of increasing or decreasing Z) containing all the full names of the files that make up the CT image, to be used in CTCREATE. For each plan, depending on the region of interest, the X, Y and Z limits were set. Also, depending on the size of the whole image, the number of voxels to be used by DOSXYZ was specified in the X, Y and Z direction. In all plans the voxel dimensions were 0.25 x 0.25 x 1.0 cm^3 in the X, Y and Z directions. Thus the size of the CT image determined the total number of voxels for each simulation.

3.8.2.2 Conversion of CT number to density in CTCREATE

CT numbers are essentially attenuation coefficients for x-rays of diagnostic energies, (section 2.6) and thus before they can be used directly for dose computation at mega voltage energies they have to be converted to electron densities relative to that of water. For a patient model to be used in the DOSXYZ MC code, each voxel (volume element) has to be associated with a specific material entry in a PEGS4 data file with a specific name and physical density. The PEGS4 data file contains the relevant cross section data for each material in the patient model. In the BEAM / DOSXYZ MC codes, either 521ICRU or 700ICRU PEGS4 data may be used depending on the transport cutoff chosen by the user. Eight materials were used for the conversion of each voxel's CT number into electron density. Table 3.2 shows the list of materials used in the conversion together with their corresponding CT number and density intervals. The 521 ICRU cross section data for materials in the PEGS4 data was used in the simulation.

Table 3.2: Materials used in the CTCREATE

Material Name	CT Number		Electron Density	
	Lower bound	Upper bound	Lower bound	Upper bound
AIR521ICRU	0	20	0.0	0.08
LUNG521ICRU	21	950	0.082	0.95
ADIPOSE521ICRU	951	980	0.951	0.977
H2O521ICRU	981	1010	0.98	1.007
BRAIN521ICRU	1011	1040	1.012	1.039
HEART521ICRU	1041	1070	1.045	1.072
CARTILAGE	1071	1100	1.08	1.107
BONE521ICRU	1101	3000	1.12	2.346

Figure 3.2 show the ramp used for converting CT values of the materials to density in CTCREATE. The density is assigned using linear interpolation between the material's density limits (Ma et al, 1995), using the equation:

$$\rho_{i,j,k} = \mathrm{M.D\_LB}_{\mathrm{i\_material}} + \left(\frac{\mathrm{M.D\_UB}_{\mathrm{i\_material}} - \mathrm{M.D\_LB}_{\mathrm{i\_material}}}{\mathrm{M.CT\_UB}_{\mathrm{i\_material}} - \mathrm{M.CT\_UB}_{\mathrm{i\_material-1}}} \right) * \left(\mathrm{M.CT\_UB}_{\mathrm{i\_material}} - \mathrm{CT}_{\mathrm{i,j,k}} \right) \quad 3.($$

Where:

- M.D_LB is material density lower bound
- M.D_UB is material density upper bound
- M.CT_UB is material CT upper bound

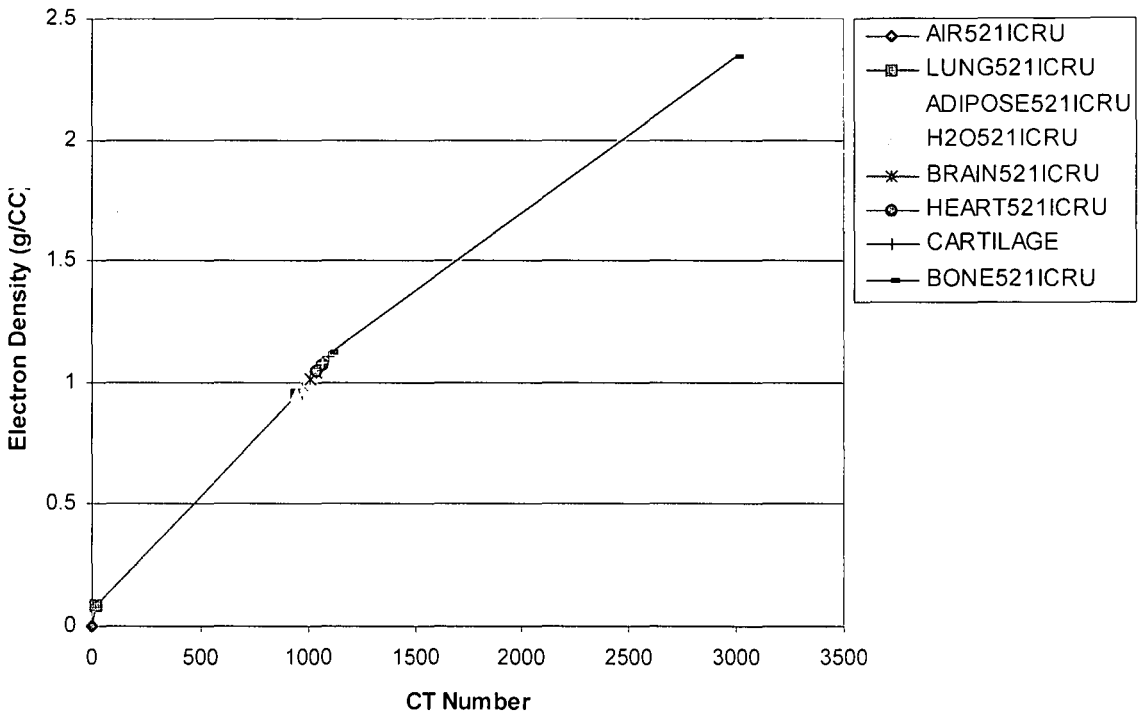

Fig 3.2:The ramp used for converting CT values to material density in CTCREATE

After running of the CTCREATE program, the CT phantom information is written into a file X.egs4phant, where X is the file name of the CT data set. DOSXYZ was run on these CT phantom files using any appropriate phase space file from the BEAM code as the source input file.

3.9 Comparison of CADPLAN and Monte Carlo dose distributions

3.9.1 The CADPLAN dose image

Methods used for the calculation of dose distributions by CADPLAN were discussed in section 2.7. CADPLAN data were stored in 2D dose calculation matrices with grid spacing of 2.5 mm for maxilla sinus and breast, and 5.0 mm for esophagus and CaCx. The dose matrices consist of arrays of 160x112 values. These files were transferred to a

Linux based PC through the network system. The TPS data is in binary or unformatted form and therefore it is machine specific. The TPS runs on a Hewlett Packard computer system and therefore bytes were swapped for the data to be read and displayed on a PC.

3.9.2 DOSXYZ dose distributions

Methods used for the calculation of dose distributions with the DOSXYZ MC code were discussed in section 3.5. The dose distribution from the DOSXYZ output file is a floating point array of i_{max} by j_{max} by k_{max} values, where i_{max}, j_{max} and k_{max} are the number of voxels in the X, Y and Z direction. The voxel size was always set to 1.0 cm in the Z direction since the CT slices were also acquired at 1.0 cm intervals. Each time the dose distributions were analyzed at one particular slice of interest and thus the dose distribution is an array of i_{max} by j_{max} values. For the MC calculation, each field was calculated separately. In cases of plans with multiple fields, a program was written in IDL (Interactive Data Language) to display and add the dose distributions.

3.9.3 The CT image

The original CT image data are an integer array of 256x256 voxels. Also, the CT images were generated on a Helwett Packard workstation. Thus, to be read and displayed on a PC the bytes were swapped. For the comparison of the DOSXYZ and TPS results, the dose distributions were displayed (overlaid) on the CT image. To ease the comparison of the dose distributions, data had to be normalized in a similar way. A program was written in IDL to read, normalize and display the dose distributions on the CT images.

3.9.4 Normalization of the dose distributions

For comparison to be meaningful, the normalization in both the CADPLAN and DOSXYZ should be the same. For the TPS the field normalization point is always located at the field central axis point, $D_{max,}$ or isocenter point (CADPLAN, 1999). For the SSD technique the dose distribution of each field is normalized to the value of the dose

obtained at the central axis maximum depth for the same field in water. For 8 MV x-rays, this occurs at a depth of 2 cm in water. Isocentric fields are normalized to 100% at the isocenter. When isocentric fields are normalized the non-normalized dose at the isocenter point A_X_DOSE is used. The correction factor for an isocentric field CF_{iso} is given by

$$CF_{iso} = \frac{100}{A_X\_DOSE} \qquad 3.7$$

where A_X_DOSE is the axis dose at the isocenter and CF_{iso} is 1.0 for fixed SSD fields.

Thus the DOSXYZ dose distributions had to be normalized in a similar way as the CADPLAN treatment planning system.

CHAPTER FOUR

4.0 RESULTS AND DISCUSSION

4.1 Introduction

In the previous chapter the methods used for the simulation of the accelerator and calculation of the dose distributions with MC methods were presented. In this chapter the results that were obtained are given. As discussed in section 3.3, the accelerator output was simulated in two stages. In the first stage, a master phase space file (MPSF) was calculated for the upper part of the accelerator and a scoring plane was created just below the mirror. The MPSF created was then analyzed using the BEAMDP program.

4.2 Analysis of the master phase space File

With the BEAMDP program it is possible to analyze the photon fluence variations with position, energy fluence variations with position, spectral distributions and angular distributions.

4.2.1 Photon fluence variation with position

The planar photon fluence for a circular field of radius 10 cm, with annular regions of equal area were calculated. The number of bins was set to 100. Figure 4.1 shows the distribution.

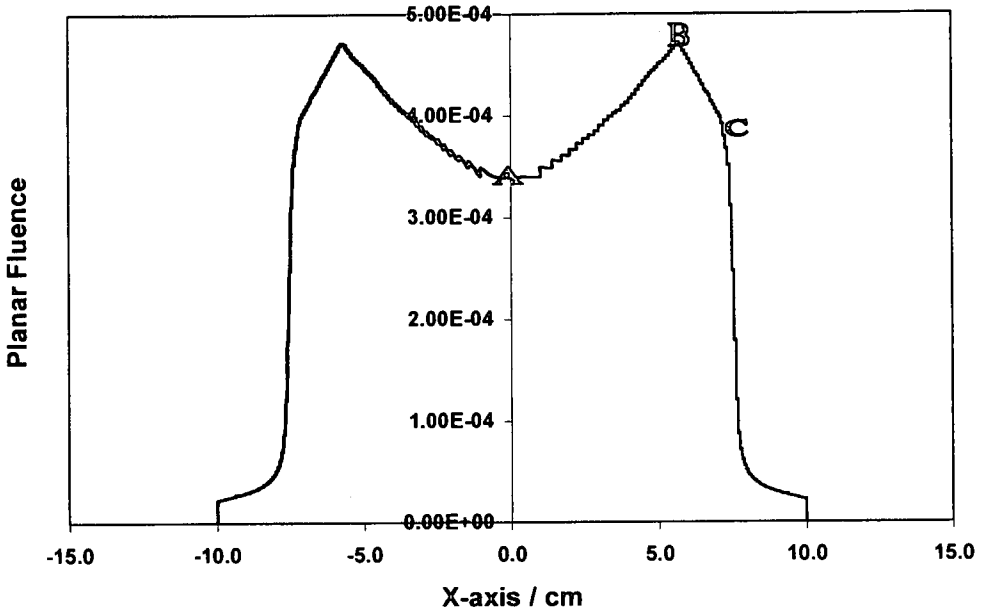

Fig 4.1: Photon fluence versus position in the X-direction

The planar fluence increases from the central axis (radius = 0 cm) to a certain maximum value at point B (radius = 5.75 cm) in figure 4.1 and then starts to decrease with increase in radius. From the geometry of figure 4.2, PQ is equal to 7.51 cm (point C in figure 4.1) and this is greater than the radius at which maximum photon fluence (PB = 5.75 cm) was observed. This is due to the spatial distribution of photons from the target, where after passing through the flattening filter, maximum intensity occurs at a certain angle. From trigonometry this angle POB can be calculated and is equal to 11.7°. Further analysis of the geometry of the accelerator indicates that actually point B coincides with the outer edge of the flattening filter.

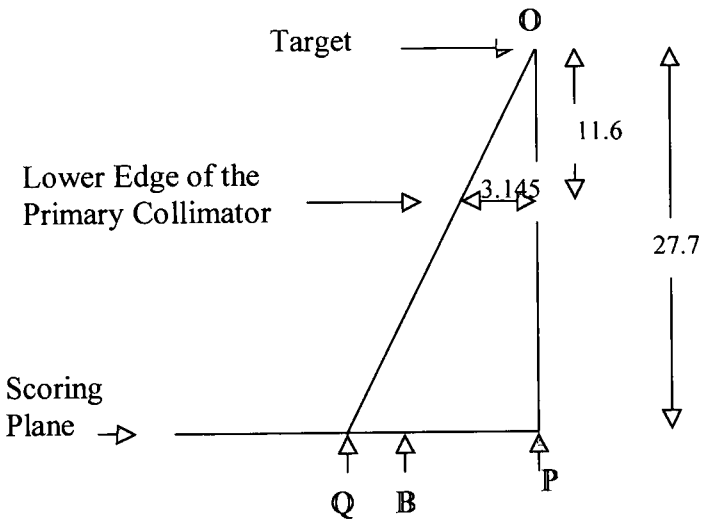

Fig 4.2: Geometry of Accelerator

4.2.2 Energy fluence variations with position.

The planar energy fluence for a circular field of radius 10 cm, with annular regions of equal area were calculated. As in section 4.2.1 also the number of bins were set to 100. Figure 4.3 shows the distribution.

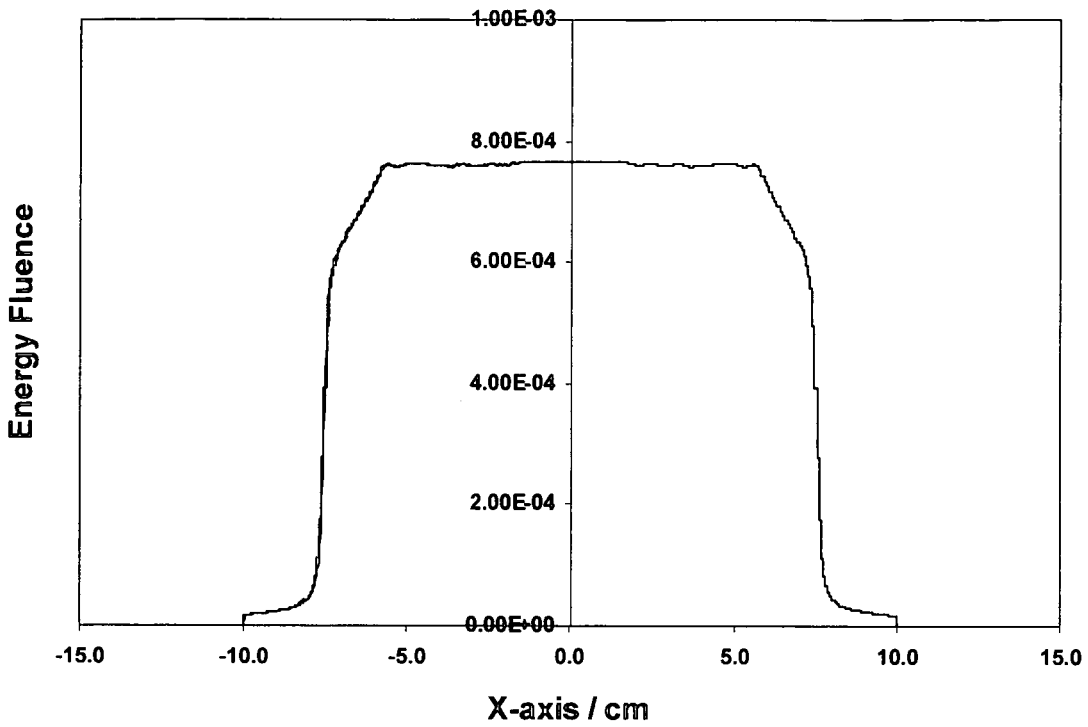

Fig 4.3 Energy fluence variations with position in X- direction

The planar energy fluence remains almost constant from the axis of the beam (radius = 0) to the point when the intensity of the photon fluence starts to decrease (radius = 5.75 cm).

4.2.3 Spectral distribution

The spectral distribution gives the total number of particles scored in each energy bin within a specified energy range. All particles within a radius of 10 cm from the central axis was analyzed and the number of bins in the energy range was set to 100. Figure 4.4 shows the distribution. The energy spectrum shows a continuous distribution, implying that photons are heterogeneous in energy. The spectrum also suggests that the maximum possible energy that bremsstralung photons can have is equal to the energy of the incident electrons and in our case 8 MeV.

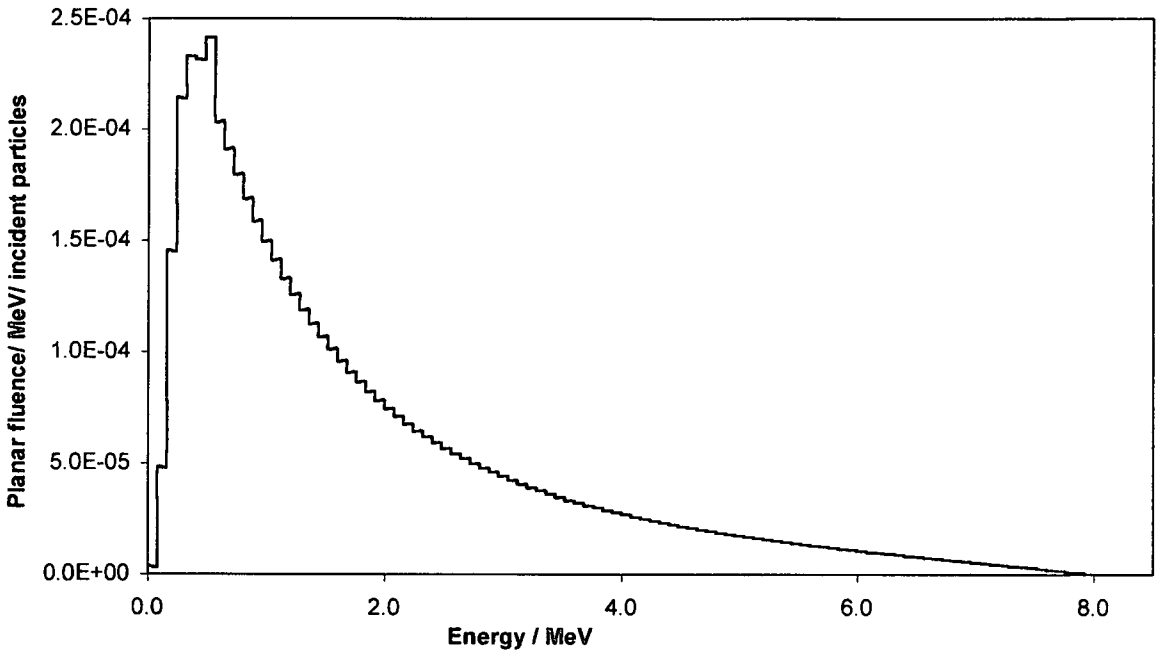

Fig 4.4: Spectral Distribution

Maximum intensity occurs at energy of 0.56 MeV. The mean energy value ($\bar{E}$) was calculated using the formula

$$\overline{E} = \frac{\sum E_i . N_i}{\sum N_i} \qquad 4.1$$

where E_i is the energy of the i^{th} bin

N_i is the number of particles in the i^{th} bin

The calculated mean energy is 1.82 MeV

4.2.4 Angular distributions

In this case the total number of particles scored in angular bin of equal bins width within a specified region is obtained. The radius was set to 10 cm, number of bins set to 40 and angles ranged from 0° to 30°. Figure 4.5 shows the photon angular distribution.

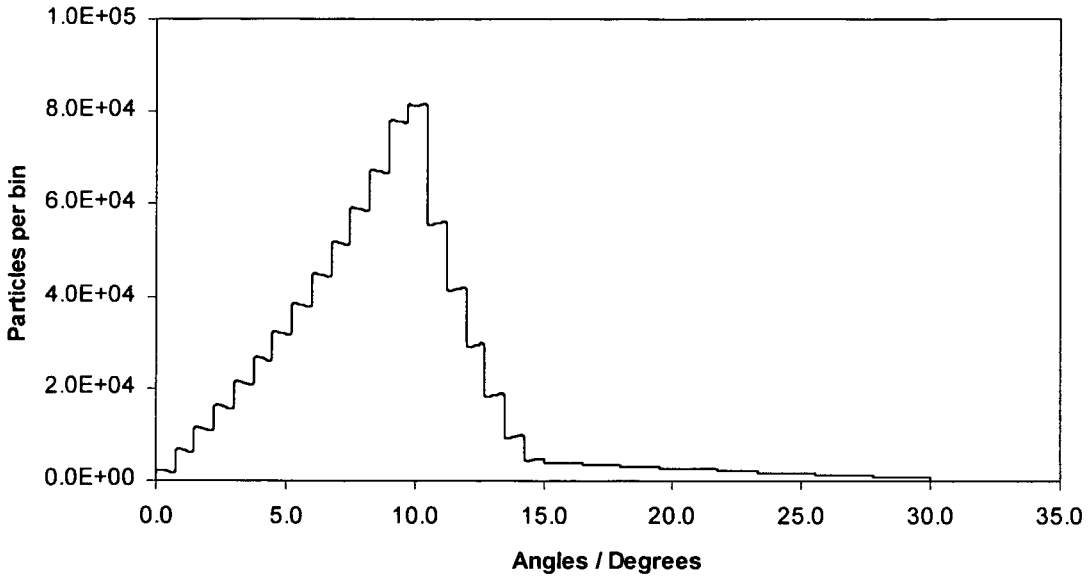

Fig 4.5: Photon Agular Distributions

The angle at which maximum intensity was observed is 11.1° and the corresponding number of particles per bin is 8.13×10^4. This angle is in close agreement with that obtained in section 4.2.1. The observed distribution is due to that at center the photons are more absorbed by the flattening filter because it is much thicker. The intensity increases with outward increase in the angle till reaches a maximum value and then starts to decrease due to beam cutoff by the primary collimator.

4.3 Simulation of the Lower Part of the Accelerator

The lower part of the accelerator was simulated by varying the field size to obtain 2, 4, 6, 8 and 10 cm square fields. The same number of particles as generated from the MPSF was used in all the simulation. Table 4.1 shows a summary of the results.

Table 4.1: Summary of the simulation results for DOSXYZ in a water phantom

Field Size (cm^2)	Particles in PSF	Number of Photons	percentage of Photons	CPU (hours)	Simulation Rate (histories/ hr)	File Size (Mbytes)
2x2	85401	84582	99.04	13.79	5285656	2.39
4x4	359654	356303	99.06	13.72	5310414	10.07
6x6	763807	756523	99.05	13.62	5349354	21.39
8x8	1373411	1360428	99.05	13.47	5411169	38.46
10x10	2169240	2148923	99.06	13.28	5489060	60.74
10x10*	2028109*	2009292*	99.07	0.19*	379202368*	56.79

The results for the 10x10 cm^2 field with a suffix (*) were obtained by setting the PCUT and ECUT values in the jaws to 8 MeV instead of 0.01 and 0.7 MeV respectively. From table 4.1, the following observations can be made:

1) The number of particles in the phase space files increase almost linearly with increase in field size.
2) For all field sizes, 99% of the particles in the phase space files are photons and the remainder are electrons and positrons. This is a bit surprising, because one would expect to see a relatively higher percentage of electrons that contribute to the dose at the surface. This unexpected result may be due to the weak dependence of the PRESTA algorithm on the ECUT value (Rogers et al, 1995).
3) For the same transport parameters, the simulation time decreases with increase in field size, although the area influence on the simulation time is negligible. The decrease in time is due to the fact that as the field size increases, there is more air space created between the jaws and therefore less attenuation and less particle interactions, hence a decrease in CPU.
4) Using high PCUT and ECUT values in the jaws results in a 7% decrease in the number of particles in the phase space file as the histories of the low energy particles are terminated by the program. This results in an increase in the simulation rate by a factor of 70, hence lowering the CPU time.

4.4 Calculation of PDDs and cross-plane profiles in a water phantom With DOSXYZ Monte Carlo code

4.4.1 Preliminary trial simulations on a 2x2 cm^2 field size

The phase space files created for each field size were used to calculate the percentage depth dose and cross-plane profiles in a water phantom using the DOSXYZ program. The number of histories to be used for each field size was reached after carrying out trial simulation tests for a 2x2 cm^2 field size. Simulations were done with the same phantom settings for 2.5, 10 and 40 million histories. The simulation times were 0.70, 2.81 and 11.23 hours respectively. Table 4.2 shows the percentage uncertainty in the calculated dose at selected depths and figure 4.6 shows the depth dose comparison for the different number of histories.

Table 4.2: Percentage uncertainty in calculated dose at selected depths in a water phantom for different numbers of histories

Depth (cm)	2.5 M Histories	10 M Histories	40 M Histories
0.125	2.79	0.96	0.36
0.5	0.84	0.45	0.19
1.0	1.06	0.49	0.22
2.0	1.03	0.42	0.24
5.0	1.21	0.55	0.30
10.0	1.24	0.67	0.25
15.0	1.80	1.18	0.29
20.0	2.10	0.76	0.39
25.0	2.33	0.93	0.51
30.0	1.46	0.80	0.68
35.0	3.23	1.71	0.59
40.0	3.06	1.25	0.70

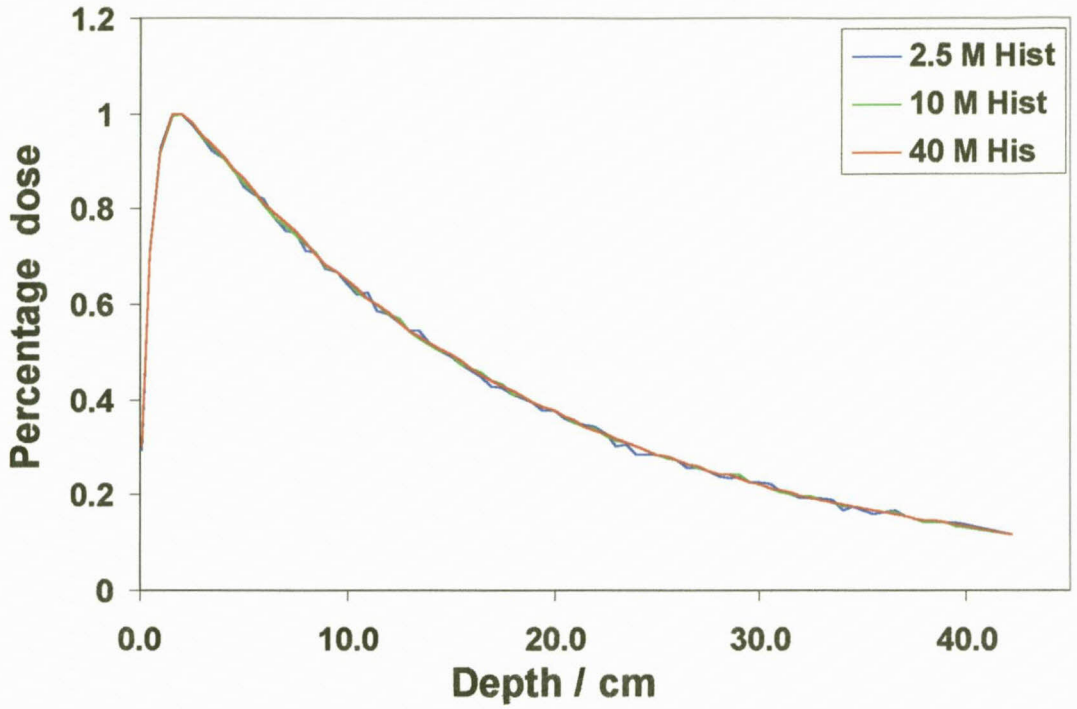

Fig 4.6: Comparison of 2.5, 10 and 40 million histories for 2x2 cm2 field sizes.

Figure 4.6 indicates that the distribution for the 10 and 40 million histories are almost indistinguishable, yet the simulation time is 4 times longer for the 40 million histories; and so does the does the disk storage space. Taking the two effects into consideration, 10 million histories were found adequate for a 2x2 cm^2 field size giving a particle density of 2.5 million per cm^2 and an uncertainty which is approximately 1% at most depths of major interest (table 4.2). This photon density was kept constant for all other field sizes. Table 4.2 indicates that the percentage uncertainty tends to increase with depths. This might be due to the fact that the number of particles decreases after most of the histories have been terminated and hence affecting the statistics.

4.4.2 DOSXYZ simulation on different field sizes

The number of histories used, CPU time and simulation rate for different field sizes, are shown in table 4.3.

Table 4.3: Summary of the DOSXYZ simulation results in a water phantom for different field sizes

Field Size (cm2)	Number of histories (Millions)	CPU time (hours)	Histories per hour	Number of times PSF was restarted
2x2	10	2.81	3564660	128
4x4	40	10.93	3661365	116
6x6	90	24.46	3679136	125
8x8	160	42.95	3725613	123
10x10	250	65.83	3797537	121

The following observations can be made from table 4.3:

- The number of histories used for each field was directly proportional to area, to obtain a uniform particle density.
- The number of histories determined the CPU time, and the two were directly proportional to each other.
- Since the number of particles stored in each phase space file were much less than what was used to minimize the uncertainty, the PSF were reused several times. The number of times the PSF were reused was almost the same for all the field sizes, since the number of particles in a file depends on area (table 4.1).

4.4.3 Comparisons of PDD obtained by chamber measurements and Monte Carlo method

Figures 4.7-a, 4.7-b, 4.7-c, 4.7-d and 4.7-e show a comparison of percentage depth dose curves obtained by the MC method and ionization chamber measurement for a 2, 4, 6, 8, and 10 cm^2. Both MC and ionization chamber data were normalized to 100%. Both methods are in good agreement. In all figures for the different field sizes, they is an initial rise in depth dose till a maximum at a depth of about 2 cm and then it starts to decrease. The dose is delivered by secondary electrons that are set in motion by photons. The dose

diminishes with depth due to the progressive disappearance of the photons. The initial increase of the dose below the entry surface is due to the accumulation of the secondary electrons over a distance equal to their ranges and this distance depends on the energy of the photon beam its self.

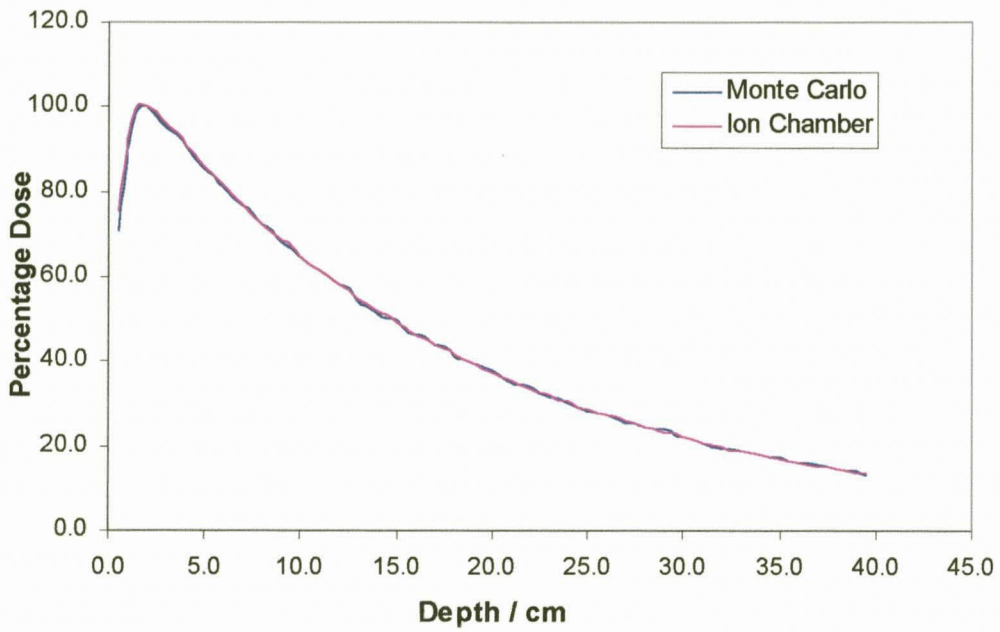

Fig 4.7-a: PDD curves MC versus chamber for 2x2 cm^2 field size.

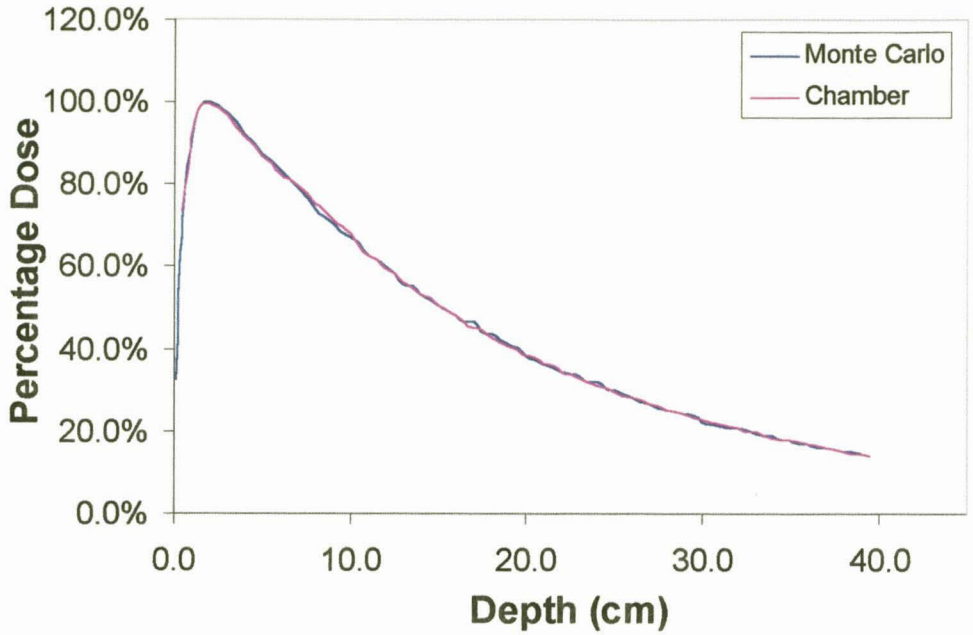

Fig 4.7-b: PDD curves MC versus chamber for 4x4 cm^2 field size.

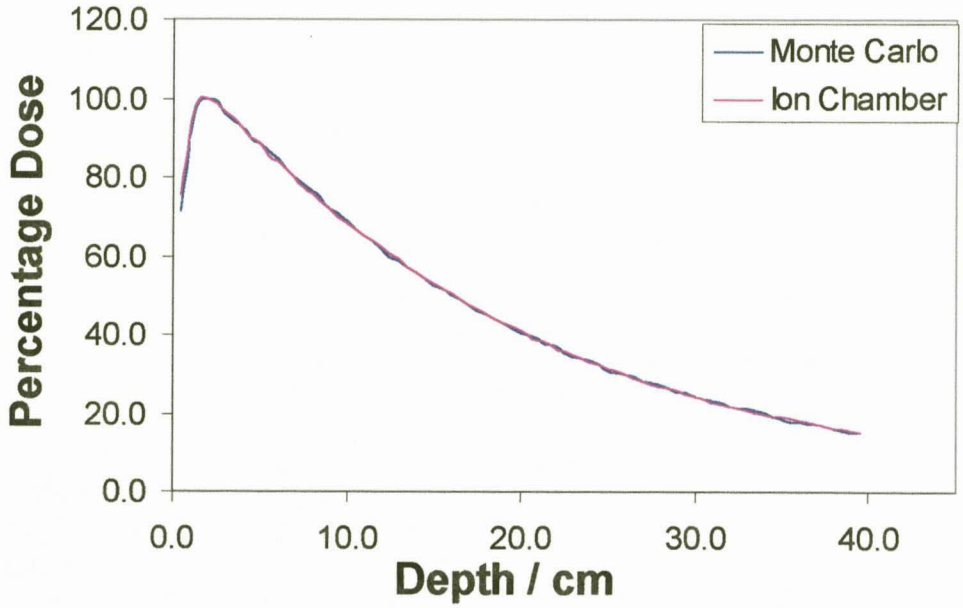

Fig 4.7-c: PDD curves MC versus chamber for 6x6 cm^2 field size

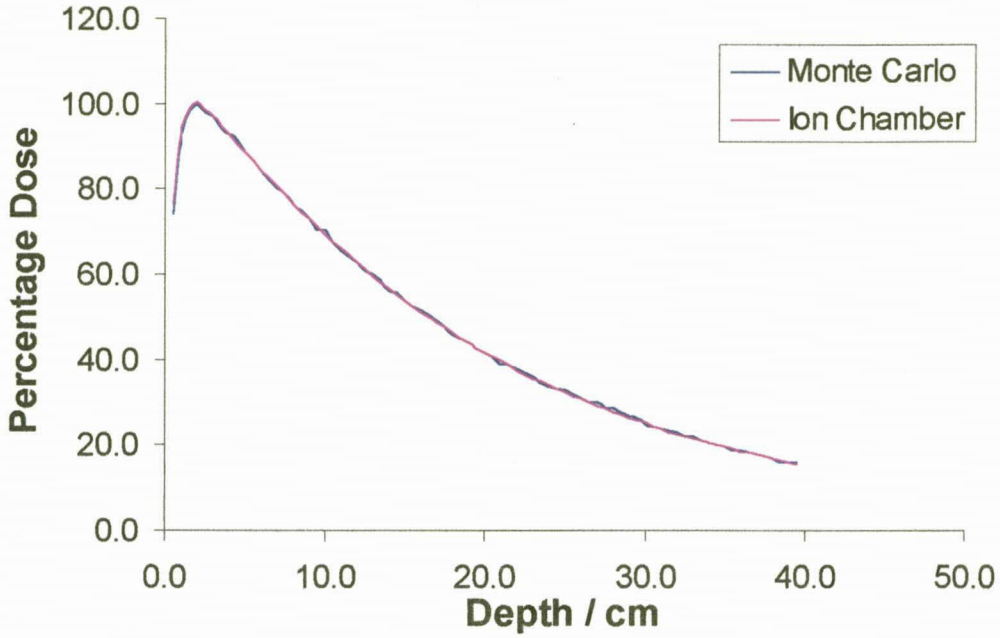

Fig 4.7-d: PDD curves MC versus chamber for 8x8 cm^2 field size

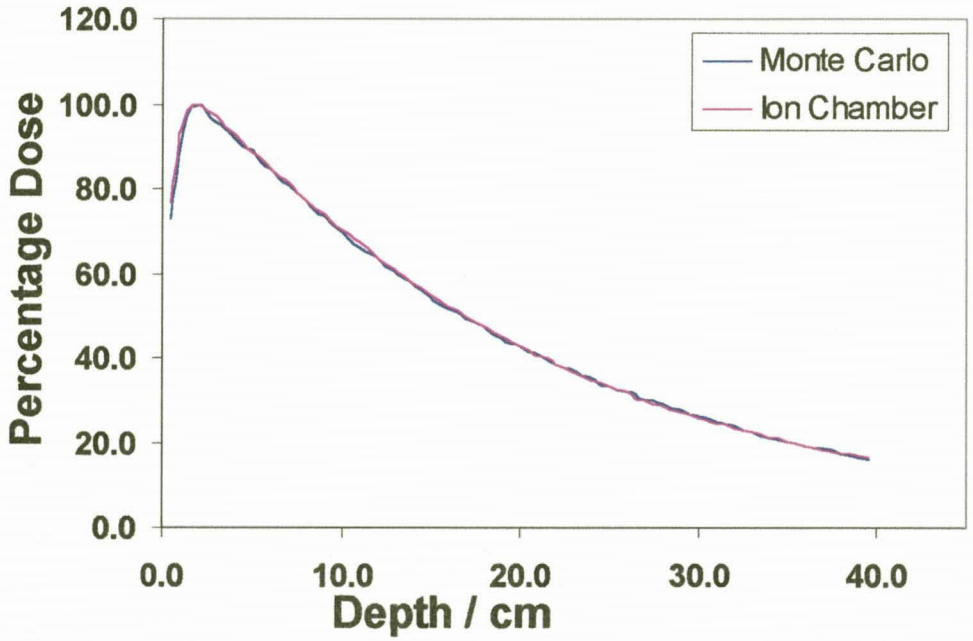

Fig 4.7-e: PDD curves MC versus chamber for 10x10 cm^2 field size

The initial buildup in dose is due to the fact that as the photons interact with the phantom (water) medium, electrons are set in motion in a forward direction and hence the number of electronic tracks will increase with depth until a depth equal to the electron range is reached. From this point onwards the dose decreases with depth due to attenuation of the photon radiation. The result is that the dose first increases and then decreases, leading to a very important phenomenon in radiotherapy: "the skin sparing effect ".

4.4.4 Comparison of Monte Carlo and chamber central axis percentage depth dose

To verify the MC calculation, it was necessary to get the uncertinity between the two methods. Table 4.4 shows the relative errors between the MC method and ionization chamber measurements on the central axis for different field sizes. The deviations for all the field sizes are highest in the buildup region. This is due to the MC method's under estimation of the dose at the surface, compared to that obtained by the ionization chamber. This discrepancy may be due to the fact that in MC, the percentage fraction of electrons in the PSS that would have increased the dose at the surface are low (less than 1%, table 4.1). However these deviations can be assumed to be insignificant since this area is within the high dose and steep dose gradient region of the beam. Large variations of more than 20% have been reported by comparing other dosimetrical methods like film and TLD with the ion chamber when used to measure dose in very high or very low dose regions (Williamson et al, 1981).

Table 4.4: Percentage relative error between MC and chamber measurements of central axis percentage depth dose

Depth (cm)	2x2 cm^2	4x4 cm^2	6x6 cm^2	8x8 cm^2	10x10 cm^2
0.5	6.5	2.9	5.6	3.1	5.6
1.0	2.4	0.4	2.6	1.3	3.3
2.0	0.0	-0.2	0.0	0.1	-0.1
5.0	-0.2	-0.3	-0.1	-0.1	-0.2
10.0	0.0	1.0	-0.1	-1.0	0.7
15.0	-0.6	-0.2	0.8	0.2	0.9
20.0	-1.3	0.0	0.5	0.7	0.7
25.0	1.0	-1.0	1.3	-0.9	0.6
30.0	-0.9	1.8	0.0	0.4	-0.8
35.0	-1.7	-0.6	1.1	-0.5	0.0
40.0	1.5	-1.4	-1.3	-1.9	1.2

4.4.5 Depth dose for different field sizes obtained by Monte Carlo

The dose data obtained by MC were plotted on the same graph to see the variation of PDD with field size. Figure 4.8 shows a comparison depth dose for different field sizes obtained by MC method. For sufficiently small fields, one may assume that the depth dose at a point is the result of primary radiation. The contribution of the scattered photons to the depth dose in this case is negligible. But as the field size is increased, the contribution of the scattered radiation to the absorbed dose increases (Khan, 1994). Since this increase in scattered dose is greater at larger depths than at the depth of d_{max}, the PDD increases with increasing field size.

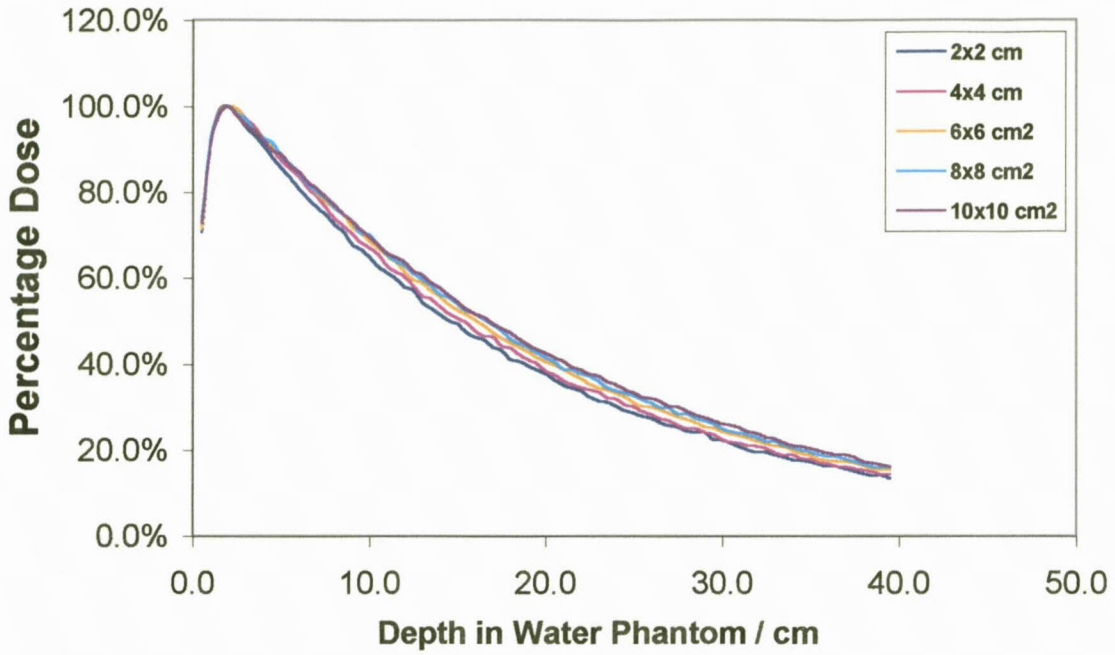

Fig 4.8: Depth Dose Curves for Different Fields Obtained by MC Method.

Figure 4.8 indicates that at a fixed depth above d_{max}, the percentage depth dose increases with increase in field size. When the field area is small, the dose received at a point below the surface is entirely due to primary radiation, since the volume that scatter radiation is very small. As the field area increases, the scatter contribution to the dose at points below the surface also increases. For small areas; depth dose is due to primary radiation alone while for large fields; depth dose is due to both primary and scattered radiation. Thus percentage depth dose increases with increase in field size, in agreement with Johns et al (1983).

4.4.6 Comparison of cross plane profiles obtained by Monte Carlo and chamber measurement

In figures 4.9-a, 4.9-b, 4.9-c, 4.9-d and 4.9-e the comparison of cross-plane profiles calculated by MC method and ion chamber measurement are shown. The profiles are for 2, 4, 6, 8 and 10 cm square fields measured at preset depths of 2, 5, 10, 15 and 25 cm measured in a water phantom. All data was normalized to the peak of the depth dose curve. The agreement is remarkable. The calculated and measured data are in good agreement even outside the beam. The observed dose outside the primary field is due to the scattered radiation from the jaws and other metallic parts of the accelerator.

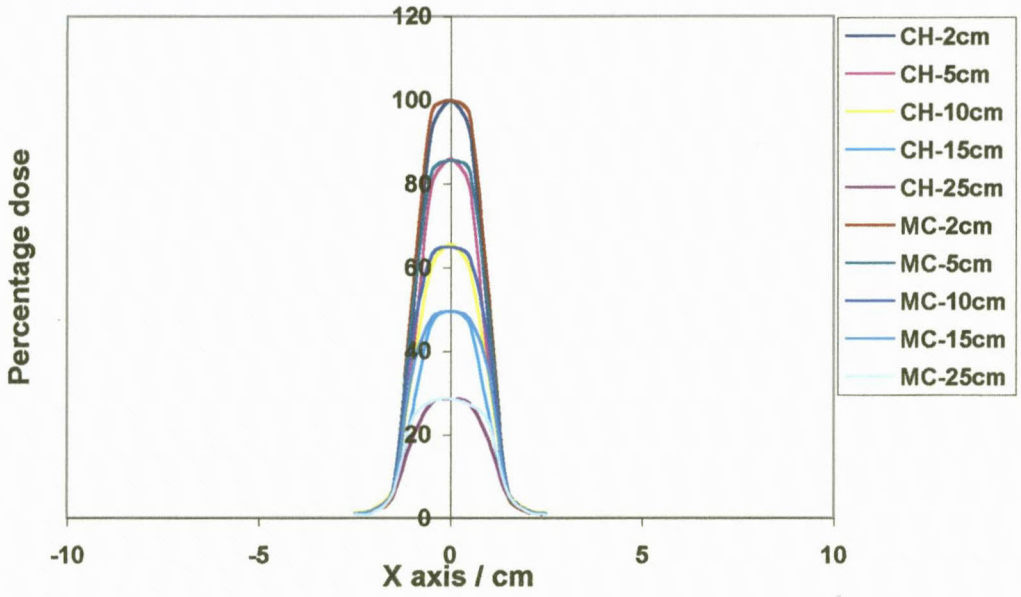

Fig 4.9-a: Cross plane profiles obtained with MC and ion chamber for 2x2 cm^2 field size at different field size

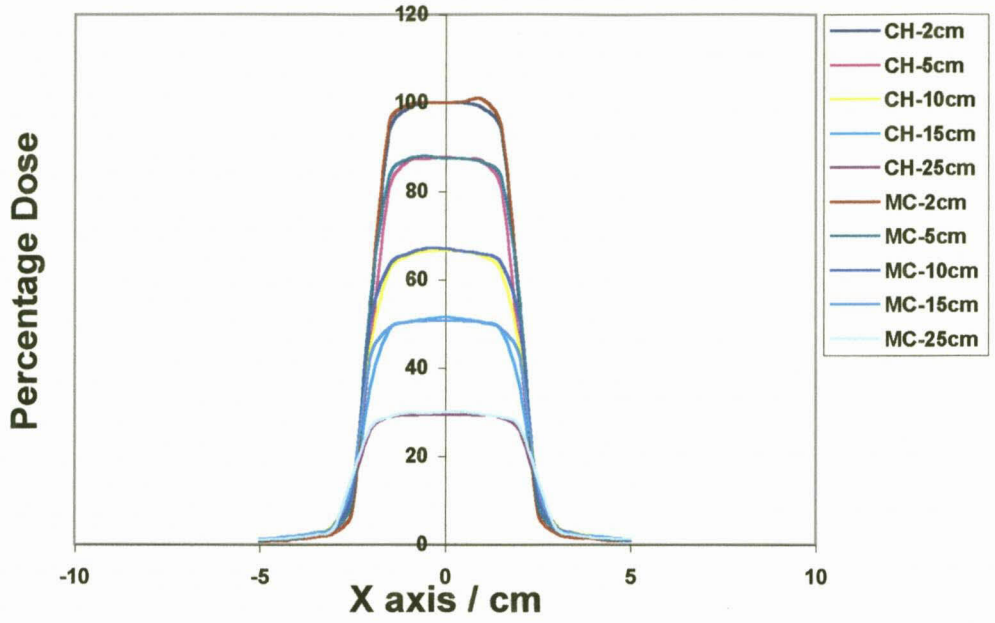

Fig 4.9-b: Cross plane profiles obtained with MC and ion chamber for 4x4 cm^2 field size at different depth

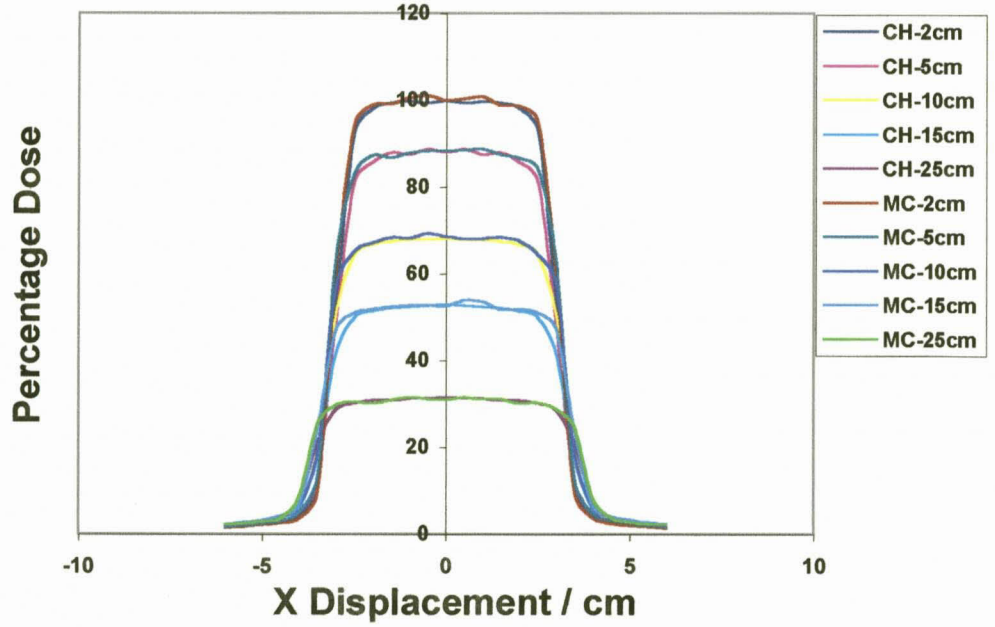

Fig 4.9-c: Cross plane profiles obtained with MC and chamber for 6x6 cm^2 field size at different depths

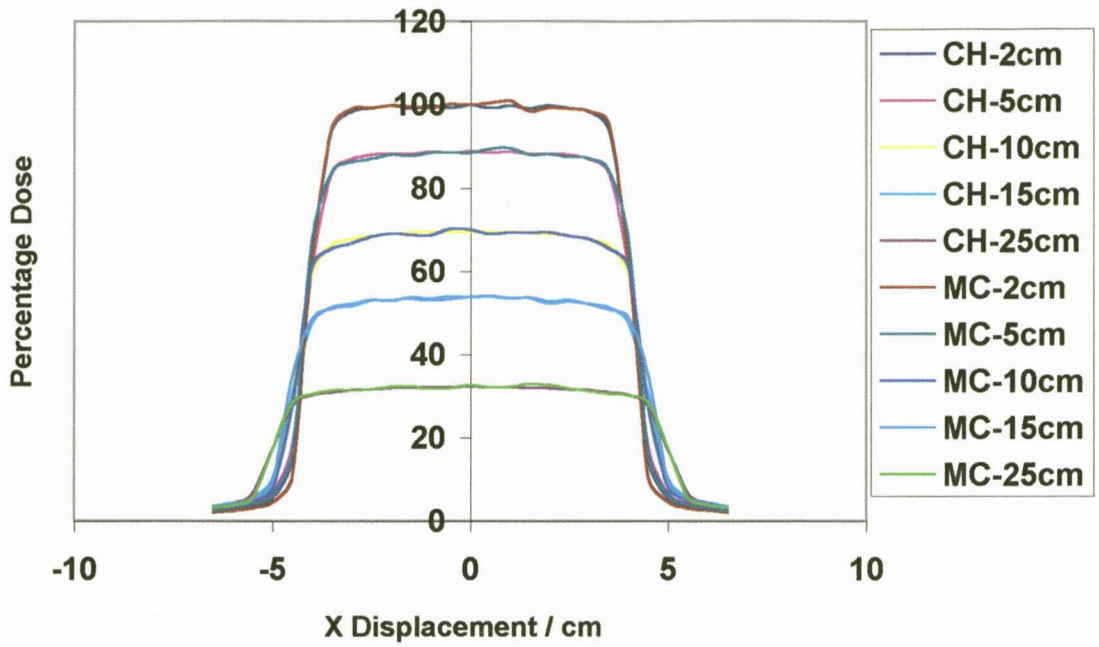

Fig 4.9-d: Cross plane profiles obtained with MC and chamber for 8x8 cm^2 field size at different depths.

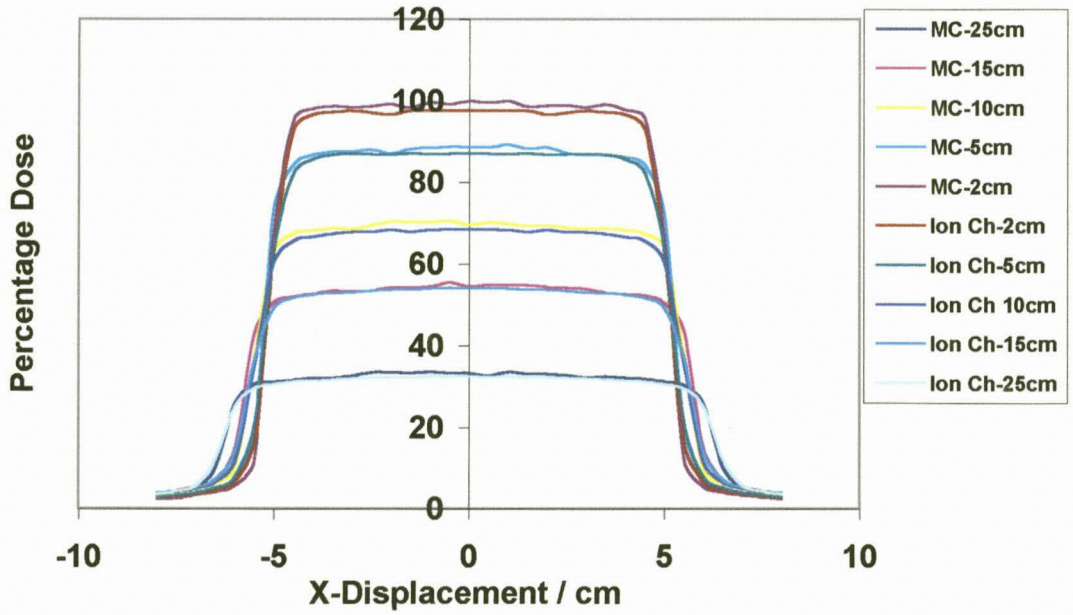

Fig 4.9-e: Cross plane profiles obtained with MC and chamber for 10x10 cm^2 field size at different depths.

4.5 Comparison of Monte Carlo with TPS dose distribution

4.5.1 Introduction

To meet the objective of the study, dose distributions for a number of field sizes were calculated using DOSXYZ code and compared with corresponding dose distributions calculated by the TPS. The ETAR and Modified BATHO inhomogeneity correction algorithms used by the TPS were both evaluated. Plans for maxillary sinus, breast, pelvis (CaCx), and esophagus were calculated using CT slices of real patients and a Rando phantom. In the calculation both SSD (used in maxillary sinus and breast) and isocentric (esophagus and pelvis) techniques were used. The number of histories used in the DOSXYZ MC was fixed depending on the field size. After carrying out trial simulations for a 2x2 cm^2 field size, we found 20 million histories to be quite adequate and this history density (i.e 5 million histories per cm^2) was maintained for all the field sizes.

4.5.2 Maxillary sinus

Single field dose distributions for different sizes (2, 4, 6 and 10 cm square fields) were calculated using MC method and TPS. In all cases, a single anterior-posterior field was used and the beam entry point was kept constant. The number of histories used in DOSXYZ for the 2, 4, 6 and 10 cm square fields were 20, 80, 180 and 500 million respectively. For the comparison of the MC and TPS to be meaningful the dose was normalized to 2 cm at the central axis of each field. The results are shown in figures 4.10, 4.11, 4.12 and 4.13.

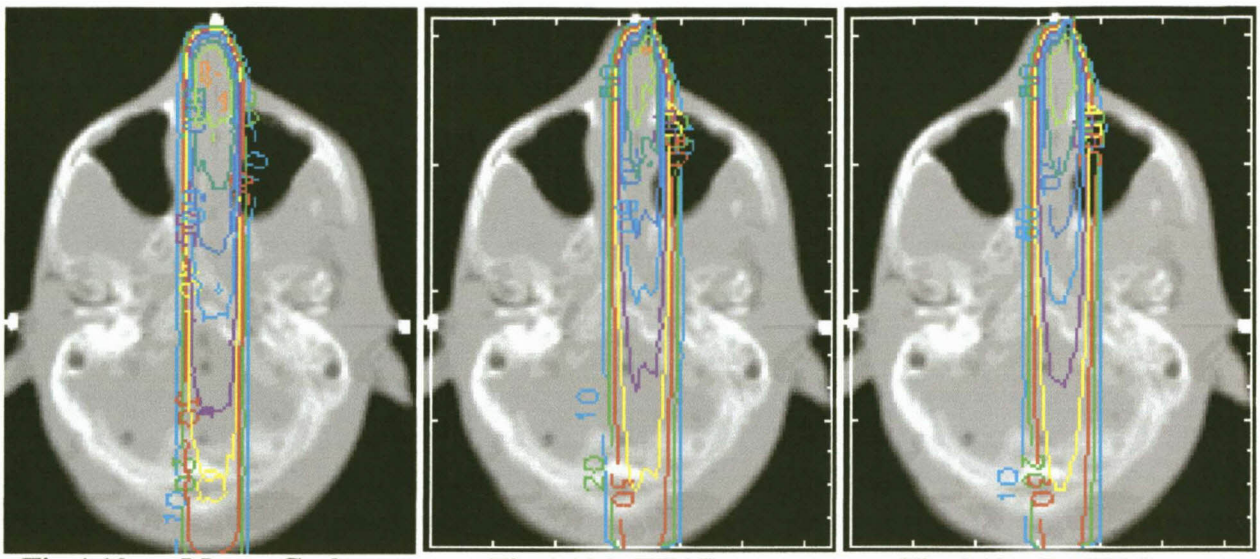

Fig 4.10. a: Monte Carlo **Fig 4.10.b:ETAR** **Fig 4.10.c:BATHO**

Fig 4.10: A comparison of the dose distributions for maxillary sinus a 2x2 cm^2 normalized at 2 cm depths

Figure 4.10 indicates that the dose distributions for the maxillary sinus calculated by DOSXYZ and the treatment planning system are very much the same. For a 4x4 cm^2 field size shown in figure 4.11, the MC calculated dose distributions show slight deviations compared to ETAR (fig 4.10.b) and BATHO (fig 4.10.c). This is indicated by the bulging of the 10% isodose distribution in the sinus and the 80% isodose level. This effect may be attributed to the fact that the ETAR and BATHO methods fail to calculate the dose accurately in and near tissue interfaces. Otherwise elsewhere the distributions are quite similar. Comparison of figures 4.11.a, 4.11.b and 4.11.c show that the TPS dose calculation algorithm do not model the lateral scatter process of the photon beam as accurately as the Monte Carlo DOSXYZ code. This effect of scatter is more prominent for the 4x4 cm^2 field size than the 2x2 cm^2, mainly because in smaller fields, the primary beam mainly contributes to the dose, with a small contributions by scattered radiation.

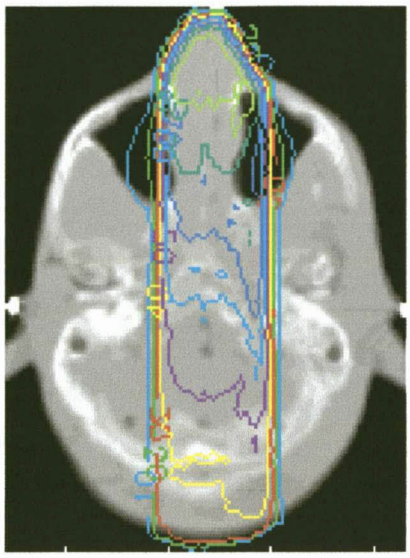

Fig 4.11.a:Monte Carlo

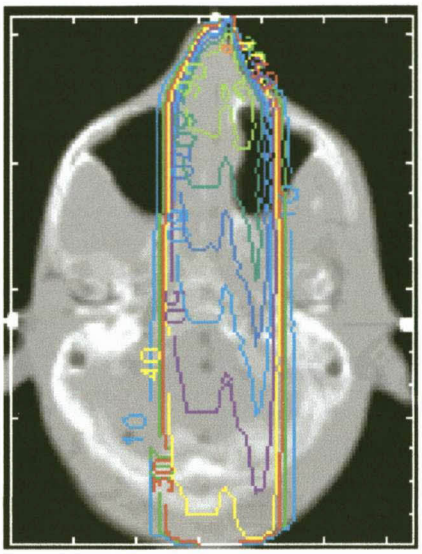

Fig 4.11.b:ETAR

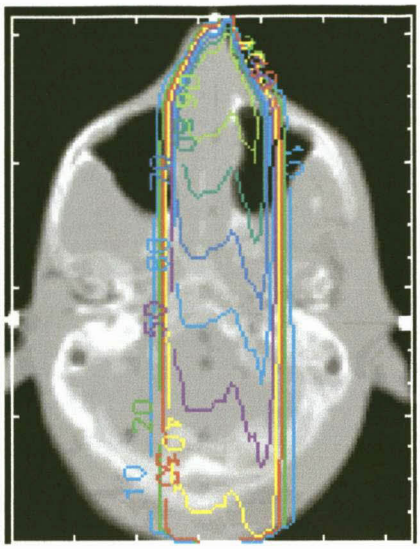

Fig 4.11.c:BATHO

Fig 4.11: A comparison of the dose distributions for a 4x4 cm^2 normalized at 2 cm depths.

Figure 4.12 shows a 6x6 cm^2 anterior field to the maxillary sinus, with the dose normalized at 2 cm depth. The dose distributions for the CT slices 2 cm above and 2 cm below the central slice are also displayed to show a three dimensional view, as calculated by MC and TPS methods. Comparison of the dose distributions at corresponding CT slices don't show any significant deviation apart from the MC dose distribution's un smooth appearance at some selected isodose levels. e.g 50% in fig 4.12.d, 70% in 4.12.g, which might be due to the poor statistics caused by low number of histories.

CT slice 2 cm above

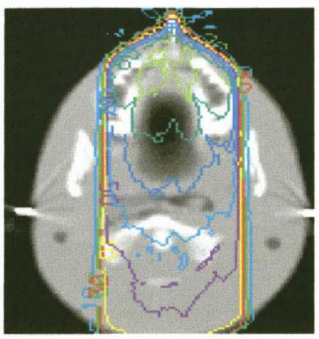

Fig 4.12.a: Monte Carlo

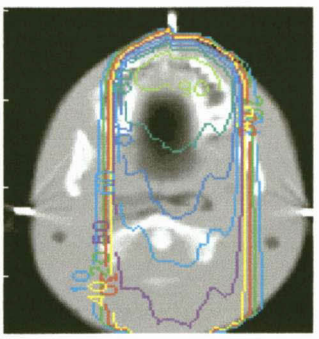

Fig 4.12.b: BATHO

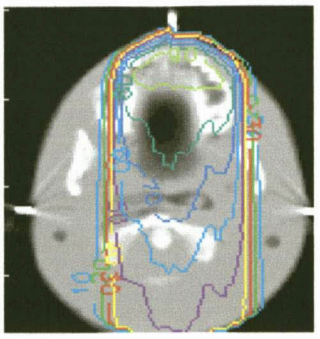

Fig 4.12.c:ETAR

Central CT slice

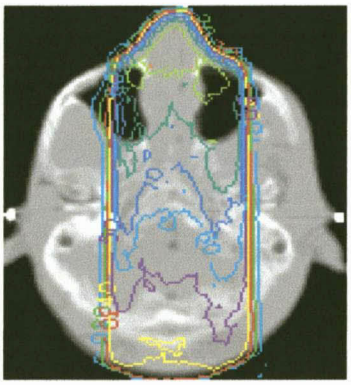

Fig 4.12.d: Monte Carlo

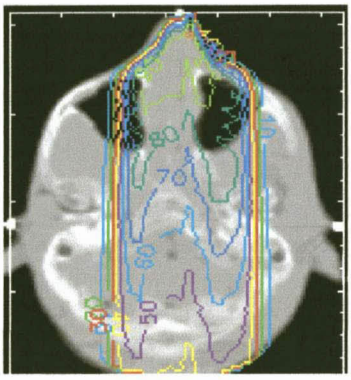

Fig 4.12.e: BATHO

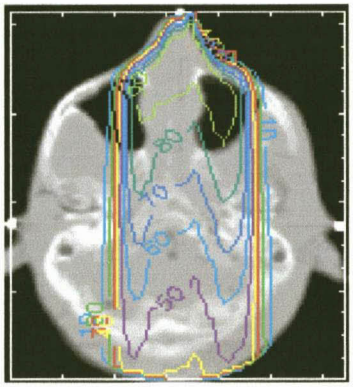

Fig 4.12.f: ETAR

CT slice 2 cm below

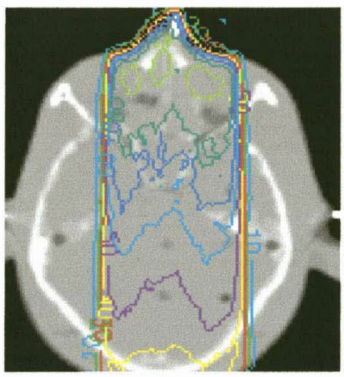

Fig 4.12.g: Monte Carlo

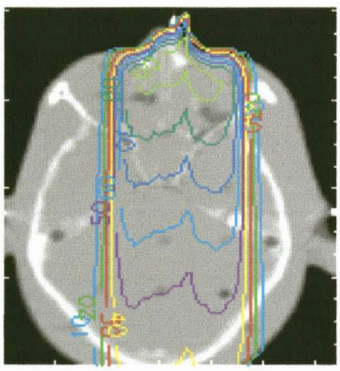

Fig 4.12.h: BATHO

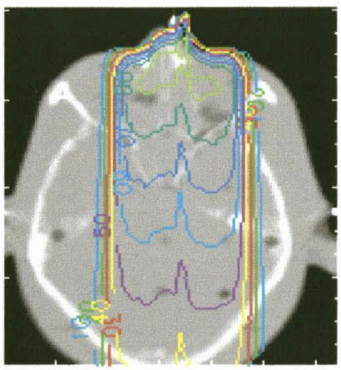

Fig 4.12.i:ETAR

Fig 4.12: A comparison of the dose distributions for a 6x6 cm^2 normalized at 2 cm depths.

CT slice 4 cm above

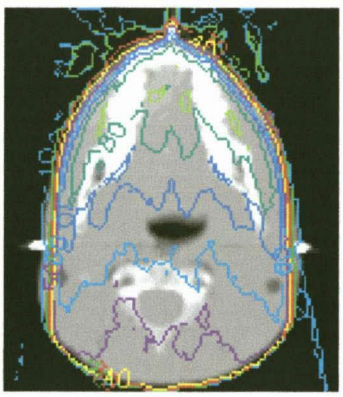

Fig 4.13.a: Monte Carlo

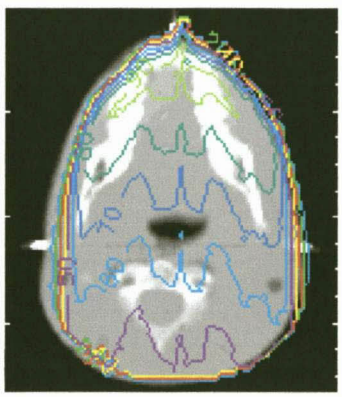

Fig 4.13.b: ETAR

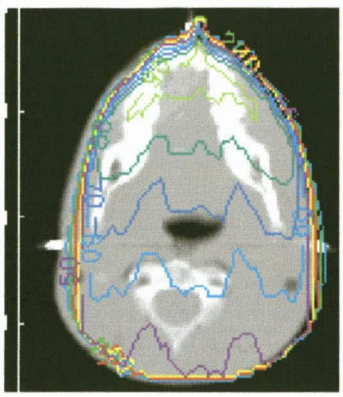

Fig 4.3.c: BATHO

Central CT Slice

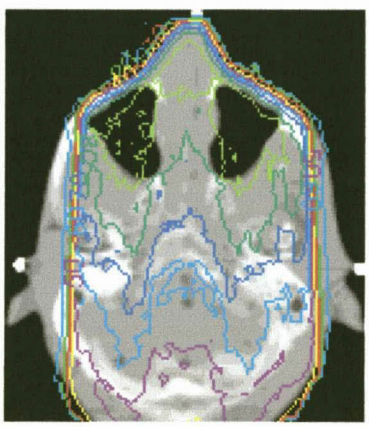

Fig 4.13.d: Monte Carlo

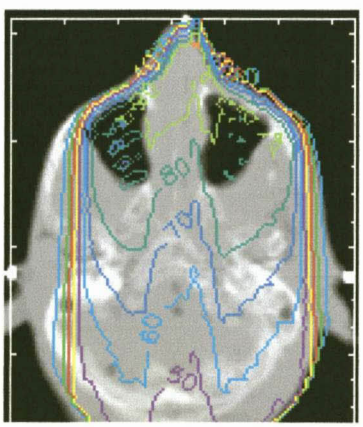

Fig 4.13.e: ETAR

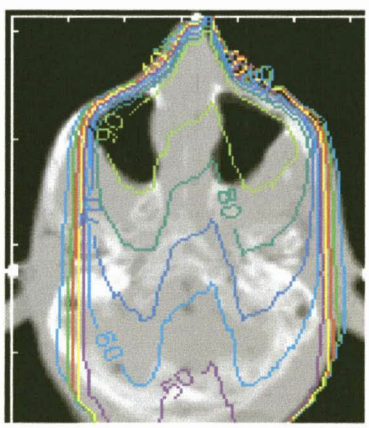

Fig 4.13.f: BATHO

CT slice 4 cm above

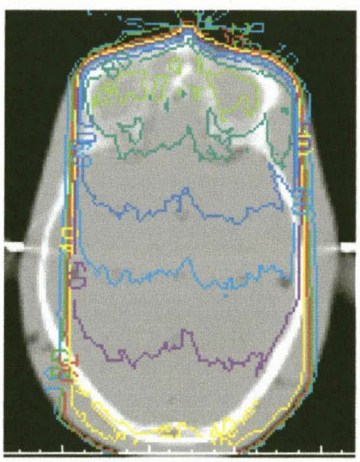

Fig 4.13.g: Monte Carlo

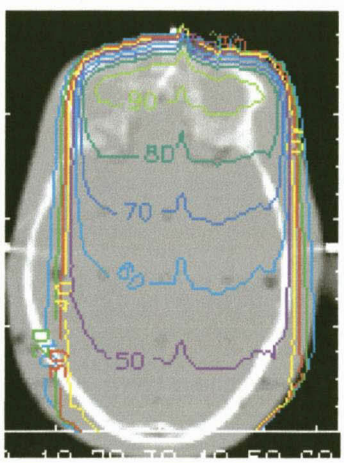

Fig 4.13.h: ETAR

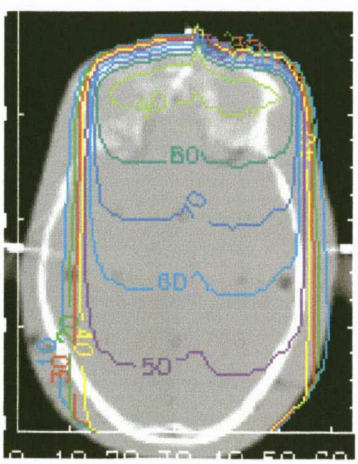

Fig 4.3.i: BATHO

Fig 4.13: Dose distributions for a 10x10 cm^2 normalized at 2 cm depths.

Figure 4.13 shows a 10x10 cm^2 anterior field to the maxillary sinus, with the dose normalized at 2 cm depth. The dose distributions for the CT slices 4 cm above and 4 cm below the central slice are also displayed to show a three dimensional view, as calculated by Monte Carlo and treatment planning system. On the central slice the BATHO and DOSXYZ calculated dose distributions are in agreement with the ETAR, figures 4.13.d, 4.13.e and 4.13.f. The dose distributions for the CT slices above and below the central slice are in good agrrement with each other.

4.5.3 Breast

Dose distributions for 10x10 cm^2 field size were calculated using MC method and TPS. In all the plans, two tangential fields were used and the beam entry points were kept constant. The gantry angles were set at 146° for the lateral oblique and 326° for the mediastinal oblique. The SSD technique was used and for the comparison of the MC and TPS to be meaningful the dose was normalized at 2 cm depth at the central axis of each field. The results are shown in figure 4.14. This plan is not a typical breast plan. The aim was to show the comparison of the dose distributions as calculated by MC and the TPS. The field size used, the beam entry angles and the volume of the lungs included in the primary beam don't reflect a typical radiotherapy treatment breast plan. On the central slice, ETAR and BATHO dose distributions are comparable to each other, figures 4.14.e, 4.14.f indicating that most of the target region is within 140%. The DOSXYZ calculated dose distribution show that most of this region is within 130%, with small spots having 140%. This difference between the TPS and the MC method can be explained by the inability of the TPS to model correctly the effect of the lower attenuation of photons by the lungs compared to water which results in higher dose distribution. Figure 4.14.a is totally different from those calculated by the TPS (figures 4.14.b and figure 4.14.c). This might be due to the slice being at the field edge where dose gradient is high. This edge effect was also observed in the esophagus plan, figure 4.16.

CT slice 5 cm Above

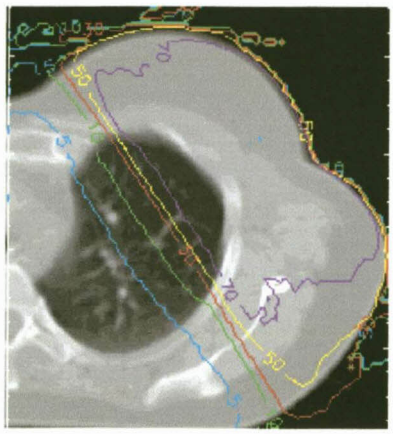

Fig 4.14.a: Monte Carlo

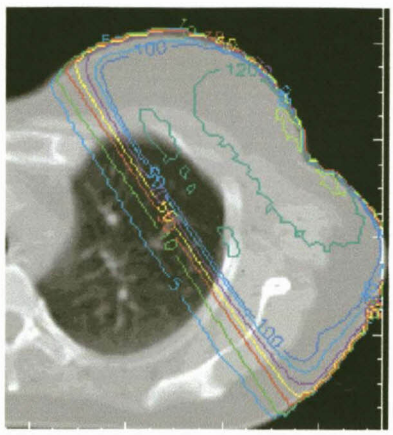

Fig 4.14.b: ETAR

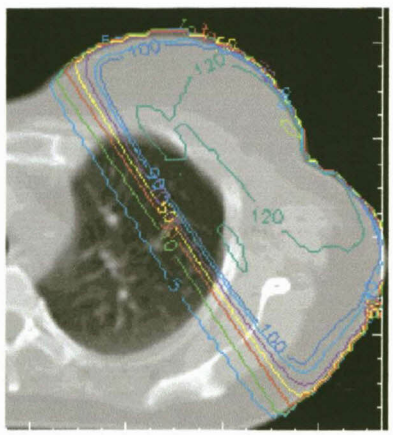

Fig 4.14.c: BATHO

Central CT slice

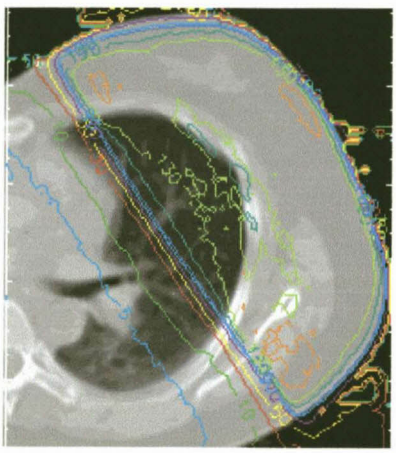

Fig 4.14.d: Monte Carlo

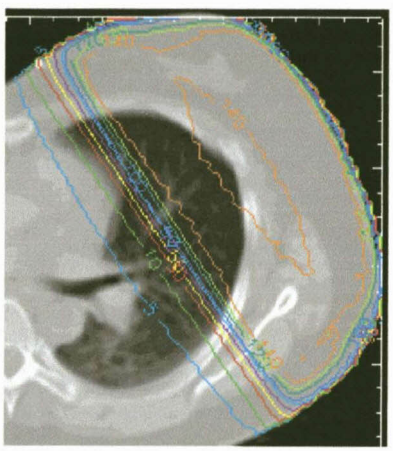

Fig 4.14.e: ETAR

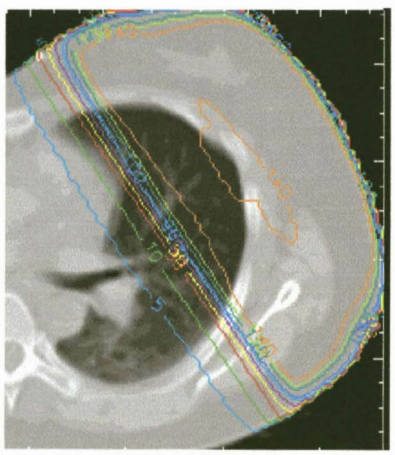

Fig 4.14.f: BATHO

CT slice 5 cm below

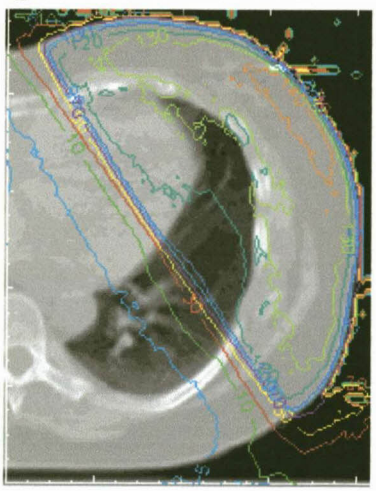

Fig 4.14.g: Monte Carlo

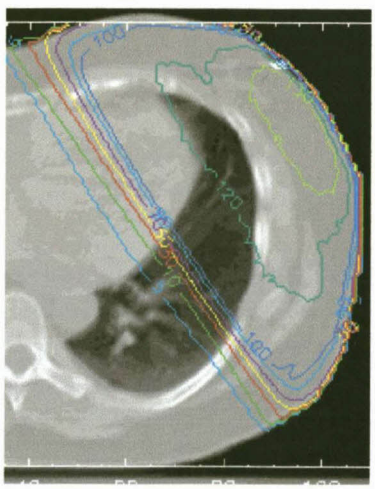

Fig 4.14.h: ETAR

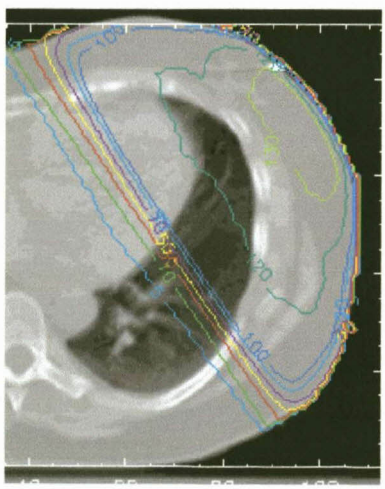

Fig 4.14.i: BATHO

Fig 4.14: Comparison of two tangential fields for 10x10 cm^2 field size to the breast

4.5.4 Oesophagus

Plans show a comparison of MC and TPS methods for a three field isocentric technique for a typical plan for the treatment of the cancer of the esophagus. One anterior-posterior and two posterior oblique fields were used, and the beam entry points were kept constant. The size of each field was 4x6 cm^2 and the angles are 0^o, 140^o and 220^o. Figure 4.15 show the distributions when the dose was normalized to the isocenter coordinate point and when the dose was normalized to the 90% isodose.

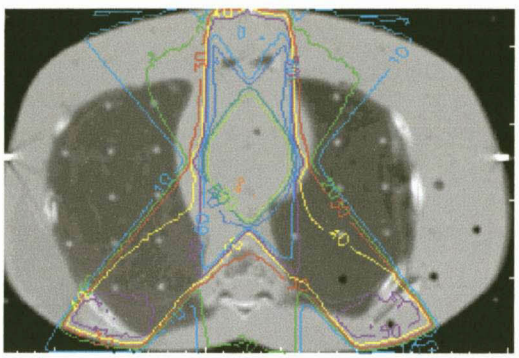

Fig 4.15.a: Monte Carlo (normalized to isocenter)

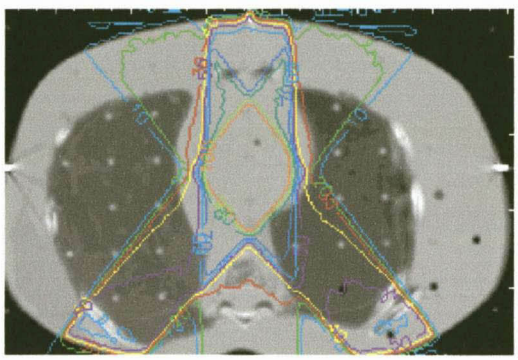

Fig 4.15.b: Monte Carlo (normalized 90%)

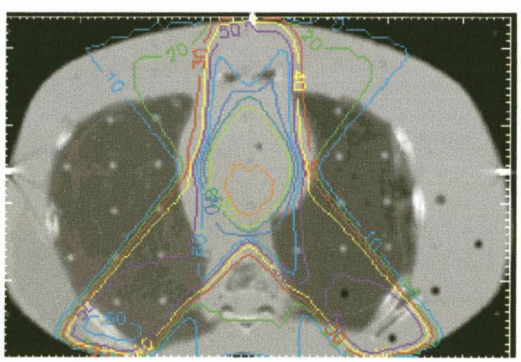

Fig 4.15.c: BATHO (normalized to isocenter)

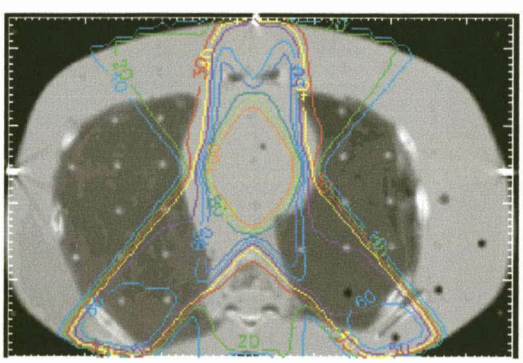

Fig 4.15.d: BATHO (normalized to 90 %)

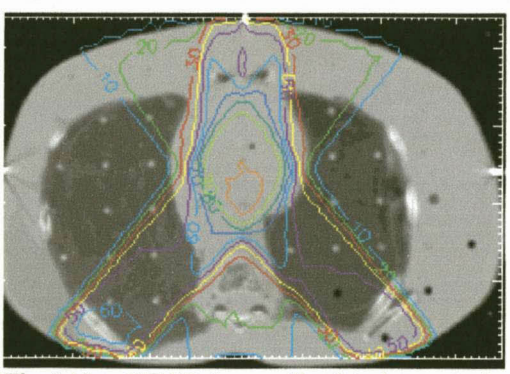

Fig 4.15.e: ETAR (normalized to icocenter)

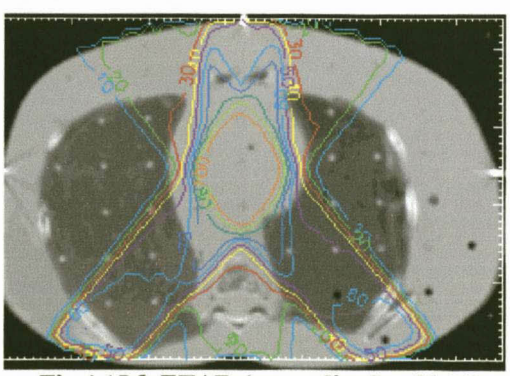

Fig 4.15.f: ETAR (normalized to 90 %)

Fig 4.15 Comparison of the dose distributions for a three field esophageal

Comparison of the dose distributions normalized at the isocenter, DOSXYZ (figure 4.15.a) indicates a 50% isodose at the entrance of both the oblique fields where as the ETAR and BATHO show a 60% and 50% entrance doses for the right and left posterior oblique fields. The normalized dose distributions for all the methods do not show any significant difference. Figure 4.16 is the same plan showing a three dimensional view by displaying the dose distributions for the CT slices 2 cm above and 2 cm below the central slice, calculated by Monte Carlo and CADPLAN ETAR and BATHO inhomogeneity correction algorithm methods. Dose distributions were normalized at the isocenter point.

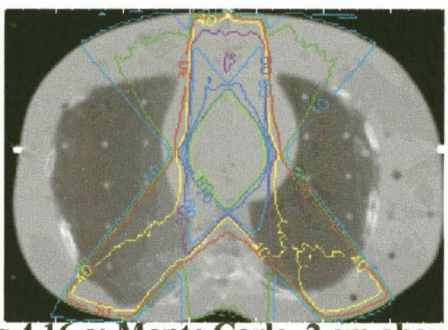

Fig 4.16.a: Monte Carlo, 2 cm above

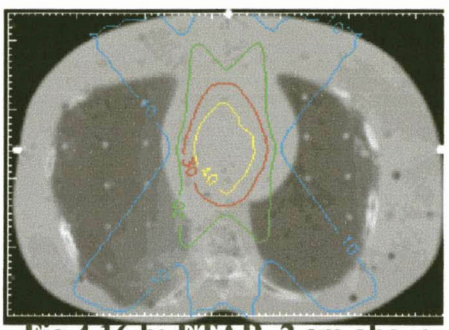

Fig 4.16.b: ETAR, 2 cm above

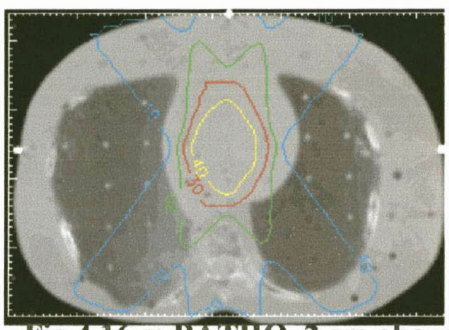

Fig 4.16.c: BATHO, 2 cm above

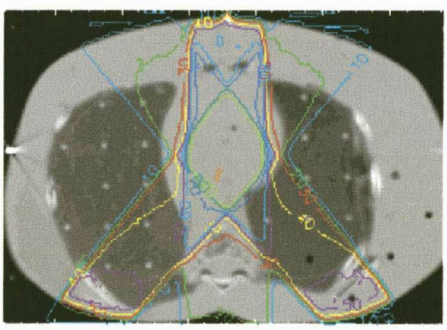

Fig 4.16.d: Monte Carlo, Central slice

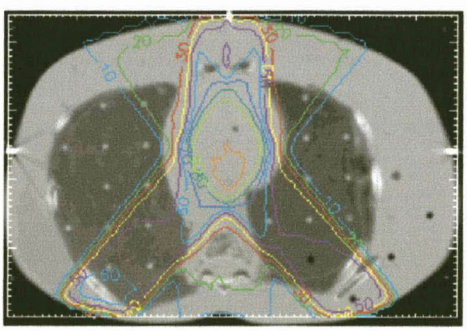

Fig 4.16.e: ETAR, Central slice

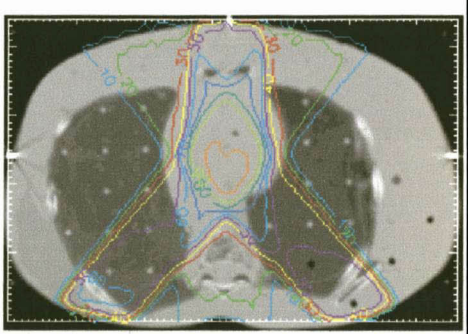

Fig 4.16.f: BATHO, Central slice

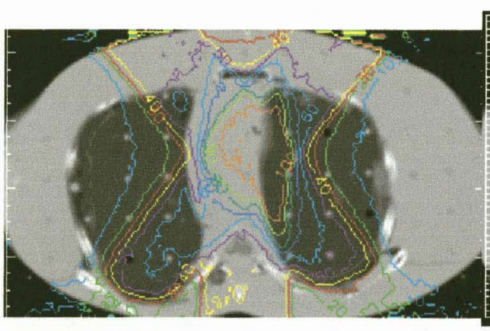

Fig 4.16.g: Monte Carlo, 2 cm below

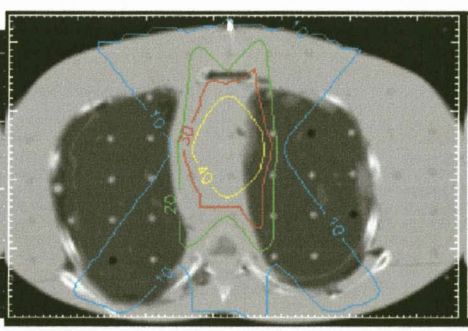

Fig 4.16.h: ETAR, 2 cm below

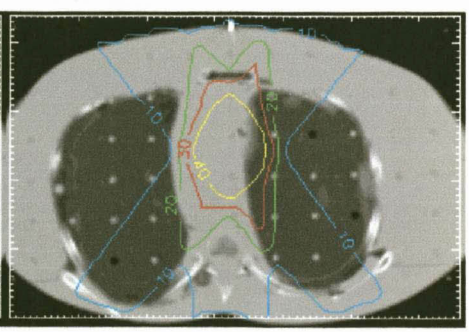

Fig 4.16.i: BATHO, 2 cm below

Fig 4.16: A 3D view showing dose distributions for slices 2 cm above and below the central CT slice

Comparison of figure 4.16 indicates that there is a big difference between the Monte Carlo and the treatment planning system dose distributions for slices 2 cm above and below the central CT slice. Figure 4.16.a: calculated by DOSXYZ is totally different compared to ETAR (fig 4.16.b) or BATHO (fig 4.16.c). Similar effect is observed on dose distributions for the CT slices 2 cm below the central slice, that is figures 4.16.g, 4.16.h and 4.16.i. This might be due to the edge effect. The field sizes used were 6x4 cm^2 and there is a possibility that we are presenting the dose distribution in the high dose gradient region such that the error is quite large. This edge effect was also observed in the breast plan, figures 4.14.a, 4.14.b, and 4.14.c or figures 4.14.g, 4.14.h, and 4.14.i.

4.5.5 Pelvis (CaCx)

Plans were calculated for a comparison of MC and TPS methods for a three field and a four field isocentric technique which is a typical plan for the treatment of the cancer of the cervix. One anterior-posterior and two lateral fields were used for the three fields technique while for the four field technique an extra posterior-anterior field was added. The beam entry points were kept constant for all the fields. The size of each AP and PA field was 10x10 cm^2 and the lateral fields were 10x6 cm^2. The angles were 0^o, 90^o, 180^o and 270^o. Figures 4.17 and 4.19 show the dose distributions calculated on the central slices for the three fields and four fields techniques respectively.

4.5.5.1 Pelvis (three fields)

Fig 4.17: Comparison of three field isocentric plan: One AP (10x10 cm^2) and two lateral fields (10x6 cm^2). The dose is normalized at the isocenter for all plans

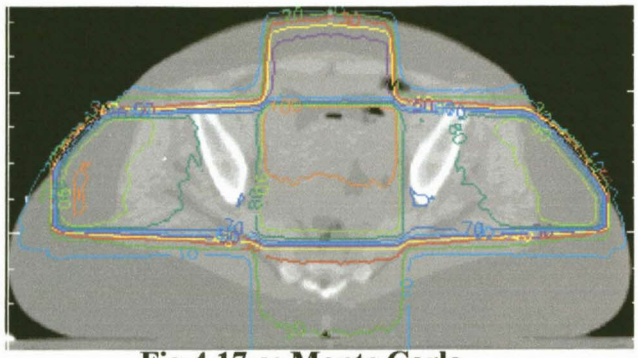

Fig 4.17.a: Monte Carlo

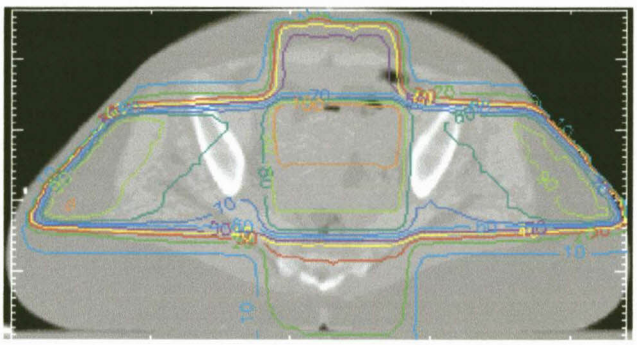

Fig 4.17.b:ETAR

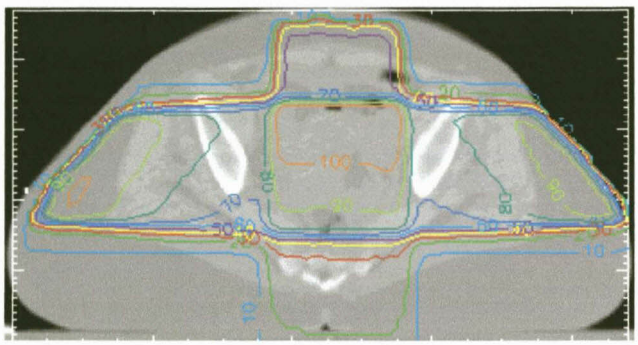

Fig 4.17.c:BATHO

The dose distributions on the central slice displayed in figure 4.17 are very much in agreement to each other. Only one noticeable difference at the 70% isodose. For the ETAR (fig 4.17.b) and BATHO (fig 4.17.c), the 70% isodose raises to the level of the left and right femoral bones while in the case of DOSXYZ (fig 4.17.a) the 70% isodose are shown as small spots at the same points. Elsewhere the dose distributions are the same.

Figure 4.18 show the three field technique comparison showing a three dimensional view by displaying the dose distributions for the CT slices 3 cm above and 3 cm below the central slice as calculated by Monte Carlo and CADPLAN ETAR inhomogeneity correction algorithm methods

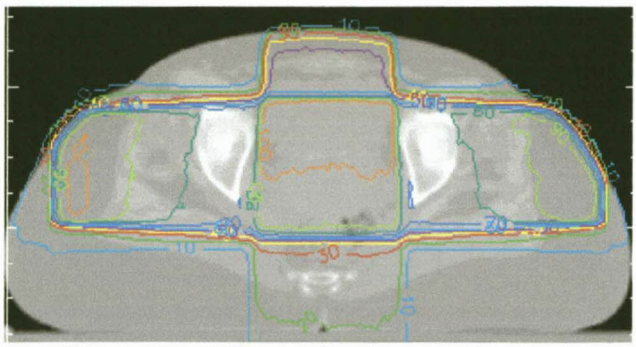

Fig 4.18.d: Monte Carlo

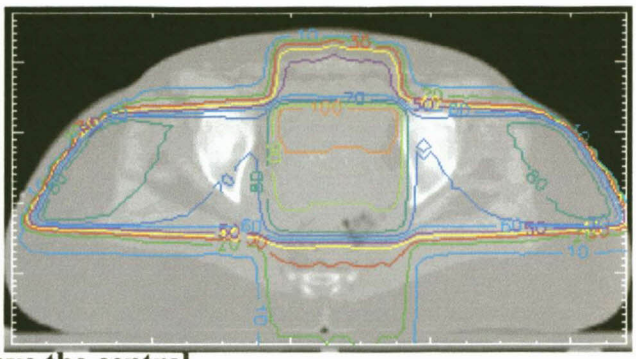

Fig 4.18.e:ETAR

Slice 3 cm above the central

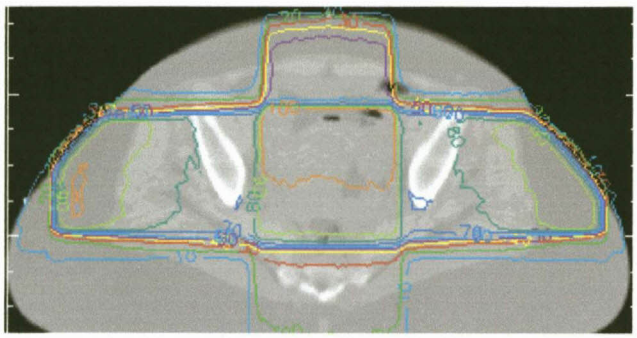

Fig 4.18.f: Monte Carlo

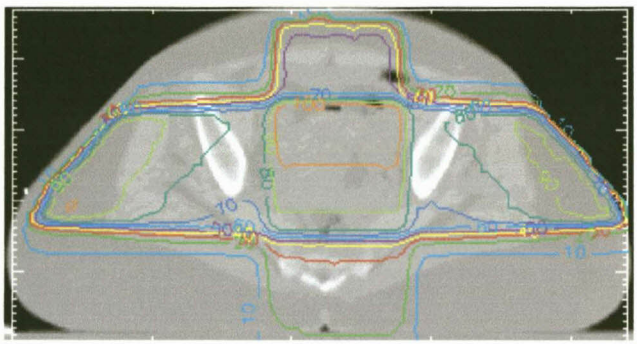

Fig 4.18.g:ETAR

Central slice

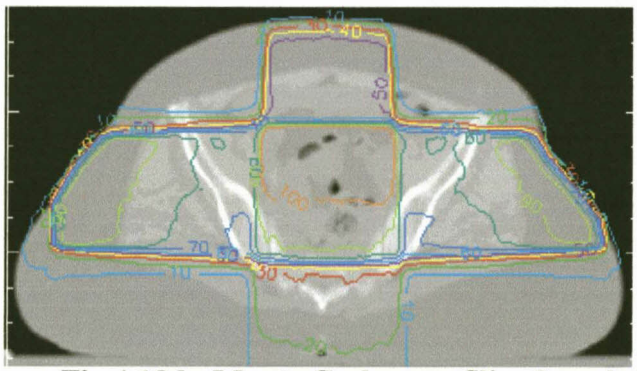

Fig 4.18.h: Monte Carlo

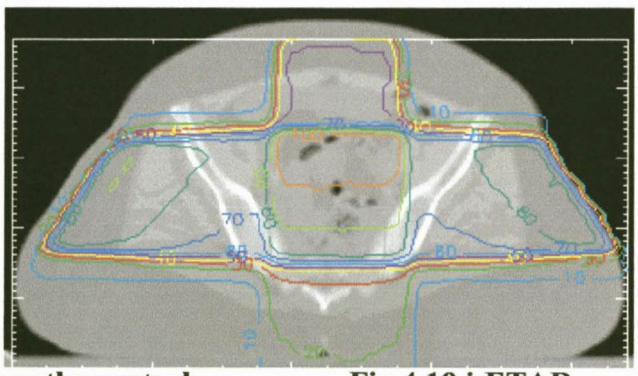

Fig 4.18.i:ETAR

Slice 3 cm below the central

Fig 4.18: Three field technique comparison showing a 3D view

For the slices above and below the central slice in Fig 4.18, Monte Carlo method (figures 4.18.d and 4.18.h) shows higher entrance dose (90%) from the lateral fields compared to the ETAR (figures 4.18.e and 4.18.i) which indicates 80% isodose level. Also there is a noticeable difference for the slice 3 cm above the central CT slice, figures 4.18.d and 4.18.e at the 70% isodose line. The difference is less marked on the opposite CT slice (figures 4.18.h and 4.18.i).

4.5.5.2 Pelvis (four fields)

Fig 4.19: A comparison of four field technique, field size 10x10 cm^2 for the AP and PA, and 10x6 cm^2 for the lateral fields. The dose is noralized to 90% isodose

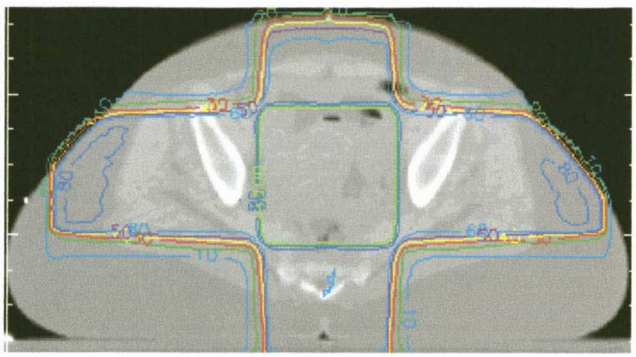

Fig 4.19.a: Monte Carlo

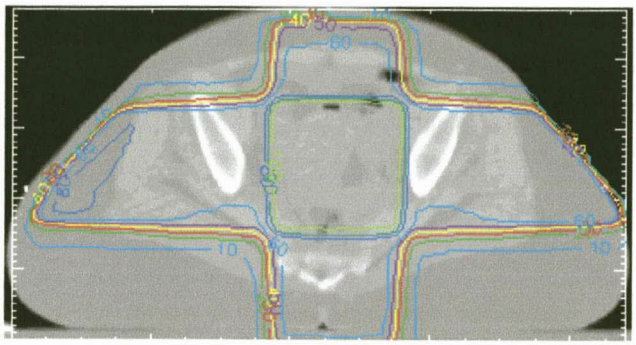

Fig 4.19.b: ETAR

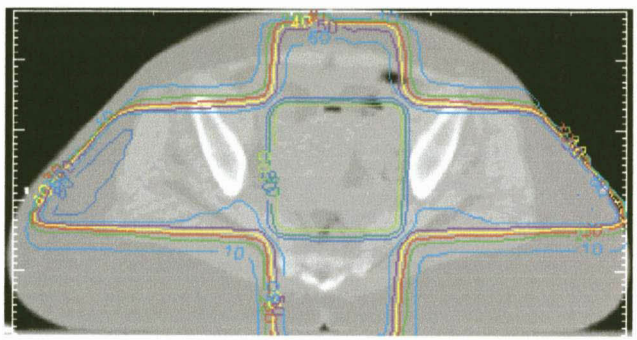

Fig 4.19.c: BATHO

The dose distributions on the central slice displayed in figure 4.19 are in good agrrement to each other. The only noticeable difference is at the 80% isodose. DOSXYZ (fig 4.19.a) indicate an 80% isodose level on both the left and right lateral entrance while for ETAR (fig 4.19.b) and BATHO (fig 4.19.c), the dose distribution around the region is 70%.

Figure 4.20 show the four field technique comparison to show a three dimensional view by displaying the dose distributions for CT slices 3 cm above and 3 cm below the central slice as calculated by Monte Carlo and CADPLAN modified BATHO inhomogeneity correction

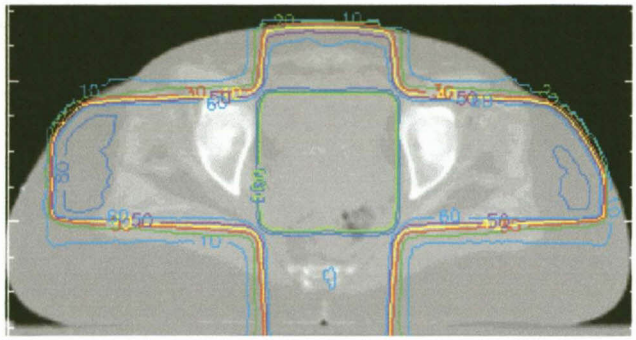

Fig 4.20.d: Monte Carlo

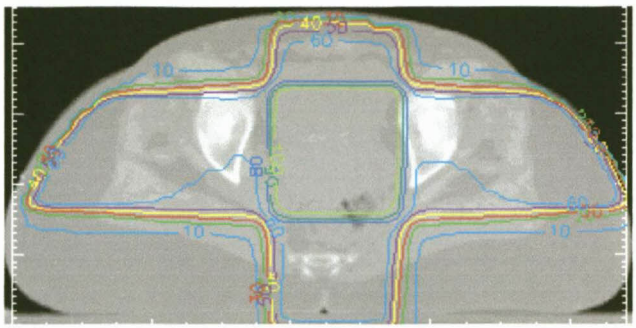

CT slice 3 cm above the central

Fig 4.20.e: BATHO

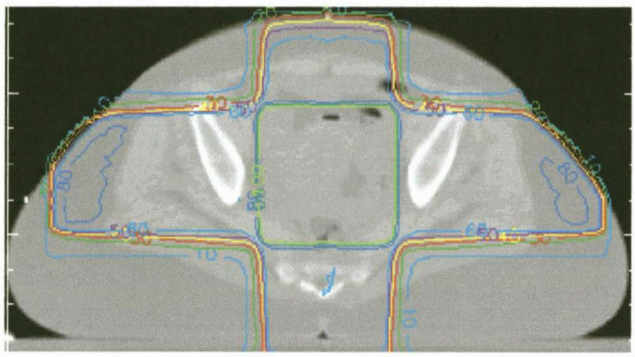

Fig 4.20.f: Monte Carlo

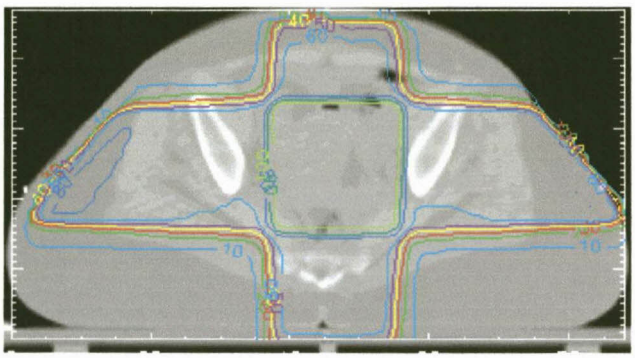

Central CT slice

Fig 4.20.g: BATHO

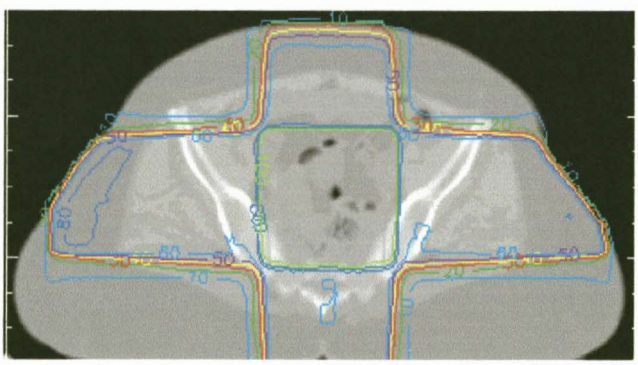

Fig 4.20h: Monte Carlo

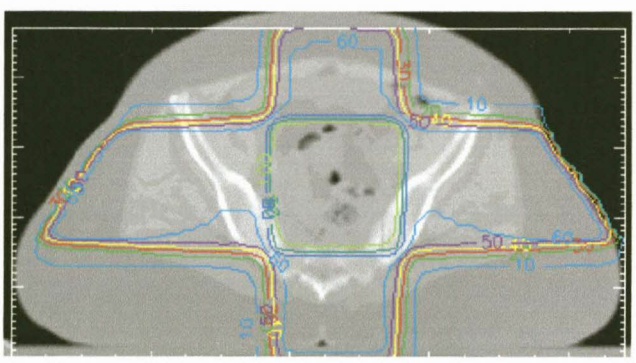

CT slice 3 cm below the central

Fig 4.20.i: BATHO

Fig 4.20: four field technique comparison showing a 3D view

For the slice above the central slice in Fig 4.20, the Monte Carlo method (figure 4.20.d) shows higher entrance dose (80%) from the lateral fields compared to the BATHO (figure 4.20.e) which indicates 60% - 70% isodose level. Also there is a noticeable difference for the CT slices 3 cm above the central (figures 4.20.d and 4.20.e) and below (figures 4.20.h and 4.20.i) the central CT slice, at the 60% isodose line.

CHAPTER FIVE

CONCLUSIONS

The main purpose of this study was to use Monte Carlo techniques to evaluate dose distributions from a treatment planning system. It is well accepted that the MC simulation of the treatment head is the most accurate and practical way to obtain a detailed information about any radiation beam distribution. This was done by simulating the 8 MV photon beams of a SL25 linear accelerator to obtain phase space files that provided source input data for the calculation of the dose distributions in realistic patient models. In the study the CADPLAN treatment planning system (TPS) was evaluated. From the previous chapters several conclusions can be made and these are:

1) The BEAM Monte Carlo code can accurately model radiotherapy units like linear accelerator, as accurate MC treatment planning cannot be performed without accurate beam phase space data. This conclusion came after analysis of some of the beam characteristics from the SL25 linear accelerator with the BEAMDP code, a subsidiary of the BEAM. The obtained fluence, energy fluence, energy spectrum and angular spectrum, analyzed from a phase space file created with in the geometry of the accelerator were in agreement with the expected. This detailed information about the radiotherapy beam increased our understanding of the clinical beam characteristics. Some investigators have used this information to improve accelerator design and improve accuracy of dosimetry.

2) Results have shown that MC methods can accurately reproduce ion chamber measurements in a water phantom. This conclusion came after using the DOSXYZ Monte Carlo code to calculate percentage depth doses and cross plane profiles in a 3D water phantom for different field sizes. The agreement between the MC calculated and similar data obtained by ion chamber on the same accelerator is remarkably excellent. Results are within less than 2% even in areas outside the primary beam.

3) Monte Carlo techniques are very useful for evaluating the accuracy of the dose distributions generated by a treatment planning system in patient based models. Dose distributions were generated by DOSXYZ code in different field sizes and in different treatment sites of varying tissue inhomogeneities. By so doing it allowed us to compare the dose distributions calculated by the treatment planning system and that obtained by DOSXYZ. Also the varying degree of inhomogeneities in the different sites aimed at testing the ETAR and modified BATHO algorithms capabilities and inefficiencies in dose distribution calculation using DOSXYZ as the benchmark.

4) The overall impression from the isodose curves is that ETAR and modified BATHO results are similar to MC in most of the areas with very limited disagreement in few areas. This is still a subject for further investigation and more especially the visual method of the dose distribution that we used in this study for the comparison of different plans. A more quantitative method involving the use of dose difference volume histograms is recommendable, where by the dose differences can be compared in every voxel. Hopefully this will then give a better impression of the performance of the ETAR and modified BATHO dose calculation methods against the Monte Carlo method that in our case is used as a benchmark.

5) The Monte Carlo simulation time is long for the computing facilities at our disposal, rendering the method to be impractical for routine treatment planning in our situation. An extremely large number of histories are required before the statistical uncertainty in the distribution is small enough for it to be compared or used in a treatment planning system. The lower the uncertainty the smoother the dose distribution. Because a large number of histories are simulated in the method, a large amount of computer time and memory is required. For example a typical four field cancer of the cervix technique takes about 30 days on a 400 MHz pentium II PC.

REFERENCES

Andreo P, "Monte Carlo techniques in medical radiation physics", Phys. Med. Biol. **36**, 861 - 920 (1991)

Attix F.H, Introduction to radiological physics and radiation dosimetry, (John Wiley & Sons, New York, USA, 1986)

Batho H.F, "Lung corrections in Co-60 beam therapy", Journal of Cancer Association and Radiology. **15**, 79-89 (1964)

Berger M.J and Wang R, "Multiple-Scattering angular deflections and Energy-loss straggling", in 'Monte Carlo transport of electrons and photons, edited by M.Jenkins, R.Nelson and A.Rindi', 21 – 57, (Plenum press, New York and London, 1988)

Bielajew A.F and Rogers D.W.O, "Variance reduction techniques", in 'Monte Carlo transport of electrons and photons, edited by M.Jenkins, R.Nelson and A.Rindi', 407 – 419, (Plenum press, New York and London, 1988)

Brahme A, "Dosimetric precision requirements in radiation therapy", Acta Radiologica Oncology. **23**, 379 – 391 (1984).

Bushberg J.T, Serbert J.A, Leidholdt E.M and Boone J.M, The essential physics of medical imaging, (Williams and Wilkins, Baltmore, USA 1994)

CADPLAN, users manual (1999)

Cunningham J.R, "Tissue inhomogeneity corrections in photon beam treatment planning", in Orton C.G (ed), Progress in medical radiation physics, **1**, Plenum, New York (1982)

Dahlin H, Lamm I.L, Landberg T, Levernes S and Ulso N, "User requirements on CT-based computed dose planning systems in radiation therapy", Acta Radiologica Oncology. **22**, 398 – 415 (1983)

Du Plessis F.C.P, "Development of a Monte Carlo simulation method for the evaluation of dose distribution calculation of radiotherapy treatment planning system", Thesis submitted for M.Med.Sc degree, University of Orange Free State, (1999)

Green D and Stewart J, "Isodose curves in non-uniform phantoms", British Journal of Radiology. **38**, 378, (1965)

Han K, Ballon D, Chui C.S and Mohan R, "Monte Carlo simulation of Co-60 beams", Med. Phys. **14**, 414 - 419 (1987)

Huizenga H and Storch P.R.M, "The use of computed tomography numbers in dose calculations for radiation therapy", Acta Radiologica Oncology. **24**, 505 – 519 (1985)

ICRU, "Use of computers in external beam radiotherapy procedures with high energy photons and electrons", International Commission on Radiation Units and Measurements, Report **42** (ICRU, Bethesda USA, 1987)

ICRU, "Determination of absorbed dose in a patient irradiated by beams of X-rays or γ-rats in radiotherapy procedures", International Commission on Radiation Units and Measurements, Report **24** (ICRU, Bethesda USA, 1976)

Jiang S.B and Ayyangar K.M; "Compesator design for photon beam intensity modulated radiation therapy", Med. Phys. **25**, 668 - 675 (1998)

Johns H.E and Cunningham J.R, The physics of Radiology, 3rd edition (Charles C.Thomas Publisher, Illinois USA 1980)

Khan F.M; The physics of radiation therapy, 2nd edition (Williams and Wilkins, Baltimore, USA 1994)

Klevenhagen S.C, Physics of electron beam therapy, first edition, Adam Hilger, Bristol (1985).

Kutcher G.J; "Quantitative plan evaluation" , in Purdy J.A, (ed), "Advances in radiation oncology physics: Dosimetry, treatment planning and brachytherapy", American Association of Physicists in Medicine, Medical physics Monograph No **19**, American Insititute of Physics (1992).

Laughlin J, Chu.F, Simpson L and Watson R, "Radiation Treatment Planning", Cancer. **39**, 719 – 728 (1977)

Lee P.C, "Monte Carlo simulations of the differential beam hardening effect of a flattening filter on a therapeutic x-ray beam", Med. Phys. **24**, 1485 - 1489 (1997)

Liu H.H, Mackie T.R and McCullough E.C, "A dual source photon beam model used in convolution/superposition dose calculations for clinical mega voltage x-ray beams", Med.Phys. **24**, 1960 - 1974 (1997)

Lovelock D.M.J, Chui C.S and Mohan R, " A Monte Carlo model of photon beams used in radiation therapy", Med. Phys. **22(9)**, 1387 – 1394 (1995)

Lovelock D.M.J, Chui C.S, Kutcher J and Mohan R, "Analysis of the photon beam treatment planning data for a scanning beam machine", Med. Phys. **21**, 1969 – 1977 (1994)

Ma C.M, Reckwerdt P, Holmes M, Rogers D.W.O and Geiser B, "DOSXYZ users manual", National Reasearch Council of Canada, Report PIRS-0509(revC), (NRC, Ottawa, 1995)

Ma C.M and Rogers D.W.O, "BEAMDP as a general purpose utility", NRCC report PIRS-0509(E), OTAWA, CANADA (1995)

Ma C.M and Jiang S.B; "Monte Carlo modeling of electron beams from medical accelerators", Phys. Med. Biol. **44** (12), 157 -187 (1999)

Ma C.M, Mok E, Kapur A, Pawhcki T, Findley D.O, Brain S, Forster K and Boyer A.L, "Clinical implementation of a Monte Carlo treatment planning system", Med. Phys. **26**, 2133 – 2143 (1999)

Mackie T.R, "Application of Monte Carlo methods in radiotherapy dosimetry of ionizing radiation" Vol **3**, eddited by K.Kase, B.Bjamgand and F.H.Attix, 541 - 620 (San Diego, CA academics, 1990)

McCall R.C, McIntyre R.D and Turnbull W.G, "Improvement of linear accelerator depth-dose curves", Med. Phys. **5**, 518 - 524 (1978)

Metcalfe P, Kron T, Hoban P, The physics of radiotherapy X-rays from linear accelerators, 1st edition (Medical Physics publishing, Wisconsin, USA, 1997)

Mohan R, "Monte Carlo simulation of radiation treatment machine heads" in 'Monte Carlo transport of electrons and photons, edited by M.Jenkins, R.Nelson and A.Rindi', 453 – 467, (Plenum press, New York and London, 1988)

Mohan R, Chui C.S and Lidofsky L, "Energy and angular distributions of photons from medical linear accelerators", Med. Phys. **12**, 592 - 597 (1985)

Mohan R, "Monte Carlo dose calculation for radiation treatment planning", Med. Phys. **24** (1997)

Nahum A.E, "Overview of photon and electron Monte Carlo", in 'Monte Carlo transport of electrons and photons, edited by M.Jenkins, R.Nelson and A.Rindi', 3 – 21, (Plenum press, New York and London, 1988)

Nilsson B and Brahme A, "Contamination of high energy photon beams by scattered photons", Strahlentherapie. **157**, 181 – 186 (1981)

Petti P.L, Goodman M.S, Gabriel T.A and Mohan R, "Investigation of buildup dose from electron contamination of clinical photon beams", Med. Phys. **10(1)**, 18 – 24, (1983)

Raeside D.E, "Monte Carlo principals and application", Med. Phys. **21(2)**, 181 – 197 (1976)

Rogers D.W.O and Bielajew A.F, "Monte Carlo techniques of electrons and photon transport for radiation dosimetry" in 'The Dosimetry of Ionizing Radiation', edited by K.Kase, B.Bjarngard and F.Attix Vol III, 427 – 435, (1990).

Rogers D.W.O, Faddegon B.A, Ding G.X, Ma C.M and We J, "BEAM: A Monte Carlo code to simulate radiotherapy treatment units", Med. Phys. **22(5)**, 503 – 524 (1995)

Rogers D.W.O, Ma C.M, Ding G.X and B Walters, "BEAM user manual" NRCC, OTAWA CANADA, (1996).

Rogers D.W.O, Ewart G.M, Bielajew A.F and Van Dyk, "Calculation of electron contamination in a Co-60 therapy beam", Proceedings of IAEA International Symposium on Dosimetry in Radiotherapy. **1**, 303 - 312 (Vienna, IAEA, 1988)

Rogers D.W.O, "The role of Monte Carlo simulation of electron transport in radiation dosimetry", International Journal of Radiation and Isotopes. **42**, 965 - 974 (1991)

Satish C.P, Glenn .P.G and Purdy J.A, "Dosimetric evaluation of a CT treatment system", Radiology. **130**, 777 – 781 (1979)

Sontag M.R, Battissa J.J, Brouskill M.J and Curningham, "Implementation of CT for inhomogeneity correction in photon beam dose calculation", Radiology. **124**, 143 – 149 (1977).

Sontag M.R and Cunningham J.R, "Corrections to absorbed dose calculations for tissue inhomogenieties", Med. Phys. **4**, 431- 440 (1977)

Sontag M.R and Cunningham J.R, "The ETAR method making absorbed dose calculation in a heterogeneous medium", Radiology. **129**, 787- 795 (1978)

Tubiana J.D, Wambersie A, Introduction to Radiobiology, (Taylor and Francis, London, UK, 1990)

Udale-Smith, "Monte Carlo calculation of electrons beam parameters for three Philips linear accelerators", Phys. Med. Biol. **37**, 85 - 105 (1992)

Van Dyk.J, Barnett R.B, Cyger J.E and Shragge P.C, "Commissioning and quality assurance of treatment planning computers", International Journal of Radiation Oncology, Biology and Physics. **26**, 719 – 728 (1977)

Verhaegen F, Nahum A.E, Van de Putte S and Namito Y, "Monte Carlo modeling of radiotherapy kilo voltage x-ray units" Phys. Med. Biol. **44**, 1767 - 1789 (1996)

Williamson J.F, "Radiation transport calculations in treatment planning", Computerised Medical Imaging and Graphics. **3** 251 - 268 (1989)

Williamson J.F, Khan F.M and Sharma S.C, "Film dosimetry of megavoltage photon beams: A practical method of isodensity- to-isodose curve conversion" Med. Phys. **8**, 94 – 98 (1981)

Woodard H.Q and White D.R, "The composition of body tissues", British Journal of Radiology. **59**, 1209 – 1219 (1986).

Young M and Gaylord J.D, "Experimental tests of correction for tissue inhomogeneities in radiotherapy", British Journal of Radiology. **43**, 49- 61 (1970)

U.O.V.S. BIBLIOTEEK